Teza de abilitare : Modelarea și analiza dinamică a structurilor mecanice de tip paralel cu jocuri și elemente elastice
Autor : Conf. Dr. Ing. Nadia Ramona Crețescu
Domeniul de doctorat : Inginerie Mecanică

1. **Rat, N.R,** Neagoe, M., Diaconescu, D., Stan, S.D. Dynamic analysis of a Triglide parallel robot, The 4th International Conference on Human System Interaction (HSI), Japan, 19-21 May 2011, pp. 245-249, ISBN 978-1-4244-9639-6, IEEE Catalog Number CFP1121D-CDR.
   https://www.researchgate.net/publication/261195536_Dynamic_analysis_of_a_Triglide_parallel_robot

   https://drive.unitbv.ro/s/2gTQ5Q84iPySQS4

2. **Cretescu N.,** Neagoe. M., Saulescu, R. Kinematic modelling and VR simulation of a 3DOF medical parallel robot with one decoupled motion, Advanced Materials Research, **ISSN**: 1662-8985, Vol. 837, p. 567-572, 2013, DOI: 10.4028/www.scientific.net/AMR.837.567.
   https://www.researchgate.net/publication/272051434_Kinematic_Modelling_and_VR_Simulation_of_a_3DOF_Medical_Parallel_Robot_with_One_Decoupled_Motion

   https://drive.unitbv.ro/s/2gTQ5Q84iPySQS4

3. Neagoe. M., **Cretescu N.,** Saulescu, R. Dynamic modelling of a 3DOF medical parallel robot with one decoupled motion, Advanced Materials Research, ISSN: 1662-8985, Vol. 837, p. 594-599, 2013, DOI: 10.4028/www.scientific.net/AMR.837.567.
   https://www.researchgate.net/publication/271571648_Dynamic_Modelling_of_a_3DOF_Medical_Parallel_Robot_with_One_Decoupled_Motion

   https://drive.unitbv.ro/s/2gTQ5Q84iPySQS4

4. **Cretescu, N.,** Neagoe, M. Rigid versus flexible link dynamic analysis of a 3DOF Delta type parallel manipulator, Applied Mechanics and Materials, Vol. 658 (2014) pp 153-158, Trans Tech Publications, Switzerland, doi:10.4028/www.scientific.net/AMM.658.153.
   https://www.researchgate.net/publication/277906770_Rigid_versus_Flexible_Link_Dynamic_Analysis_of_a_3DOF_Delta_Type_Parallel_Manipulator

   https://drive.unitbv.ro/s/2gTQ5Q84iPySQS4

5. **Cretescu, N. R.**, Kinematic and Dynamic Simulation of a 3DOF Parallel Robot, BULLETIN OF THE TRANSILVANIA UNIVERSITY OF BRASOV • VOL. 8 (57) No.1 – 2015, SERIES I - ENGINEERING SCIENCES, ISSN 2065-2119 (Print), ISSN 2065-2127 (CD-ROM), pag 73-78.
https://webbut.unitbv.ro/index.php/Series_I/article/view/4146

https://drive.unitbv.ro/s/2gTQ5Q84iPySQS4

6. **Cretescu, N.,** Neagoe, M., Saulescu, R. Kinematic and Dynamic Analysis of a 4DOF Parallel Robot with Flexible Links, Proceedings of The Joint International Conference of the XII International Conference on Mechanisms and Mechanical Transmissions (MTM) and the XXIII International Conference on Robotics (Robotics '16), Aachen, 26-27 October 2016, New Advances in Mechanisms, Mechanical Transmissions and Robotics, Editors Burkhard Corves, Erwin-Christian Lovasz, Mathias Husing, Inocentiu Maniu, Corina Gruescu, Ed. Springer, pp. 473-481, ISBN 978-3-319-45449-8, Mechanisms and Machine Science 46, DOI 10.1007/978-3-319-45450-4_48 (ISI Proceedings).
https://www.researchgate.net/publication/308842630_Kinematic_and_Dynamic_Analysis_of_a_4DOF_Parallel_Robot_with_Flexible_Links

https://drive.unitbv.ro/s/2gTQ5Q84iPySQS4

7. **Cretescu, N.,** Neagoe, M. Dynamic Modelling of an Isoglide T3 Type Parallel Robot. In: Lovasz, EC., Maniu, I., Doroftei I., Ivanescu, M., Gruescu. C.M. (eds) New Advances in Mechanisms, Mechanical Transmissions and Robotics. Joint International Conference of the International Conference on Mechanisms and Mechanical Transmissions and the International Conference on Robotics, MTM&Robotics 2020, 14-16 October 2020, Timişoara, Romania. Mechanisms and Machine Science, Vol. 88, 2021. Springer, Cham, p. 235-248, DOI: 10.1007/978-3-030-60076-1_21, ISBN 978-3-030-60075-4.
https://www.researchgate.net/publication/346222736_Dynamic_Modelling_of_an_Isoglide_T3_Type_Parallel_Robot

https://drive.unitbv.ro/s/2gTQ5Q84iPySQS4

8. **Cretescu, N.,** Neagoe, M., Saulescu. R. Dynamic Analysis of a Delta Parallel Robot with Flexible Links and Joint Clearances. Applied Sciences. 2023; 13(11):6693. https://doi.org/10.3390/app13116693. FI: 2.838, SRI: 0.885, ISSN: 2076-3417.
https://www.mdpi.com/2076-3417/13/11/6693

https://drive.unitbv.ro/s/2gTQ5Q84iPySQS4

7.07.2025

Dynamic analysis of a Triglide parallel robot

4 authors, including:

Nadia Ramona Cretescu
Universitatea Transilvania Brasov
29 PUBLICATIONS **105** CITATIONS

SEE PROFILE

Mircea Neagoe
Universitatea Transilvania Brasov
102 PUBLICATIONS **601** CITATIONS

SEE PROFILE

Dynamic analysis of a Triglide parallel robot

Nadia Ramona Rat[1], Mircea Neagoe[1], Dorin Diaconescu[1] and Sergiu Dan Stan[2]

[1]Transilvania University of Brasov, Romania, [2]Technical University of Cluj-Napoca, Romania,

ncretescu@unitbv.ro, mneagoe@unitbv.ro, dvdiaconescu@unitbv.ro, sergiustan@ieee.org

Abstract. **This paper presents the analytical dynamic modeling of a Triglide parallel robot and numerical simulation using Maple and Adams software. The Lagrange with multipliers method was successfully applied to develop the closed-form dynamic model using the Maple software. Next, an equivalent dynamic virtual model of the Triglide parallel robot was developed and simulated in ADAMS program on different task. The simulation of the theoretical dynamic models (closed-form model) and ADAMS numerical approach confirm the validity of the analytical dynamic model.**

***Keywords*: Parallel robot, dynamic model, Triglide structure.**

I. INTRODUCTION

THE parallel robots have begun to make the object of study in priority at the last three decades. In this period, important contributions were done specially on the parallel robot modelling: kinematics [1] and dynamics [2].

Because the parallel robots are closed kinematics chains, constituted by a mobile platform with n degree of freedom, connected to the fixed base by serial or complex kinematics chains, the dynamic modelling proves to be complex even in the rigid body hypothesis.

Regarding the dynamic modelling of the parallel robots, different methods can be applied. A method using the Lagrange – D'Alembert formulation has been applied by Yen and Lai [3] for obtaining the dynamic equations of a 3-DOF translational parallel robot.

The virtual work principle was usefully applied by Wu et al. [4] for obtaining the dynamic equation for a 3DOF parallel robot and the obtained driving forces were optimized by applying the least-square method.

Li and Xu [5] derived the analytical dynamic model of a translational parallel robot using the dynamic equations obtained via the virtual work principle and validated on a virtual prototype with the ADAMS software.

In this paper, a kinematical and dynamical modeling for the Triglide parallel robot is presented.

A kinematical analyzes and simulation of Triglide parallel robot has done by Arochia Aelvakumar et al [6].

A kinematical model of the TRIGLIDE parallel robot is presented in [7-8].

The Lagrange method with multipliers was used to derive the closed form dynamic model in the rigid links hypothesis. Based on numerical examples, the dynamic closed form models were validated through MBS prototyping in ADAMS environments.

II. KINEMATICS OF THE CONSIDERED TRIGLIDE PARALLEL ROBOT

The considered Triglide parallel robot (Figure 1) has 3 degrees of freedom (DOF) and is derived of Delta parallel robot. This parallel robot has three legs of type parallelogram (Figure 1), connected to the mobile platform by spherical joints and to the fixed base by linear motors (translational joints – q_1, q_2 and q_3). Each leg has 4 spherical joints and one driving translational joint.

Typically, the study of the robot kinematics is divided into two parts: inverse kinematics and forward (or direct) kinematics. The inverse kinematics problem involves a known pose (position and orientation)/ velocity/ acceleration of the moving platform to obtain the active joint movement (joint displacements/ velocities/ acceleration) that will achieve that imposed end-effector movements.

The forward kinematics problem involves the mapping from a known set of input joint variables/ velocities/ accelerations to a pose of the moving platform that results from those given input displacement/velocity/acceleration. However, the inverse and forward kinematics problems of the former parallel robots can be described in closed form. The direct kinematical model describes the moving platform absolute velocity (v_{xp}, v_{yp}, v_{zp}) in relation with driving velocities ($\dot{q}_1, \dot{q}_2, \dot{q}_3$):

$$\begin{bmatrix} v_{xp} \\ v_{yp} \\ v_{zp} \end{bmatrix} = J_p \cdot \begin{bmatrix} \dot{q}_1 \\ \dot{q}_2 \\ \dot{q}_3 \end{bmatrix}, \qquad (1)$$

where Jp is the robot Jacobian analytically established.

The inverse geometrical modeling of the considered Triglide parallel robot permits to obtain the liaison between independent joint variables {q_1, q_2, q_3} and the moving platform coordinates {x_p, y_p, z_p}:
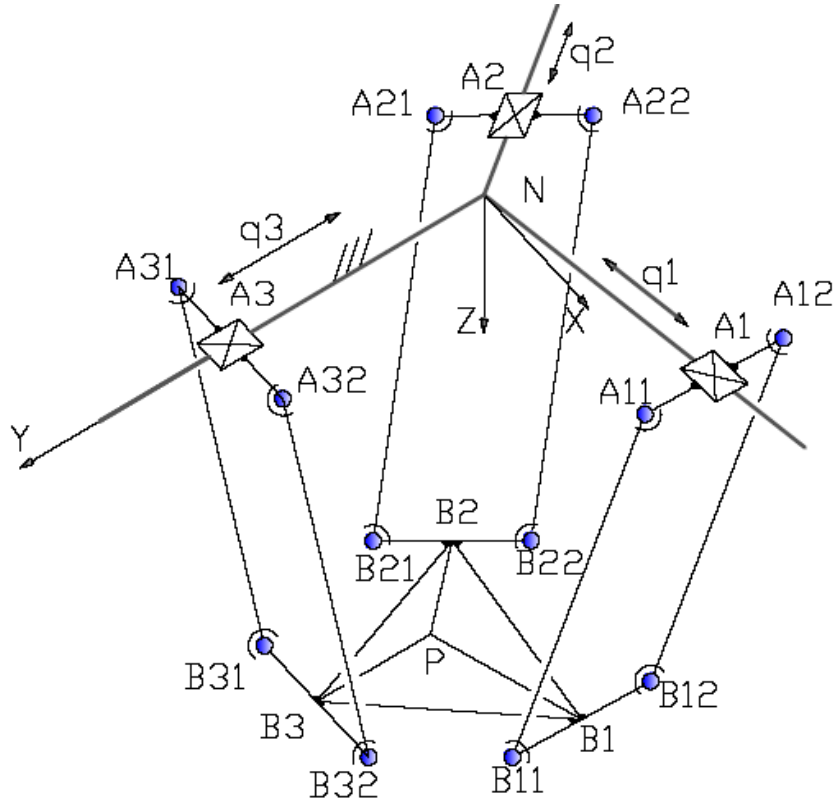
Fig. 1. The kinematical structure of the considered Triglide parallel robot

$$\begin{cases} q_1 = -\dfrac{1}{2}y_p + x_p\sqrt{3} - L_4 + L_3 + \\[2mm] \quad \dfrac{1}{2}\sqrt{-3y_p{}^2 - 2y_p x_p\sqrt{3} - x_p{}^2 + 4L_2{}^2 - 4z_p{}^2} \\[4mm] q_2 = -\dfrac{1}{2}x_p\sqrt{3} - L_4 - \dfrac{1}{2}y_p + L_3 + \\[2mm] \quad \dfrac{1}{2}\sqrt{-x_p{}^2 + 2y_p x_p\sqrt{3} - 3y_p{}^2 - 4z_p{}^2 + 4L_2{}^2} \\[4mm] q_3 = y_p - L_4 + L_3 + \sqrt{L_2{}^2 - x_p{}^2 - z_p{}^2} \end{cases} \quad (2)$$

where: $L_1 = A_{i1}A_{i2}$; $L_2 = A_{i1}B_{i1}$; $L_3 = NB_i$; $L_4 + q_i = NA_i$; with i=1, 2, 3.

Deriving the relation 2, the inverse kinematical model is obtained:

$$\begin{bmatrix} \dot{q}_1 \\ \dot{q}_2 \\ \dot{q}_3 \end{bmatrix} = J_p{}^{-1} \cdot \begin{bmatrix} v_{xp} \\ v_{yp} \\ v_{zp} \end{bmatrix}, \quad (3)$$

where:

$$J_p{}^{-1} = \begin{bmatrix} a_{11} & a_{12} & a_{13} \\ a_{21} & a_{22} & a_{23} \\ a_{31} & a_{32} & a_{33} \end{bmatrix}, \quad (4)$$

with:

$$a_{11} = \frac{1}{2}\sqrt{3} + \frac{1}{4}\frac{-2y_p\sqrt{3} - 2x_p}{\sqrt{-3y_p{}^2 - 2y_p x_p\sqrt{3} - x_p{}^2 + 4L_2{}^2 - 4z_p{}^2}}$$

$$a_{12} = -\frac{1}{2} + \frac{1}{4}\frac{-6y_p\sqrt{3} - 2x_p\sqrt{3}}{\sqrt{-3y_p{}^2 - 2y_p x_p\sqrt{3} - x_p{}^2 + 4L_2{}^2 - 4z_p{}^2}}$$

$$a_{13} = -2\frac{z_p}{\sqrt{-3y_p{}^2 - 2y_p x_p\sqrt{3} - x_p{}^2 + 4L_2{}^2 - 4z_p{}^2}}$$

$$a_{21} = -\frac{1}{2}\sqrt{3} + \frac{1}{4}\frac{2y_p\sqrt{3} - 2x_p}{\sqrt{-x_p{}^2 + 2y_p x_p\sqrt{3} - 3y_p{}^2 + 4L_2{}^2 - 4z_p{}^2}}$$

$$a_{22} = -\frac{1}{2} + \frac{1}{4}\frac{2x_p\sqrt{3} - 6y_p}{\sqrt{-x_p{}^2 + 2y_p x_p\sqrt{3} - 3y_p{}^2 + 4L_2{}^2 - 4z_p{}^2}}$$

$$a_{23} = -2\frac{z_p}{\sqrt{-x_p{}^2 + 2y_p x_p\sqrt{3} - 3y_p{}^2 + 4L_2{}^2 - 4z_p{}^2}}$$

$$a_{31} = -\frac{x_p}{\sqrt{-x_p{}^2 + L_2{}^2 - z_p{}^2}}$$

$$a_{32} = 1$$

$$a_{33} = -\frac{z_p}{\sqrt{-x_p{}^2 + L_2{}^2 - z_p{}^2}}$$
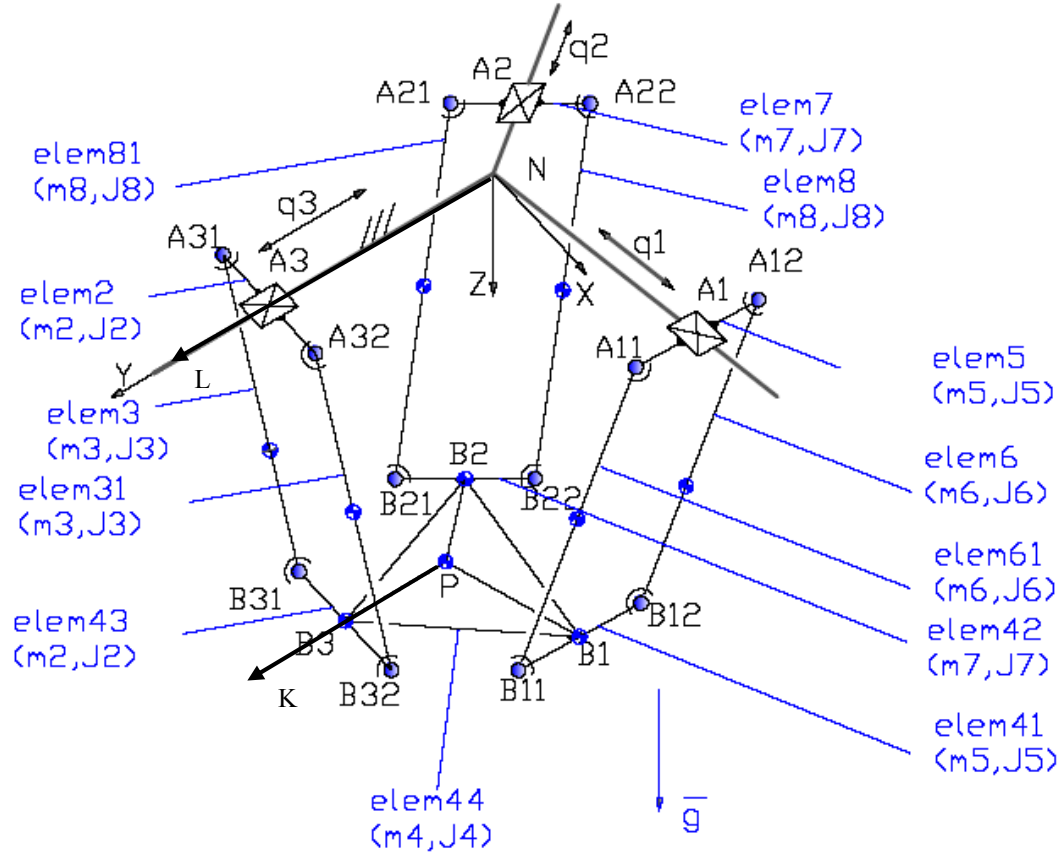
Fig. 2. The dynamical diagram of the Triglide parallel robot

III. DYNAMICAL MODELING OF TRIGLIDE PARALLEL ROBOT

The dynamic modeling has been done in the following prerequisites:
a) The elements are rigid bodies;
b) The gravity vector is oriented in negative sense of the z axis (Figure 2);
c) No external load on the moving platform;
d) The inertial matrix $J_3 = J_6 = J_8$ and $J_2 = J_5 = J_7$;
e) The mobile platform (the element no. 4) contains four parts (sub-elements): 41, 42, 43 and 44.

Considering rigid elements with distributed masses, the dynamic model can be analytically developed using the Lagrange multipliers method:

$$\sum_{i=1}^{k} \lambda_i \frac{\partial \Gamma_i}{\partial q_j} = \frac{d}{dt}\left(\frac{\partial L}{\partial \dot{q}_j}\right) - \frac{\partial L}{\partial q_j} - \hat{Q}_j$$

(5)

where: λ_i - Lagrange multipliers;

q_j - Displacements from the actuators;

$\hat{Q}_j$ - Generalized external forces;

L - Parallel robot Lagrangean:

$$L = \sum_{i=1}^{n} K_i + \sum_{i=1}^{n} P_i,$$

(6)

where: Ki – the kinetic energy of the link i;
Pi – the potential energy of the link i.

The Lagrange multipliers (λ_i) are identified introducing the following set of geometric equations:

❖ $dist(B_1, B_2) = a$, where a is the side of $\Delta B_1 B_2 B_3$;

❖ $dist(B_2, B_3) = a$;

❖ $dist(B_1, B_3) = a$;

❖ Coordinate after Z of point B1 and B2 need to be the same;

❖ Coordinate after Z of point B2 and B3 need to be the same;

❖ Cosine director between L si K (Figure 2) is equal with 1.

Finally, the analytical expression of the driver forces Fq_1, Fq_2 and Fq_3 (see Figure 2) are obtained using Maple software.

Even the obtained analytical dynamic model is complex; this method used can be usefully applied to solve the dynamical model of any 3 DOF parallel robots and can be extended to 4 and more DOF parallel robots.

IV. THE CAD MODEL OF THE TRIGLIDE PARALLEL ROBOT AND SIMULATION RESULTS

The CAD model of the Triglide parallel robot is obtained using ADAMS software and the simple elements of type cylinders (see Figure 3).
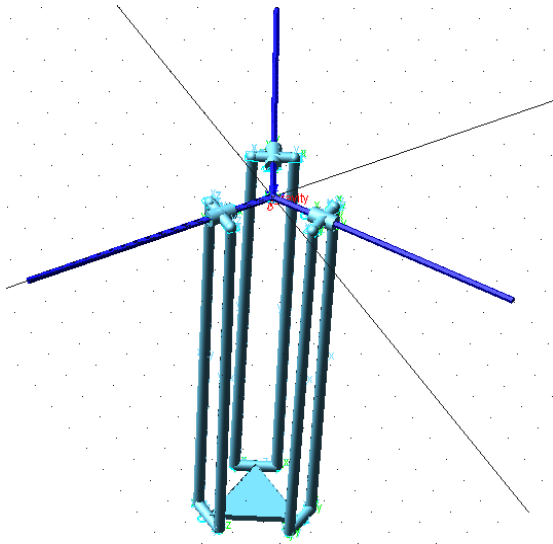
Fig. 3. The CAD model of the Triglide parallel robot

The mass and inertial parameters of CAD model obtained (see Table 1) were used also for simulation the analytical model obtained using Maple software.

Numerical simulations of the obtained models are carried out considering a linear trajectory in the operational space, using a three degree polynomial low of movement of motor B3 (see Figure 1) with 0.1m in 10s (presented in Figure 4).

	M	Ixx	Iyy	Izz	Ixy, Iyz, Izx
	[kg]	[kg*m^2]	
Element 3, 6, 8	0.941	2.824×10^{-2}	2.824×10^{-2}	3.011×10^{-5}	0
Element 4	0.570	8.015×10^{-4}	4.055×10^{-4}	4.055×10^{-4}	0

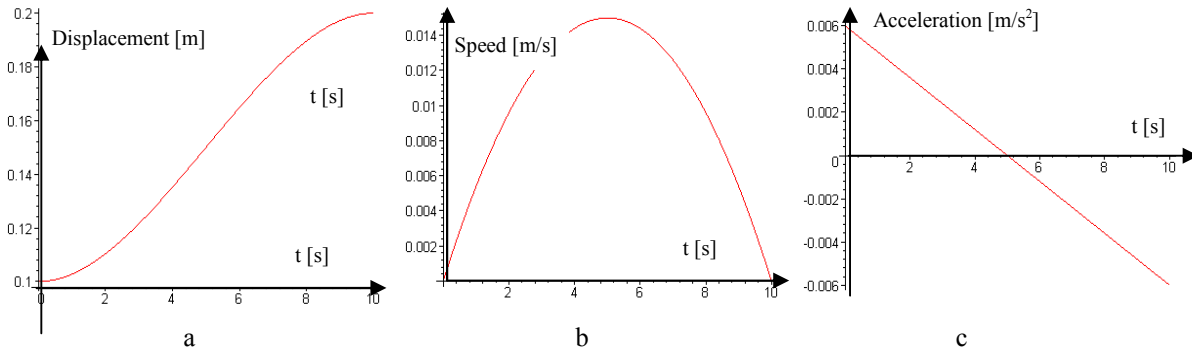Table 1: The elements' inertial property of the considered Triglide parallel robot

Fig. 4. The q_3 movement (a-displacement; b-speed, c-acceleration) of the Triglide parallel robot
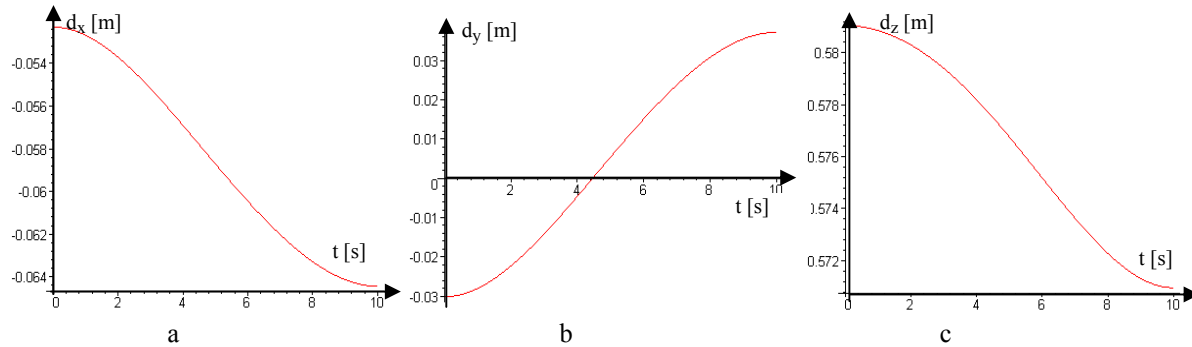

Fig. 5. The displacement of the mobile platform (of the Triglide parallel robot) after X (a), Y (b) and Z (c) axis

In this way, for the movement in active joint q_3 of 0.1m we obtain a maximal speed major then 0.014m/s and an acceleration major then 0.006m/s^2 (Figure 4).

The displacements of the mobile platform (Figure 5) have the same rate of curve with displacement of motor q_3, obtaining a displacement of 0.012m after X axis, 0.067m after Y axis and 0.01m after Z axis.

The driving force (presented in Figure 6) have the same rate of curve with the displacement impose in active joint q_3, obtaining a maximal value for driving force F_{q2} (4.3N). For verify the correctitude of the analytical model, the same simulation was made in Maple and Adams.
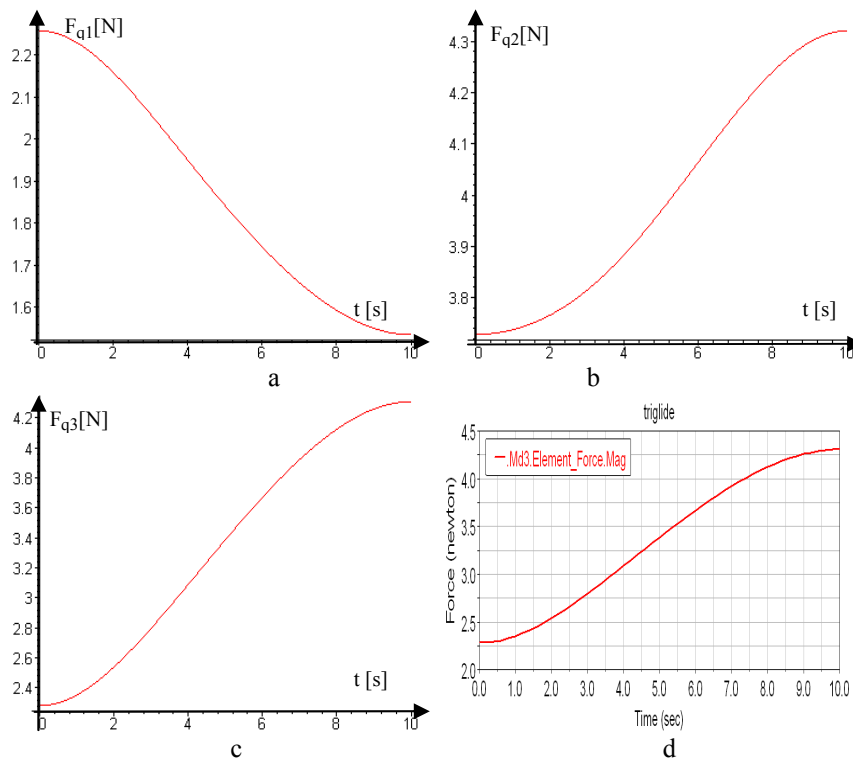
Fig. 6. The driving force of the Triglide parallel robot: F_{q1} (a), F_{q2} (b) and F_{q3} (c) from Maple and F_{q3} (d) from Adams

In Figure 6 is presented for exemplification the result obtained for driving force F_{q3} in the both case (Maple and Adams); the results obtained is the same witch can give the conclusion the analytical model obtained is correct and can be utilized in command and control model of the considered Triglide parallel robot.

V. CONCLUSION

The study highlights the following conclusions:

- The Lagrange with multipliers method for obtaining the dynamic analytical method was successfully applied for this parallel robot using Maple software;
- This numerical simulations effectuated allow to obtain the quantitative dates regarding the kinematical and dynamic response of the parallel robot when the movements from the active joints are known;
- A CAD model was successfully implemented in Adams software to allow to making the numerical simulation in Maple (using the masse and inertial proprieties of the elements of Adams) and also to compare the results obtained for verify the correctitude of the analytical model;
- The results obtained in both models (Maple and Adams) are the same in kinematical and dynamical cases, which go to at the conclusion that the analytical model obtained in Maple is correct;
- In this way, the analytical model obtained can be utilized for obtaining the model of command and control of the considered Triglide parallel robot;
- The presented methodology used for obtaining the analytical dynamic model, with its numerical simulation, can be extended for more type of parallel robot.

REFERENCES

[1] Merlet, J. P.: Les robots parallèles. Paris: Hermès, 1st ed.1990, 2nd ed. 1997 (in French).

[2] Tsai, L. W.: Mechanism Design: Enumeration of kinematic structures according to function. CRC Press, 2000.

[3] Yen, P.-L., Lai, C.C.: Dynamic modeling and control of a 3-DOF Cartesian parallel manipulator. Mechatronics (2009) No. 19, p 390–398.

[4] Wu, J. et al.: Dynamics and control of a planar 3-DOF parallel manipulator with actuation redundancy. Mechanism and Machine Theory (2009) No. 44, p 835–849.

[5] Li, Y., Xu, Q.: Dynamic modeling and robust control of a 3-PRC translational parallel kinematic machine. Robotics and Computer-Integrated Manufacturing (2009), No. 25, p 630– 640.

[6] Arochia Aelvakumar A. et al.: Simulation and Kinematic Analysis of Tri-glide parallel manipulator. International Journal of Mechanics and Solids, ISSN 0973-1881 Volume 4, Number 1 (2009), pp. 127-135.

[7] Stan, S.D. et al.: Evolutionary Approach to Optimal Design of 3 DOF Translation Exoskeleton and Medical Parallel Robots, HSI 2008, IEEE Conference on Human System Interaction, Krakow, Poland, May 25-27, 2008.

[8] Verdes D. et al.: Kinematics analysis, Workspace, Design and Control of 3-RPS and TRIGLIDE medical parallel robots. HSI 2009, IEEE Conference on Human System Interaction, Catania, Italy, May 21-23, 2009.

Kinematic Modelling and VR Simulation of a 3DOF Medical Parallel Robot with One Decoupled Motion

3 authors:

Nadia Ramona Cretescu
Universitatea Transilvania Brasov
29 PUBLICATIONS   105 CITATIONS

SEE PROFILE

Mircea Neagoe
Universitatea Transilvania Brasov
102 PUBLICATIONS   601 CITATIONS

SEE PROFILE

Radu Saulescu
Universitatea Transilvania Brasov
95 PUBLICATIONS   433 CITATIONS

SEE PROFILE

KINEMATIC MODELLING AND VR SIMULATION OF A 3DOF MEDICAL PARALLEL ROBOT WITH ONE DECOUPLED MOTION

Cretescu Nadia[1, a], Neagoe Mircea[1,b] and Saulescu Radu[1,c]

[1]University *Transilvania* of Brasov, Bd. Eroilor, No. 29, Brasov, Romania

[a]ncretescu@unitbv.ro, [b]mneagoe@unitbv.ro, [c]rsaulescu@unitbv.ro

Keywords: parallel robots, medical robot, kinematic modelling, VR simulation.

Abstract.

The robot studied in the paper has a 3DOF parallel structure of type 1PRRR+2PRPaR, with two coupled motions and one decoupled motion, composed by a mobile platform connected to the fixed base by three kinematic chains (one open kinematic chain of Prismatic – Revolute – Revolute – Revolute type and two kinematic chains of Prismatic – Revolute – Parallelogram – Revolute type). An analytical kinematic modelling of the parallel robot of type 1PRRR+2PRPaR is firstly presented in this paper, followed by a numerical simulation of the closed-form kinematic model and by a Virtual Reality (VR) application with control aspects. An innovative user interface for high-level control of the parallel 1PRRR+2PRPaR type robot is developed in MATLAB - Simulink and SimMechanics environment.

Introduction

In the last couple of decades parallel robots have been studied and developed from theoretical view point and also for practical applications. The advantages offered by parallel manipulators (PMs) are high stiffness, excellent load-to-weight ratio, positioning accuracy and good dynamic behavior [1]. The parallel robots are mechanisms with closed kinematics chains, composed by a mobile platform (the end-effector) with *n* degrees of freedom, connected to the fixed base by two or more kinematical chains called limbs or legs. A simple or a complex kinematics chain can be associated with each limb [2].

Jin et al. [3] studied the kinematic design of a family of partially decoupled parallel manipulators (DPMs) with 3-limb symmetrical structure, in which 3-DOF spatial motion composed by a vertical translation and two horizontal rotations can be independently controlled. The concept of group decoupling (GD) is introduced for classification and synthesis of decoupled motion PMs.

Also, a kinematical analyze is made by Stan et al. [4], where a kinematics analysis and control of a 3DOF parallel robot is presented. A kinematical modeling of a 3DOF medical parallel robot is detailed in [5].

The Virtual Reality (VR) immerses the user in a three-dimensional (3D) environment that can be actively interacted and explored. Virtual reality environment tool is used by many researchers in design, development and manufacturing of the robotic industry [6].

Using the virtual reality simulation with a virtual robot, a three dimensional design and the real-time behavior of the robot can be observed; that fact is relatively new and allows testing the robot before accomplishment a physical implementation. In this way, resources (money and time) can be saved and various problems can be solved from the design stage.

This paper presents the kinematical modeling of a parallel robot of type 1PRRR+2PPPaR [7] and the necessary steps for developing the virtual environment for kinematic simulation, starting from the SolidWorks model [8].

Description and kinematical modeling of 1PRRR+2PRPaR parallel robot

The parallel robot of type 1PRRR+2PRPaR (1Prismatic, Revolute, Revolute + 2Prismatic, Revolute, Parallelogram, Revolute) has 3 degrees of freedom (DOF) with one decoupled motion along X axis and two coupled motions (see Fig. 1).
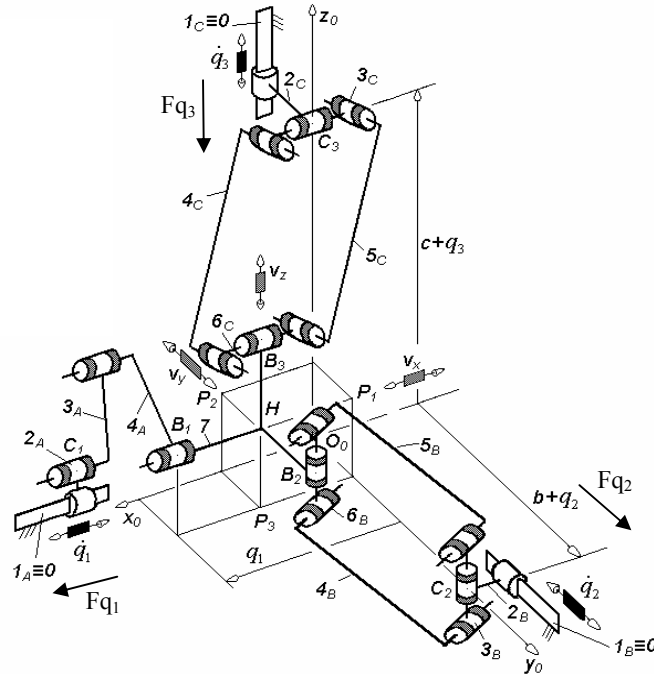

Fig. 1 Kinematic structure of parallel robot of type 1PRRR+2PRPaR [7]

This parallel robot is composed by a mobile platform 7 connected to the base by three kinematic chains A, B and C:
- A: simple open kinematic chain with one active prismatic joint (q1) and three passive revolute joints ($\varphi2a$, $\varphi3a$ and $\varphi4a$) – see Fig. 2,b;
- B and C: complex kinematic chains of parallelogram type with one active prismatic joint (q2 and respectively q3) and six passive revolute joints ($\varphi2i$, $\varphi3i$, $\varphi3i1$, $\varphi4i$, $\varphi4i1$, and $\varphi5i$ – where i = b,c) – see Fig. 2,a.
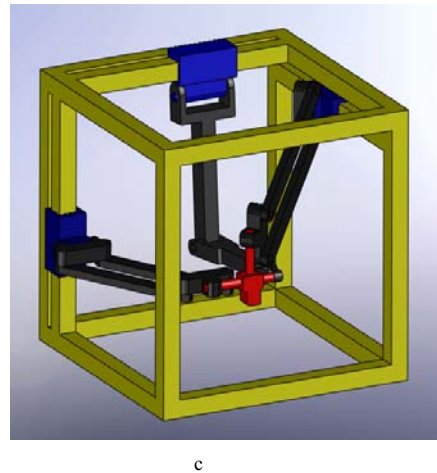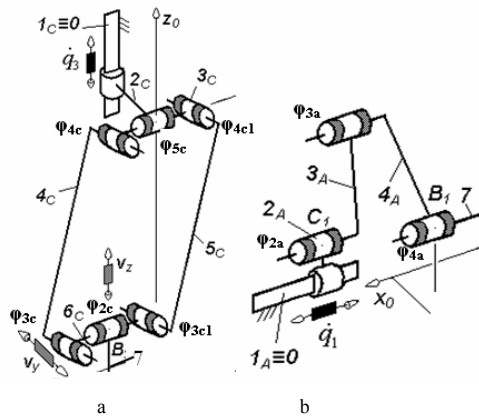

Fig. 2 Parametrization of the 1PRRR+2PRPaR parallel robot (a and b) and its CAD model (c)

Direct and inverse kinematic model of 1PRRR+2PRPaR parallel robot

The direct geometrical (Eq. 1) and the kinematical model (Eq. 2) have been derived to compute the mobile platform displacement (x_h, y_h, z_h) and velocity (V_{xh}, V_{yh}, V_{zh}) in function of drivers' motion.

$$\begin{cases} x_h = q_1 - l_{7a} \\ y_h = l_{3a}\cos(\varphi_{2a}) + l_{4a}\cos(\varphi_{2a} + \varphi_{3a}), \\ z_h = l_{3a}\sin(\varphi_{2a}) + l_{4a}\sin(\varphi_{2a} + \varphi_{3a}) \end{cases} \tag{1}$$

$$\begin{bmatrix} v_{xh} \\ v_{yh} \\ v_{zh} \end{bmatrix} = J_h \cdot \begin{bmatrix} \dot{q}_1 \\ \dot{q}_2 \\ \dot{q}_3 \end{bmatrix}, \tag{2}$$

where: J_h is the robot Jacobian.

The inverse geometric model allows obtaining the liaison between geometrical parameters (q1, q2, q3) and (xh, yh, zh) – eq. 3 for 1PRRR+2PRPaR parallel robot (with notations presented in Fig. 1 and 2):

$$\begin{cases} q_1 = x_h + l_{7a} \\ q_2 = \sqrt{l_{4b}^2 - z_h^2 - x_h^2} + l_{7b} + y_h \\ q_3 = \sqrt{l_{4c}^2 - x_h^2 - y_h^2} + l_{7c} + z_h \end{cases} \tag{3}$$

Deriving the eq. 3, the inverse kinematical model (eq. 4) is obtained:

$$\begin{bmatrix} \dot{q}_1 \\ \dot{q}_2 \\ \dot{q}_3 \end{bmatrix} = J_h^{-1} \cdot \begin{bmatrix} v_{xh} \\ v_{yh} \\ v_{zh} \end{bmatrix}, \tag{4}$$

where J_h^{-1} is the inverse Jacobian matrix of the 1PRRR+2PRPaR parallel robot:

$$J_h^{-1} = \begin{bmatrix} 1 & 0 & 0 \\ -\dfrac{x_h}{\sqrt{l_{4b}^2 - z_h^2 - x_h^2}} & 1 & -\dfrac{z_h}{\sqrt{l_{4b}^2 - z_h^2 - x_h^2}} \\ -\dfrac{x_h}{\sqrt{l_{4c}^2 - x_h^2 - y_h^2}} & -\dfrac{y_h}{\sqrt{l_{4c}^2 - x_h^2 - y_h^2}} & 1 \end{bmatrix}. \tag{5}$$

Virtual Reality tools for parallel robot prototyping

An interface for high-level control of robot manipulators is presented in this section and is based on a virtual reality approach in order to provide the user with an interactive 3D graphical representation of the parallel robot.

The actuators and the control algorithm were modeled in Simulink. The dynamic model of the mechanical structure was imported from SolidWorks using SimMechanics from MATLAB/ Simulink.

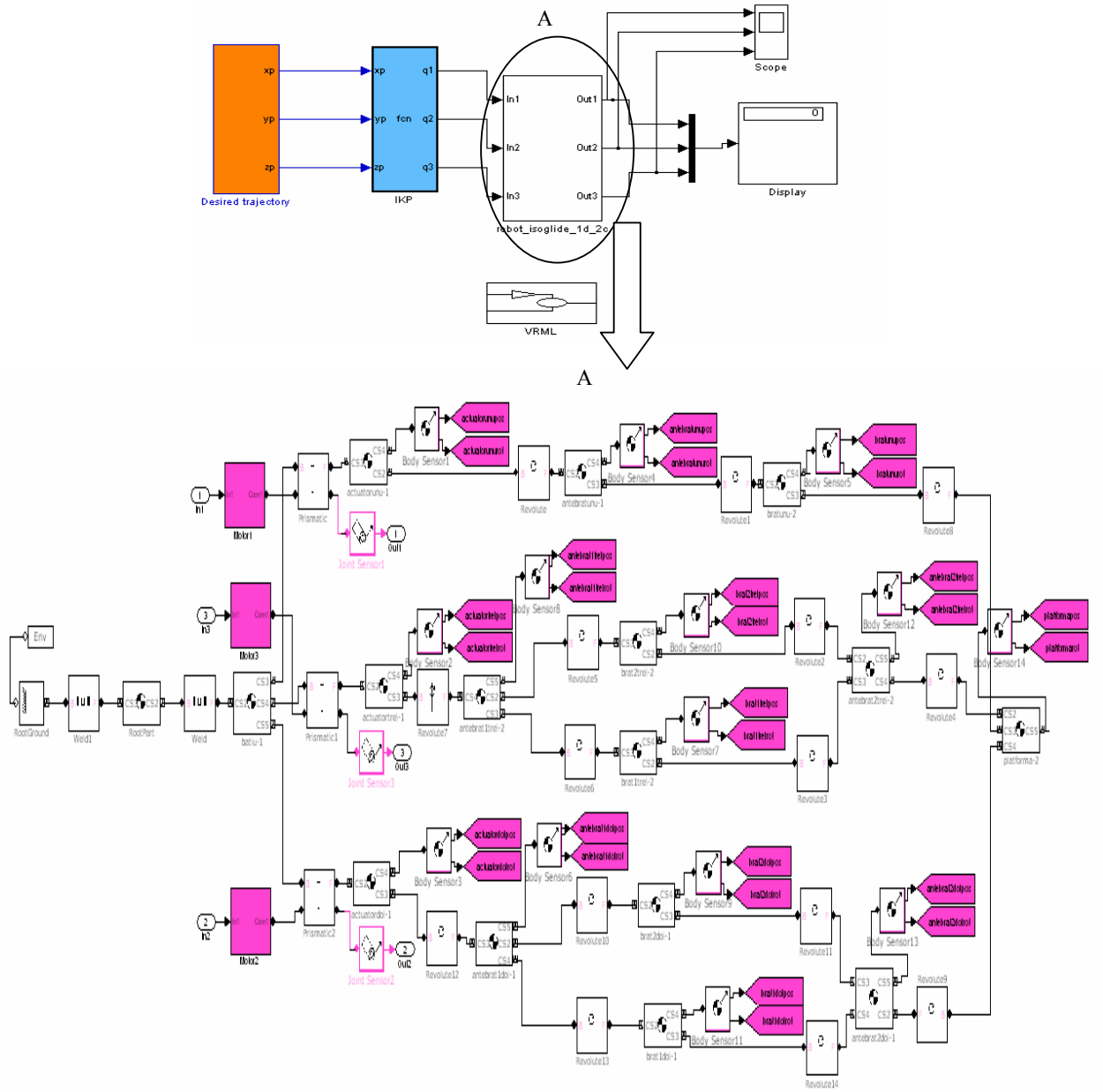In fig. 3 is presented the complete model with VR of the parallel robot.

Fig. 3 The complete model for 1PRRR+2PRPaR parallel robot with VR

Virtual Reality Toolbox for MATLAB makes more realistic renderings of bodies possible. Arbitrary virtual worlds can be designed with Virtual Reality Modeling Language (VRML), and interfaced to the SimMechanics model. The user simply describes the geometric properties of the robot first. Then, in order to move any part of the robot through 3D input devices, the inverse kinematics is automatically calculated in real time. The interface was also designed to provide the user decision capabilities when problems such as singularities are encountered.

In particular, the interface allows user to understand the behaviour of an existing robot, and to investigate the performance of a newly designed structures without the need and the cost associated with the hardware implementation.

SimMechanics offers the possibility to visualize and animate the robot. The visualization tool can also be used to animate the motion of the system during simulation. The bodies of the robot can be represented as convex hulls (fig. 4).

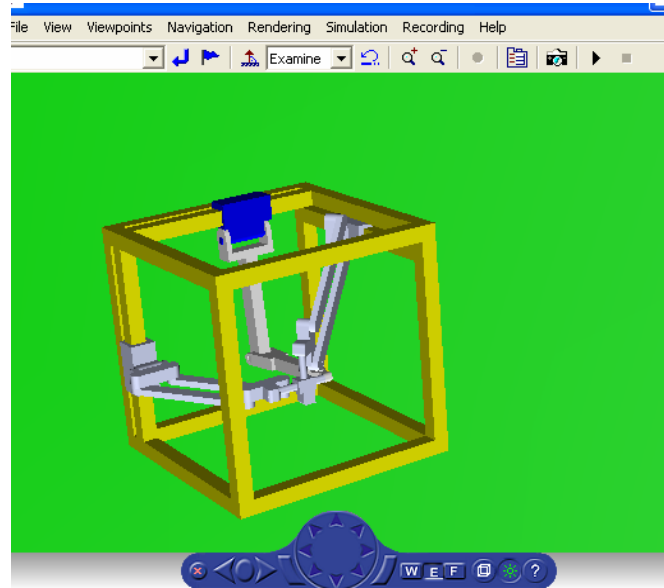The models obtained allow the opening for a control strategy implementation.

Fig. 4 Virtual Reality model of 1PRRR+2PRPaR parallel robot

Simulation Results

For testing the obtained model, it has been chosen a linear trajectory between two defined points, considering a movement low in Cartesian space of fifth degree polynomial type. The simulation is done by numerical simulation of the analytical model and by numerical simulation of the CAD model from Fig. 2.c.

Regarding the displacements (Fig. 5), it can be noted that for the same desired displacement of the end-effector, the required displacements in motor joints q2 and q3 are bigger.
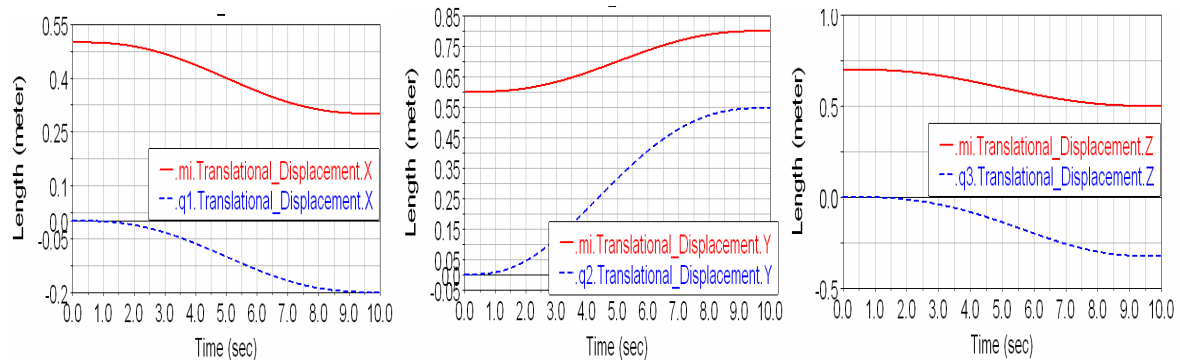

Fig. 5. Displacements of the end-effector (red-continues line) and of the independent variables $q_{1,2,3}$ (blue – dashed line) of the parallel robot of 1PRRR+2PRPaR type

The results obtained by numerical simulation (Fig. 5) reach at the conclusion: to obtain a displacement of 200 mm along each of the three axis, a 1.5-2.5 more displacement for motor q_2 and q_3 are needed, and exactly the same displacement for motor q_1, due at the decoupling motion.

Conclusions

The main advantages of this parallel manipulator are that all the actuators can be attached directly to the base, that closed-form solutions are available for the forward and inverse kinematics, and that the moving platform maintains the same orientation throughout the entire workspace. The paper presents a closed-form kinematic modelling and a novel Virtual Reality Interface for 3 DOF medical parallel robots control. An evaluation model from the Matlab/SimMechanics environment was used for the simulation and an interactive tool for kinematic system modeling and analysis was presented and exemplified on the Virtual Reality environment for the 1PRRR+2PRPaR medical parallel robot. By means of SimMechanics, the robotic system in represented as a block of functional diagrams. Besides, such software packages allow visualizing the motion of mechanical system in 3D virtual space.

With the obtained analytical kinematic model, a numerical simulation is done, on a given trajectory, emphasizing the influence of decoupled/coupled motions on the robot kinematic behaviour.

Especially non-experts will benefit from the proposed visualization tools, as they facilitate the modeling and the interpretation of results. The research presented will lay a good foundation for the development of medical parallel robots.

References

[1] Zhao Y. and Gao F., Dynamic formulation and performance evaluation of the redundant parallel manipulator, Robotics and Computer-Integrated Manufacturing, Vol. 25, (2009), pp. 770–781.

[2] Gogu G., Structural synthesis of parallel robots. Part 1: Methodology, Springer Verlag, (2008), pp.282.

[3] Jin, Y., Chen, I-M., and Yang, G., Kinematic design of a family of 6-DOF partially decoupled parallel manipulators. Mechanism and Machine Theory, Vol. 44, (200), pp. 912–922.

[4] Stan, S.D, Manic, M., Maties and M., Balan, R., Kinematics Analysis, Design, and Control of an Isoglide3 Parallel Robot (IG3PR), IECON08, The 34th Annual Conference of the IEEE Industrial Electronics Society, Nov. 10-13, (2008), Orlando, Florida, pp. 2636-2641.

[5] Sergiu-Dan Stan, Vistrian Mătieş, Radu Bălan, Nadia Raţ, Workspace and Kinematics Analysis of a Medical Parallel Robot for Cardiopulmonary Resuscitation, IEEE-ICIT'09, 2009, Melbourne, Australia.

[6] Stan, S.-D, Manic, M., Mătieş, M., Bălan, R., Kinematics Analysis, Design, and Control of an Isoglide3 Parallel Robot (IG3PR), IECON 2008, The 34th Annual Conference of the IEEE Industrial Electronics Society, Orlando, USA, November 10-13, (2008).

[7] Gogu, G., Evolutionary morphology: a structured approach to inventive engineering design, Invited paper, Proceedings of the 5th International Conference on Integrated Design and Manufacturing in mechanical Engineering, Bath, 5-7 April 2004.

[8] Raţ, N.R., Neagoe, M., Stan, S.D. Comparative Dynamic Analysis of Two Parallel Robots, The 2010 International Conference on Robotics (ROBOTICS'10), Cluj-Napoca, Romania, September 23-25, 2010, In Robotics and Automation Systems, doi:10.4028/www.scientific.net/SSP.166-167, Solid State Phenomena Vols. 166-167 (2010) pp 345-356, Online available since 2010/Sep/10 at www.scientific.net©(2010) Trans Tech Publications, Switzerland doi:10.4028/ www.scientific.net/ SSP.166-167.345.

Dynamic Modelling of a 3DOF Medical Parallel Robot with One Decoupled Motion

3 authors:

Mircea Neagoe
Universitatea Transilvania Brasov
102 PUBLICATIONS   **601** CITATIONS

SEE PROFILE

Nadia Ramona Cretescu
Universitatea Transilvania Brasov
29 PUBLICATIONS   **105** CITATIONS

SEE PROFILE

Radu Saulescu
Universitatea Transilvania Brasov
95 PUBLICATIONS   **433** CITATIONS

SEE PROFILE

DYNAMIC MODELLING OF A 3DOF MEDICAL PARALLEL ROBOT WITH ONE DECOUPLED MOTION

Neagoe Mircea [1, a], Cretescu Nadia [1,b] and Saulescu Radu[1,c]

[1]*Transilvania* University of Brasov, Blvd. Eroilor, No. 29, Brasov, Romania

[a]mneagoe@unitbv.ro, [b]ncretescu@unitbv.ro, [c]rsaulescu@unitbv.ro

Keywords: parallel robots, medical robots, dynamic modeling, Lagrange multipliers method, numerical simulations.

Abstract

The paper presents the dynamic modeling of a 3DOF parallel robot of 1PRRR+2PRPaR type using the Lagrange multipliers method in the rigid link assumption. Numerical simulations of the analytical dynamic model, developed using Maple software, on representative trajectories are carried out and these results are finally validated trough numerical simulations in the MBS ADAMS software. Final conclusions are drawn, useful for researchers and practitioners in the robotic field.

Introduction

The parallel robots are known as mechanism with high accuracy due to the non cumulative joint errors. The advantages offered by parallel manipulators (PMs) are: excellent load-to-weight ratio, high stiffness and positioning accuracy and good dynamic behavior [1].

The parallel robots are mechanisms with closed kinematic chains, composed by a mobile platform connected to the fixed base by minimum two kinematic chains (simple or complex) [2].

Different methods can be applied for obtaining the dynamical model of the parallel robots. Using the Lagrange-D'Alembert formulation, Yen and Lai [3] obtained the dynamic equations of a 3DOF translational parallel manipulator.

Lu and Xu [4] developed a dynamic model for a translational parallel robot, deriving the dynamic analytical model using the simplified dynamic equations obtained via the virtual work principle and validated on a virtual prototype with the ADAMS software.

Khoukhi et al. [5] applied the method Euler-Lagrange to obtain the dynamic model for a parallel kinematic machine. A new approach to multi-objective dynamic trajectory planning of parallel kinematic machines (PKM) under task, workspace and manipulator constraints is also presented.

A recursive model for developing kinematics and dynamics of a 3-PRR planar parallel robot was used by Staicu [6]. The principle of virtual work is applied for solving the inverse dynamic problem.

By means of the principle of virtual work and the concept of link Jacobian matrices, Zao and Gao [7] developed the inverse dynamic model of the redundant parallel manipulator, obtaining six linear consistent equations with eight unknown quantities.

Zhang et al. [8] proposed an innovative design for a parallel manipulator with 3-DOF, including the rotations of a moving platform along X and Y axis and translation of this platform along the Z axis. Kinematic aspects are investigated and a dynamic model using a Newton-Euler approach is implemented. The global system stiffness of the parallel robot is formulated and the kinetostatic analysis is conducted. Finally, a case study was presented to demonstrate the applications of the kinematic and dynamic models and to verify the concept of the new design.

The methodology of the dynamic optimum design of a three translational degrees of freedom parallel robot (Delta robot) while considering anisotropic property is presented [9].

The paper [10] presents a dynamics identification of kinematically redundant parallel robots based on the Lagrange equations of the first kind and using the coordinate partitioning method the

dynamic equations of the considered mechanism are derived analytically in a reduced symbolic form. For this parallel robot, a set of minimal dynamic parameters is automatically obtained.

The inverse dynamic model for a 5-DOF hybrid parallel robot is detailed in [11]. The virtual work method based on the dynamically equivalent lumped masses is used.

The paper [12] presents the methodology of the dynamic optimum design of a three translational degrees of freedom parallel robot (Delta) while considering anisotropic property. Taking the acceleration, velocity, and gravity components into account, the torque and power indices are adopted as the objective functions for the dynamic optimum design.

The dynamic modelling of a medical parallel robot is developed in the paper using the Lagrange multipliers method in the rigid link hypothesis. The results of numerical simulations on a given trajectory emphasize the influence of the parallel robot kinematic and dynamic properties on the driving forces. Furthermore, numerical simulations on representative trajectories of the analytical dynamic model, developed using Maple software, are fulfilled and the results are finally validated trough simulations in MBS ADAMS software. Final conclusions are drawn, useful for researchers and practitioners in the robotic field.

Description of 1PRRR+2PRPaR parallel robot

The parallel robot of type 1PRRR+2PRPaR (1Prismatic, Revolute, Revolute, Revolute + 2Prismatic, Revolute, Parallelogram, Revolute) has 3 degrees of freedom (DOF) with one decoupled motion along X axis and two coupled motions (Fig. 1).
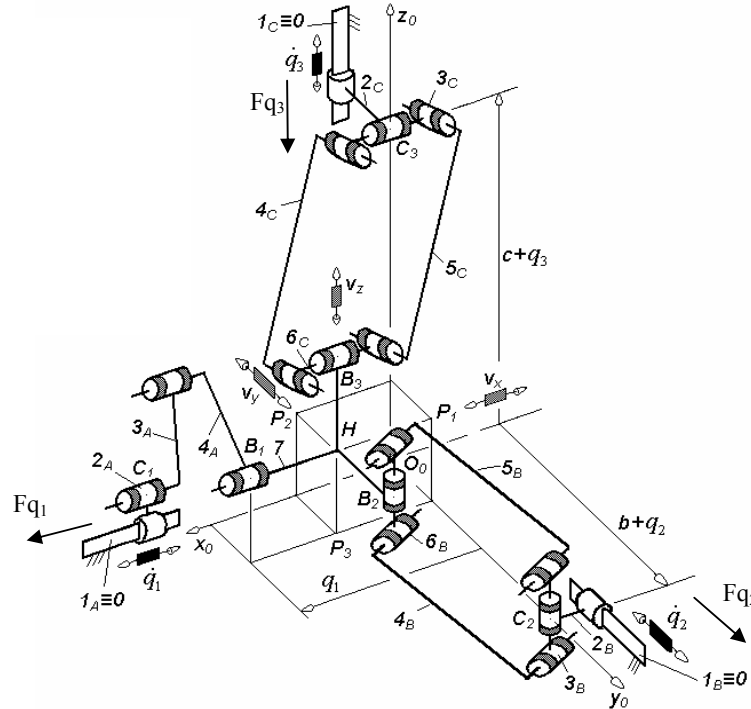

Fig. 1 Kinematic scheme of the parallel robot of 1PRRR+2PRPaR type [9].

This parallel robot is composed by a mobile platform 7 connected to the base by three kinematic chains:

- A: simple open kinematic chain with one active prismatic joint (independent joint parameter q_1) and three passive revolute joints (dependent joint parameters φ_{2a}, φ_{3a} and φ_{4a}) – see Fig. 2,b;
- B and C: complex kinematic chains of parallelogram type with one active prismatic joint (independent joint parameter q_2 and respectively q_3) and six passive revolute joints (dependent joint parameters φ_{2i}, φ_{3i}, $\varphi_{3i'}$, φ_{4i}, $\varphi_{4i'}$, and φ_{5i} – where i = b,c) – Fig. 2,a.
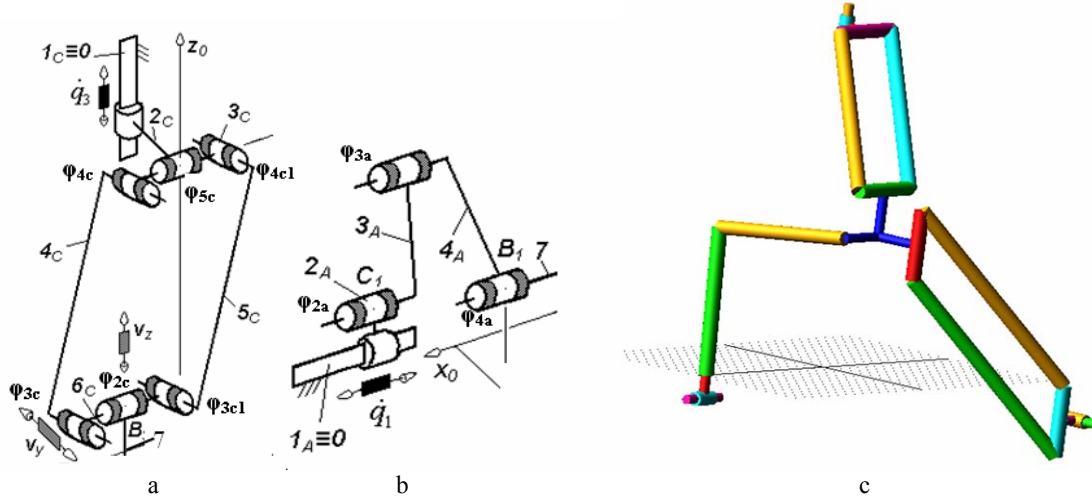
Fig. 2 Parameterization of the 1PRRR+2PRPaR parallel robot (a and b) and its simplified CAD model in ADAMS (c)

Dynamical modeling of 1PRRR+2PRPaR parallel robot in the rigid links hypothesis

Based on rigid links hypothesis, the dynamic modelling has been approached in the assumptions of: a) the gravity vector is oriented in negative sense of the z_0 axis (Fig. 1), and b) no external load on the moving platform 7.

Considering rigid elements with distributed masses (see Fig. 3), the dynamic model can be analytically derived using the Lagrange multipliers method:

$$\sum_{i=1}^{k} \lambda_i \frac{\partial \Gamma_i}{\partial q_j} = \frac{d}{dt}\left(\frac{\partial L}{\partial \dot{q}_j}\right) - \frac{\partial L}{\partial q_j} - \hat{Q}_j \quad , \tag{1}$$

where: λ_i - Lagrange multipliers; q_j - independent joint variables; $\hat{Q}_j$ - generalized external forces;

L - parallel robot Lagrangean: $L = \sum_{i=1}^{n} K_i + \sum_{i=1}^{n} P_i$,

(2)

where: K_i – the kinetic energy of the link i; P_i – the potential energy of the link i.

The Lagrange multipliers (λ_i) are identified introducing the following set of geometric equations derived from the condition of obtaining the same coordinates (x_H, y_H, z_H) of the characteristic point H for each of the arms A, B and C:

$$(\Gamma_i): \begin{cases} Ec_1 = \cos(\varphi_{2a}) \cdot l_{3a} + l_{4a} \cdot \cos(\varphi_{2a} + \varphi_{3a}) - q_2 - \cos(\varphi_{2b}) \cdot \cos(\varphi_{3b}) \cdot l_{4b} + l_{7b} \\ Ec_2 = \sin(\varphi_{2a}) \cdot l_{3a} + l_{4a} \cdot \sin(\varphi_{2a} + \varphi_{3a}) - q_3 - \cos(\varphi_{2c}) \cdot \cos(\varphi_{3c}) \cdot l_{4c} + l_{7c} \\ Ec_3 = \sin(\varphi_{2b}) \cdot \cos(\varphi_{3b}) \cdot l_{4b} - q_1 + l_{7a} \\ Ec_4 = \sin(\varphi_{3b}) \cdot l_{4b} - q_3 - \cos(\varphi_{2c}) \cdot \cos(\varphi_{3c}) \cdot l_{4c} + l_{7c} \\ Ec_5 = \sin(\varphi_{3c}) \cdot l_{4c} - q_1 + l_{7a} \\ Ec_6 = \sin(\varphi_{2c}) \cdot \cos(\varphi_{3c}) \cdot l_{4c} - q_2 - \cos(\varphi_{2b}) \cdot \cos(\varphi_{3b}) \cdot l_{4b} + l_{7b} \end{cases} \tag{3}$$
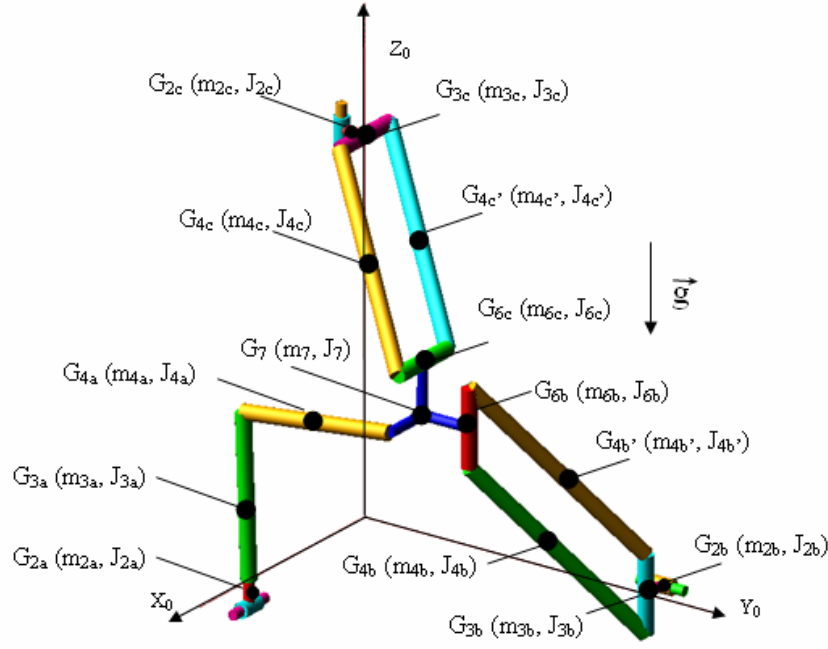
Fig.3 Dynamic scheme of the parallel robot of 1PRRR+2PRPaR type

Finally, the analytical expressions of the driving forces Fq1, Fq2 and Fq3 (see Fig. 1) are obtained using Maple software.

Even the obtained analytical dynamic model is of high complexity, the Lagrange multipliers method can be usefully applied to derive the dynamical model of any 3 DOF parallel robots and can be extended to 4 and more DOF parallel robots.

Numerical simulation of 1PRRR+2PRPaR parallel robot

Numerical simulation of the dynamic analytical model is carried out considering a linear trajectory in the Cartesian space between the point 1(0.5, 0.6, 0.7) and point 2(0.3, 0.8, 0.9), using a fifth degree polynomial movement low (see Fig. 4).

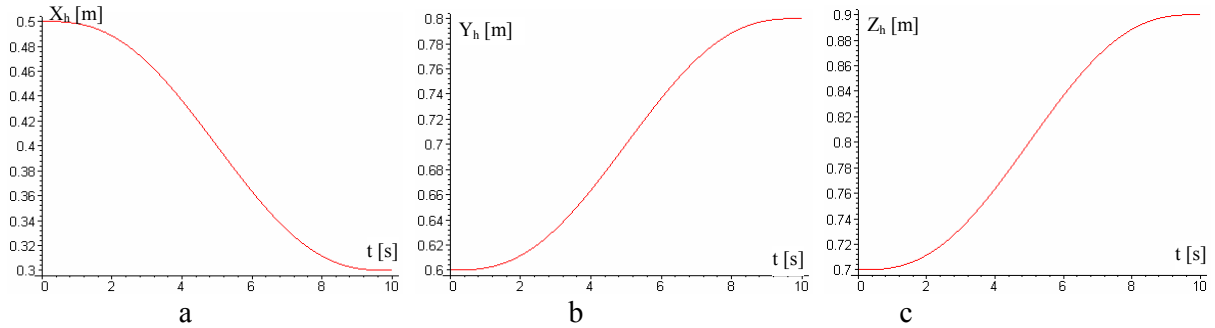a   b   c

Fig. 4 Displacement of the end-effector characteristic point H along X axis (a), Y axis (b) and Z axis (c)

For these imposed movements of the characteristic point H, the relative movement (displacements, velocities and accelerations) in the three active joints were obtained and drawn in Fig. 5. The maximum velocity and acceleration on the desired end-effector trajectory are obtained in driving joint (q_2). To validate the analytical results, numerical simulations are performed in Adams for the same values of the input parameters as used in the Maple simulation; as the same

driving force variations were obtained (see Fig. 6, 7 and 8), it can be conclude that the analytical model was correctly developed.
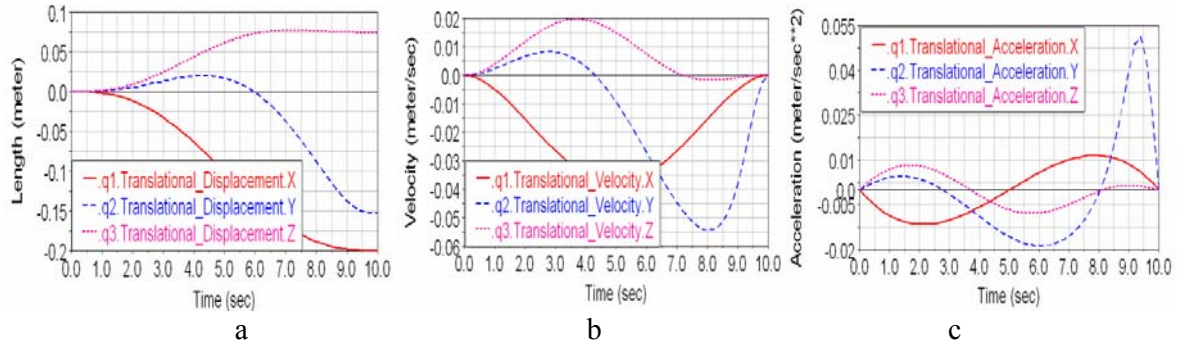

a   b   c

Fig. 5 The relative movement of the active joints: displacements $q_{i,\,i=1..3}$ (a), velocities $\dot{q}_{i,\,i=1..3}$ (b) and accelerations $\ddot{q}_{i,\,i=1..3}$ (c)
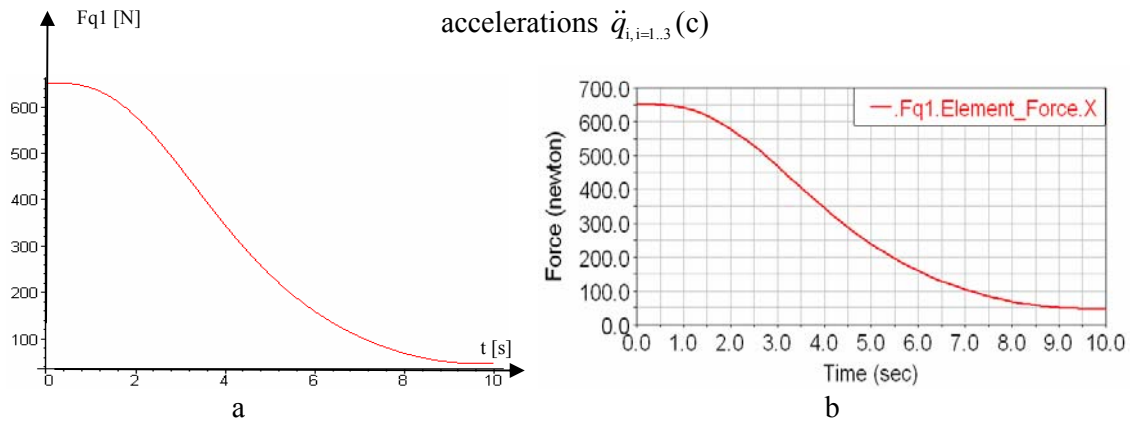

a   b

Fig. 6 The variation of driving force Fq1 in Maple (a) and Adams (b)
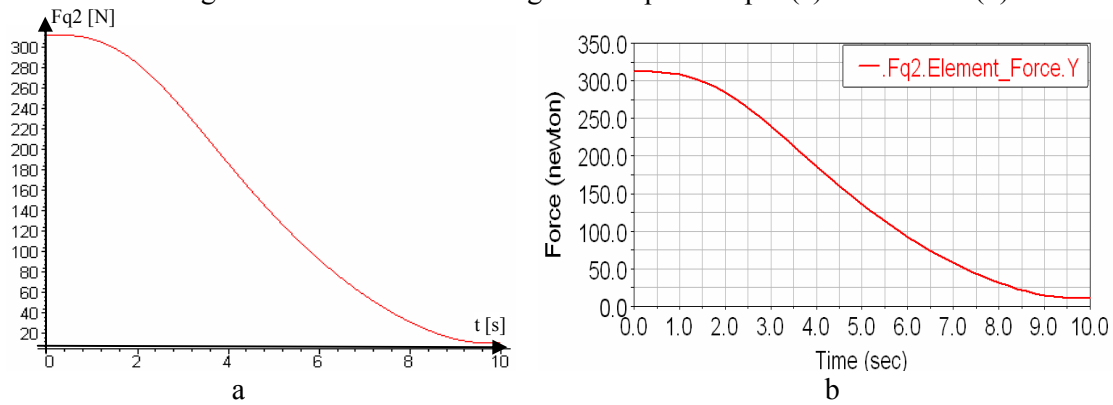

a   b

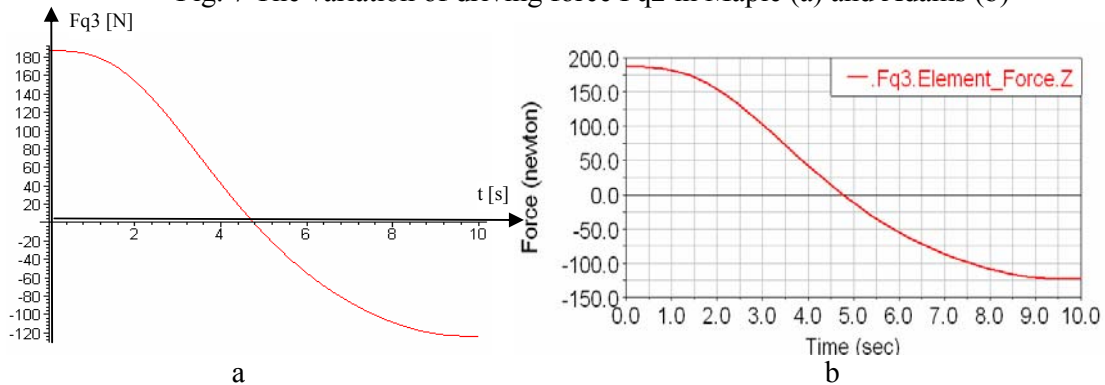Fig. 7 The variation of driving force Fq2 in Maple (a) and Adams (b)

a   b

Fig. 8 The variation of driving force Fq3 in Maple (a) and Adams (b)

Fig. 6-8 highlight that the maximum driving force is achieved in the X linear motor (Fq1) with decoupled motion.

Conclusions

A dynamic modeling of maximally regular parallel robots [2], with application to the coupled topology, has been presented in this paper. The closed-form dynamic model was developed in the rigid link hypothesis using Lagrange with multipliers method. With the obtained analytical dynamic model, a control model can be added to complete the study.

The numerical simulations, performed for the obtained dynamic analytical model and a correspondent CAD model using ADAMS software, highlighted identical robot behavior and thus the closed form dynamic model was validated.

References

[1] Y. Zhao and F. Gao, "Dynamic formulation and performance evaluation of the redundant parallel manipulator", Robotics and Computer-Integrated Manufacturing, Vol. 25, (2009), pp. 770–781.

[2] G. Gogu, Structural synthesis of parallel robots. Part 1: Methodology, Springer Verlag, (2008), pp.282.

[3] Yen, P.-L. and Lai, .C.-C., "Dynamic modeling and control of a 3-DOF Cartesian parallel manipulator", Mechatronics, Vol. 19, (2009), pp. 390–398.

[4] Lu, Y.and Xu, Q., "Dynamic modeling and robust control of a 3-PRC translational parallel kinematic machine", Robotics and Computer-Integrated Manufacturing, Vol. 25, (2009), pp. 630–640.

[5] Khoukhi, A., Baron, L. and Balazinski, M., "Constrained multi-objective trajectory planning of parallel kinematic machines", Robotics and Computer-Integrated Manufacturing, Vol. 25, (2009), pp. 756–769.

[6] Staicu, S., "Inverse dynamics of the 3-PRR planar parallel robot". Robotics and Autonomous Systems, Vol. 57,(2009), pp 556-563.

[7] Y. Zhao and F. Gao, "Dynamic formulation and performance evaluation of the redundant parallel manipulator", Robotics and Computer-Integrated Manufacturing, Vol. 25, 2009, pp. 770–781.

[8]Zhang, D., Bi, Z. and Li, B., "Design and kinetostatic analysis of a new parallel manipulator", Robotics and Computer-Integrated Manufacturing, Vol. 25, 2009, pp 782–791.

[9] Gogu, G., "Evolutionary morphology: a structured approach to inventive engineering design", Invited paper, Proceedings of the 5th International Conference on Integrated Design and Manufacturing in mechanical Engineering, Bath, 5-7 April 2004.

[10] Thanh T.D., Kotlarski J., Heimann B., Ortmaier T., "Dynamics identification of kinematically redundant parallel robots using the direct search method", Mechanism and Machine Theory, Volume 52, June 2012, pp. 277–295.

[11] Gherman B., Pisla D., Vaida C., Plitea N., "Development of inverse dynamic model for a surgical hybrid parallel robot with equivalent lumped masses", Robotics and Computer-Integrated Manufacturing, Volume 28, Issue 3, June 2012, pp. 402–415.

[12] Zhao Y., "Dynamic optimum design of a three translational degrees of freedom parallel robot while considering anisotropic property", Robotics and Computer-Integrated Manufacturing, Volume 29, Issue 4, August 2013, pp. 100–112.

Rigid versus flexible link dynamic analysis of a 3DOF Delta type parallel manipulator

Nadia Ramona CRETESCU[1, a *], Mircea NEAGOE[1,b]

[1]Transilvania University of Brasov, Bd. Eroilor, 29, Romania

[a]ncretescu@unitbv.ro, [b]mneagoe@unitbv.ro

Abstract. This paper presents a comparative kinematic and dynamic analysis of a Delta parallel robot based on numerical simulations of the rigid vs. flexible links robot models. The flexible links numerical models are derived using AutoFlex module of Adams software. Finally, the conclusions regarding the obtained results useful in manipulator constructive design are presented.

Introduction

The Delta parallel robot it's a very studied type of parallel robot in literature, due at the great advantages likes speed, precision and accuracy.

A method to obtained normal and inverse pose solution to Delta parallel robot using ADAMS software is presented in [1].

In [2] a design methodology of a Delta parallel robot it's proposed and developed.

A simplified dynamics modelling of a Delta parallel robot is presented in [3]. The analytical results are verified by the model obtained in ADAMS.

Performance analysis of Delta parallel robot is performed in [4] using criteria like: workspace, manipulability, dexterity, etc.

A modelling taking in consideration flexible links hypothesis is presented in [5], using ANSYS software, taking into account the dynamic forces of inertia, as well as stress analysis along the selected critical trajectory.

This paper deals with a Delta parallel robot of IRB 340 Flexpicker type from ABB [6], designed for high-speed pick and place tasks, able to perform 150 picks per minute, with capability of 1kg payloads.

Kinematic simulation of Delta parallel robot

The IRB340 Delta parallel robot developed by ABB is a 3DOF manipulator with 3 active revolute joints (with basis) and 18 passive joints (12 spherical joints and 6 revolute joints).

This parallel robot have the possibility to achieve a maximum speed of 10m/s and a maximum acceleration of $100m/s^2$ and a cycle time for 1 kg payload of 0.38s.

Starting from Delta parallel robot developed by ABB (Fig.1,a) with technical specification described in [6], a simplified numerical model was obtained using ADAMS software (Fig.1,b).

The principal objective of this paper was to optimize the diameter of the long bars of parallelograms analyzing error positions, speed and acceleration trajectory assuming flexible elements - only these long bars of four-bar kinematic chain of parallelograms, relative to the robot with rigid elements.
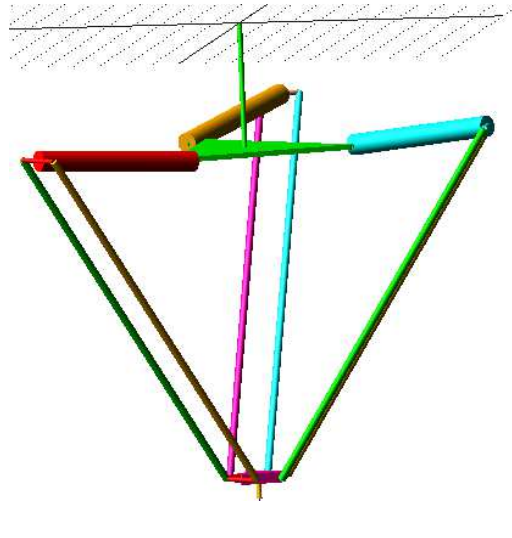
a

b

Fig.1 Delta parallel robot of ABB (a) and its simplified ADAMS model (b)
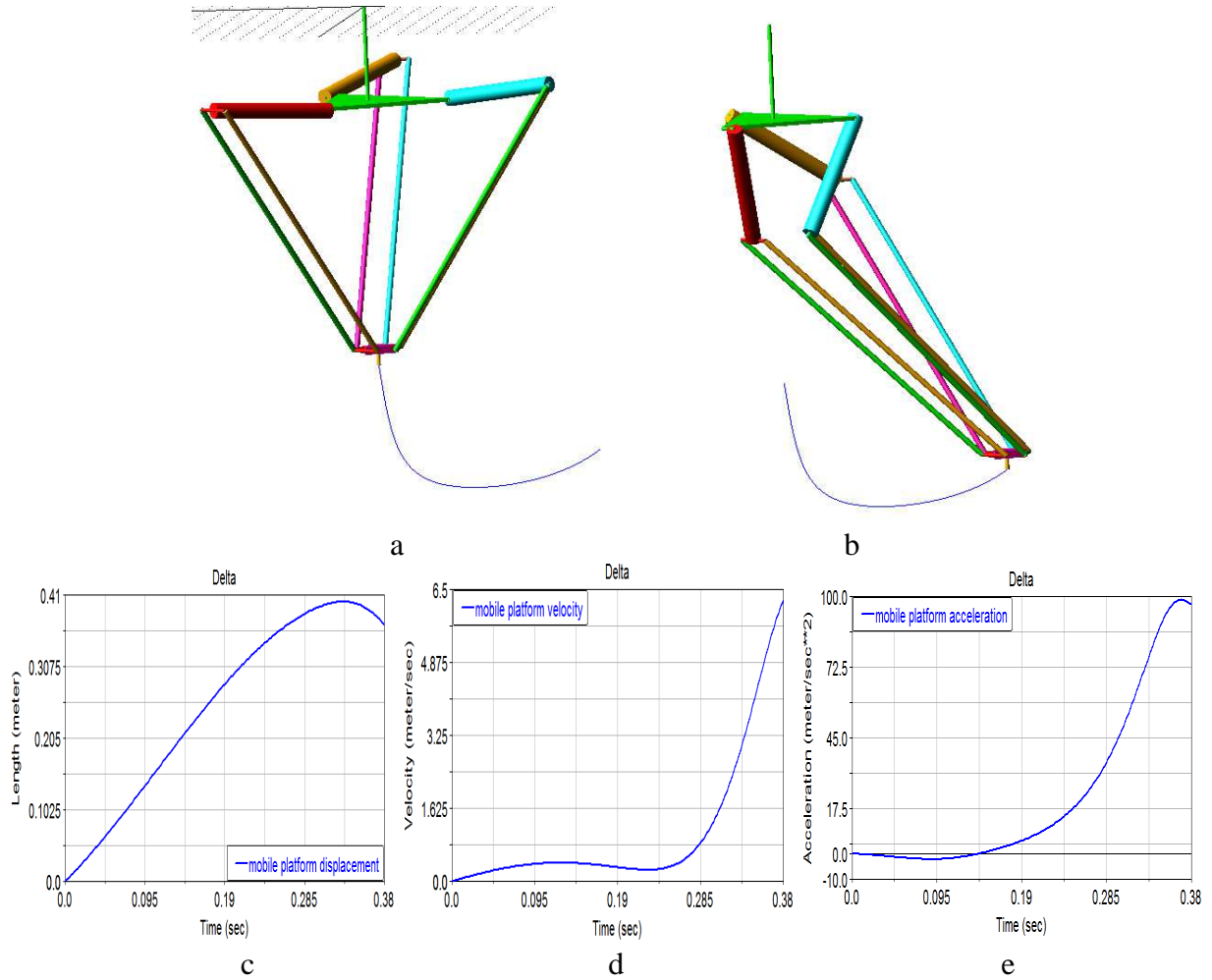

a

b

c

d

e

Fig.2 ADAMS kinematic simulation of rigid link Delta paralelel robot: its configuration on the starting point of the trajectory (a) and on the end point the trajectory (b), time variation of the end-efector relative resultant displacement (c), its trajectory velocity (d) and acceleration (e)

For obtaining the model in flexible links hypothsis, Adams AutoFlex module from Adams software is used (Fig.3.a). In this study, only the 6 long bars of the 3 parallelogram chains are considered as flexible link, due at their higher suppleness.

In analyze of the comportement in flexible links hypothesis of the long bars of the parallelogram, all 12 natural frequencies has taken in consideration (Fig.3.b).
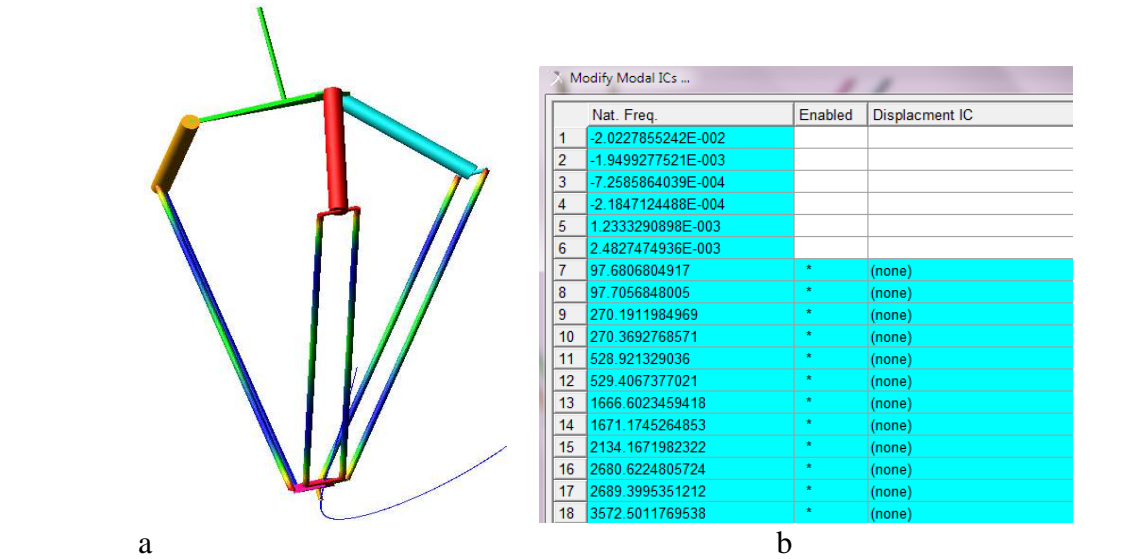
	Nat. Freq.	Enabled	Displacment IC
1	-2.0227855242E-002		
2	-1.9499277521E-003		
3	-7.2585864039E-004		
4	-2.1847124488E-004		
5	1.2333290898E-003		
6	2.4827474936E-003		
7	97.6806804917	*	(none)
8	97.7056848005	*	(none)
9	270.1911984969	*	(none)
10	270.3692768571	*	(none)
11	528.921329036	*	(none)
12	529.4067377021	*	(none)
13	1666.6023459418	*	(none)
14	1671.1745264853	*	(none)
15	2134.1671982322	*	(none)
16	2680.6224805724	*	(none)
17	2689.3995351212	*	(none)
18	3572.5011769538	*	(none)

a   b

Fig.3 Delta parallel robot with flexble links modeled in ADAMS Autoflex (a) and natural frecquencies of the 6 long flexible bars of the paralelogram chains (b)

For the simulation maded in the same condition like rigid links hypotesis, the movements errors it's presented in fig. 4. The displacement errors have a maximum of 0.5mm, a velocity errors until 35mm/s and an acceleration errors until 4.4m/s^2 (Fig. 4).
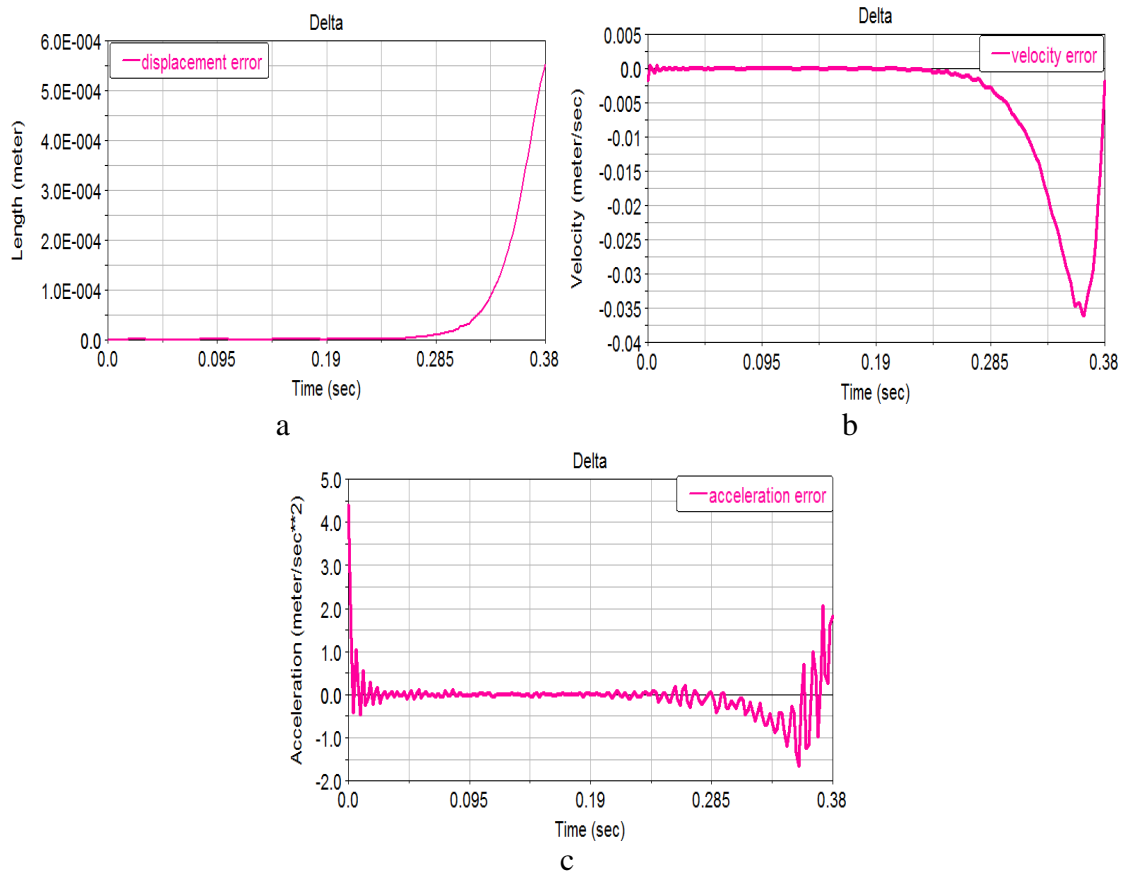
a   b

c

Fig.4 The end-effector movement errors of Delta parallel robot with flexible links on the considered trajectory: displacement errors (a), velocity errors (b) and acceleration errors (c)

The smaller error displacement obtained emphise a good comportment of this parallel robot even in flexible links hypothesis and the diameter of this bars can be the start of optimization procces with decrease of this diameter (0.75*diameter and 0.5*diameter).

The displacement errors are inverse proportional with the bar diameter, until 1.8mm for the smaller diameter, and 0.475mm for the bigger diameter (Fig. 5).
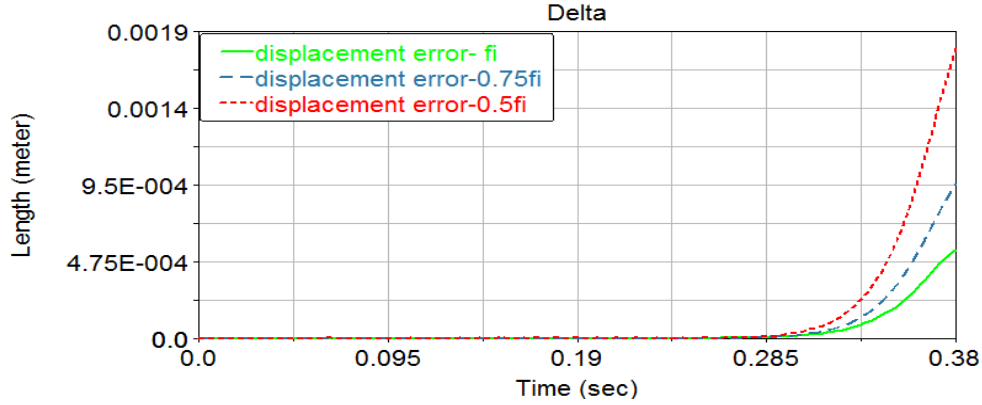

Fig.5 The mobile platform displacement errors of Delta parallel robot for differents diameters of the parallelogram long bars

The velocity errors respects the same rule, it's inverse proportional with the decrease of diameter, until 0.11m/s for the smaller diameter, and 0.010m/s for the bigger diameter (Fig. 6).
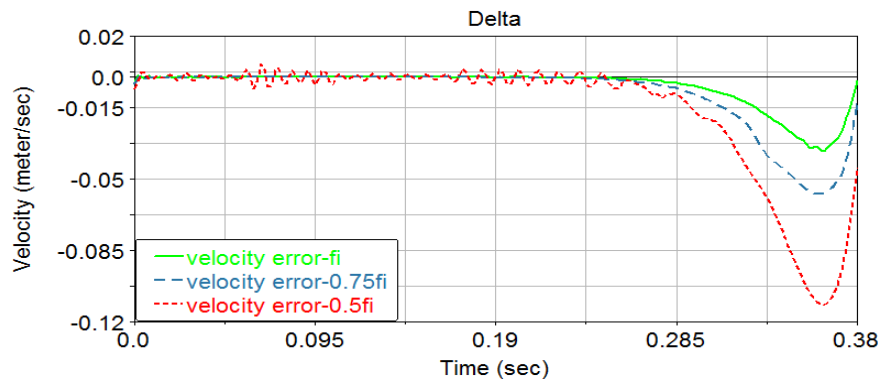

Fig.6 The mobile platform velocity errors of Delta parallel robot for differents diameters of the parallelogram bars

The acceleration errors it's also inverse proportional with the decrease of diameter, from 13m/s^2 for the smaller diameter, and 2m/s^2 for the bigger diameter (Fig. 7).
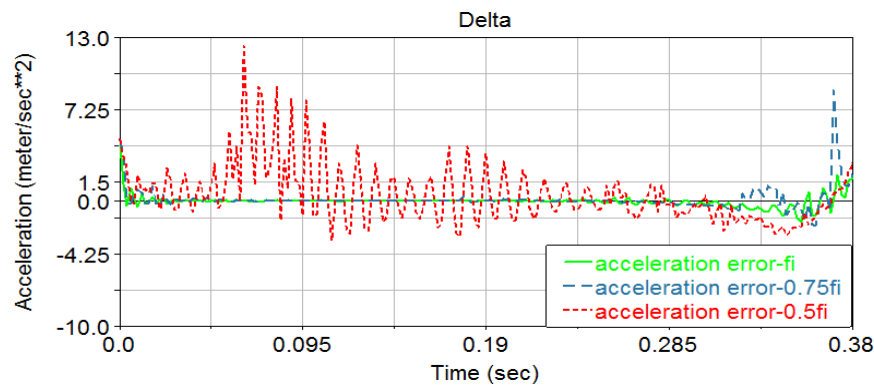

Fig.7 The mobile platform acceleration errors of Delta parallel robot for differents diameters of the parallelogram bars

Dynamical simulation of Delta parallel robot

Regarding the dynamic analyse, [7] presents the analytical dynamic modeling of a parallel robot and numerical simulation using Adams software.

Regarding the torque movements M1, M2 and M3 (Fig. 8), a comparative results it's presented in Fig. 10-12 between the obtained movement in rigid links hypothesis and flexible links hypothesis for this three cases presented (with diameter of 0.014m, and the two cases: 0.75*diameter and 0.5*diameter).
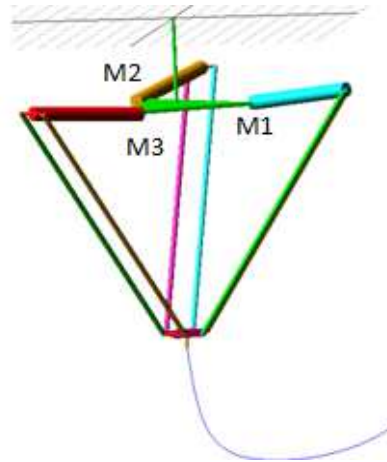

Fig.8 Delta parallel robot with active movements representation

In the results obtained and presented in fig. 9-11, can see difference between the maximal value obtained, due of the total masse of the robot witch decrease with the diameter of the link bars.

From fig. 9-11, it can be remarked that the links natural flexibility directly influences the torque motions. Comparatively with rigid links case, the needed acting torque are decreasing slowly without modifying significantly the motion shape for M1 and M3 torque motion, but with modification of the shape for M2 torque.
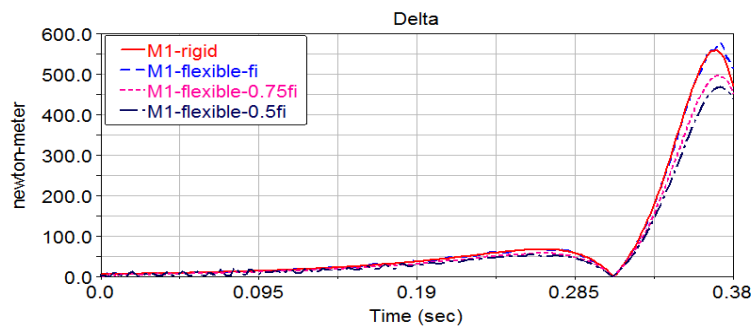

Fig.9 Torque motion M1 of Delta parallel robot in rigid vs flexible links hypothesis
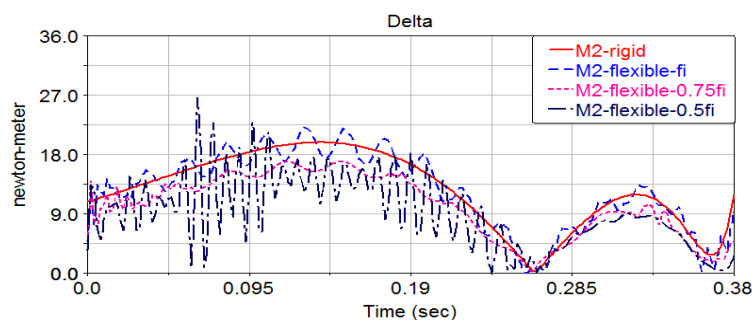

Fig.10 Torque motion M2 of Delta parallel robot in rigid vs flexible links hypothesis
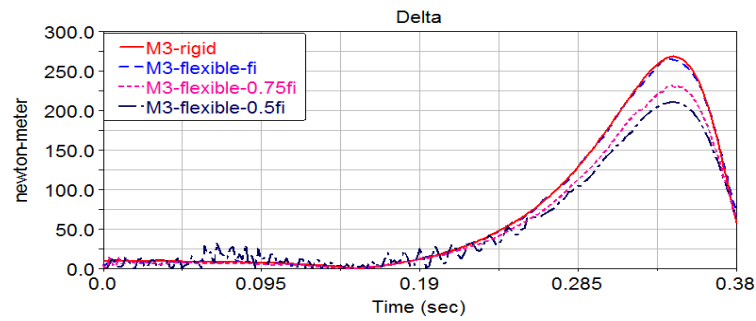
Fig.11 Torque motion M3 of Delta parallel robot in rigid vs flexible links hypothesis

Conclusion

A numerical kinematical and dynamical simulation of a Delta parallel robot with rigid vs. flexible links hypothesis taken in consideration was successfully obtained in this paper.

The purpose of this paper was to see the comportment of the robot for three different diameters of the long bars of the three parallelogram of the robot.

The results obtained from kinematical and dynamical point of view emphases the importance of the diameter bars of movements errors.

In conclusion, the initial value of the diameter of the long bars of this parallel robot it's a good solution to have a good accuracy of this parallel robot.

References

[1] J. Zhang, L. Shi, R. Gao, C. Lian, Method for obtaining direct and inverse pose solution to Delta parallel robot based on ADAMS, International Conference on Mechatronics and Automation (2009), pp. 1332-1336.

[2] L. Angel, J. Bermudez, O. Munoz, Dynamic Optimization and Building of a Parallel Delta-Type Robot, International Conference on Robotics and Biomimetics (2013) , pp.444-449.

[3] S. B. Park ,H. S. Kim, C. Song, K. Kim, Dynamics Modeling of a Delta-type Parallel Robot, ISR (2013).

[4] S.-D. Stan, M. Manic, C. Szep, R. Balan, Performance analysis of 3 DOF Delta parallel robot, HSI (2011), pp. 215-220.

[5] J.D. Rueda, L. Angel, Structural Analysis of a Delta-Type Parallel Industrial Robot Using *Flexible Dynamic* of ANSYS 11.0 Performance analysis of 3 DOF Delta parallel robot, IEEE (2009), pp. 2247-2252.

[6] Infirmation on: http://www04.abb.com/global/seitp/seitp202.nsf/c71c66c1f02e6575c125711f004660e6/d3900b3 c7489746bc12571b700351d6c/$FILE/Data%20Sheet%20IRB%20340HR.pdf

[7] N.R. Rat, M. Neagoe, D. Diaconescu, S.D. Stan, Dynamic analysis of a Triglide parallel robot, The 4th International Conference on Human System Interaction (HSI), (2011), pp. 245-249.

KINEMATIC AND DYNAMIC SIMULATION OF A 3DOF PARALLEL ROBOT

Nadia Ramona CREȚESCU[1]

Abstract: *This paper presents a kinematic and dynamic study of a 3DOF parallel structure of type 1PRRR+2PRPaR, with one decoupled motion and two coupled motions, composed by a mobile platform connected to the fixed base by three kinematic chains. A numerical simulation of the kinematic and dynamic behaviour of this parallel robot in the assumption of rigid links is presented comparatively with an equivalent structure with two flexible links, modelled with ADAMS AutoFlex module. The results show a significant influence of the natural flexibility of links on the effector speed and acceleration, along with large variation of the active forces in the three linear actuators. Thus, the results on the robot behaviour in the flexible links' assumption are useful input data in and control systems.*

Key words: *parallel robot, kinematic, dynamic, simulation, ADAMS software, ADAMS AutoFlex module.*

1. Introduction

In the last years, the parallel robots have been more and more studied and developed from theoretical view point and also for practical applications. The advantages offered by parallel manipulators (PMs) are high stiffness, excellent load-to-weight ratio, positioning accuracy and good dynamic behaviour [8]. The parallel robots are mechanisms with closed kinematic chains, composed by a mobile platform (the end-effector) with n degrees of freedom, connected to the fixed base by two or more kinematic chains called limbs or legs. A simple or a complex kinematic chain can be associated with each limb [3].

A kinematic modelling of a 3DOF parallel robot is detailed in [6] and an analytical model following by numerical simulation is presented in [1].

Regarding the dynamic model of parallel robots, different methods can be applied. Yen and Lai [7] obtained the dynamic equations of a 3DOF translational parallel manipulator using the Lagrange-D'Alembert formulation.

Euler-Lagrange method applied to obtain the dynamic model of a parallel kinematic machine is presented in [4]. Also, a new approach to multi-objective dynamic trajectory planning of parallel kinematic machines (PKM) under task, workspace and manipulator constraints is presented here.

The inverse dynamic model of a 5-DOF hybrid parallel robot is detailed in [2]. The virtual work method based on the dynamically equivalent lumped masses is used.

This paper presents the kinematic and dynamic simulation of a 3DOF parallel

---

[1] Product Design, Mechatronics and Environment Dept., *Transilvania* University of Brașov.

robot of type 1PRRR+2PPPaR based on analytical models presented in [1] and [5] and simplified models with rigid links developed in ADAMS software. In the second part of the paper, the influence of links' flexibility on the robot kinematic and dynamic behaviour is also approached considering a fifth degree polynomial low of movement in motor joints. The comparative numerical simulations on a representative trajectories of this parallel robot in both rigid vs. flexible links assumptions are developed to draw useful recommendations for researchers and practitioners from the robotic field.

2. Description of the 1PRRR+2PRPaR Parallel Robot

The parallel robot of type 1PRRR+ 2PRPaR (1Prismatic, Revolute, Revolute,

Revolute + 2Prismatic, Revolute, Parallelogram, Revolute) has 3 degrees of freedom (DOF) with one decoupled motion along X axis and two coupled motions [3], (Figure 1).

This parallel robot is composed by a mobile platform 7 connected to the base 0 by three kinematic chains (Figure 1):
- one simple open kinematic chain with one active prismatic joint and three passive revolute joints;
- two complex kinematic chains of parallelogram type with one active prismatic joint and six passive revolute joints.

3. Kinematic Simulation

Starting from the kinematical model developed in Maple and presented in [1], a numerical simulation of this model is
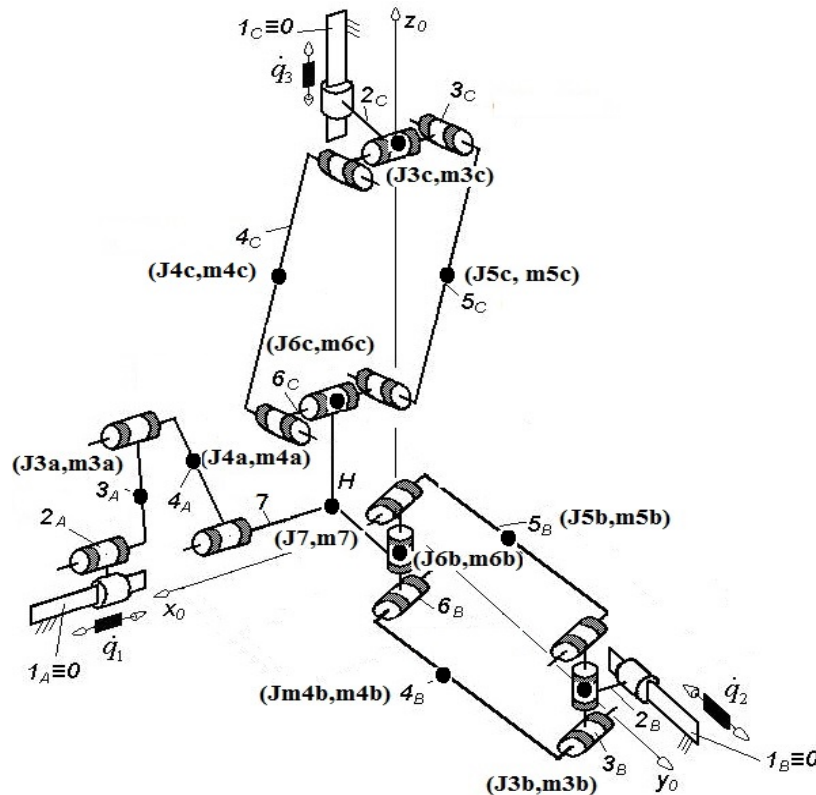

Fig. 1. *Dynamic scheme of the parallel robot of 1PRRR+2PRPaR type*

carried out considering a linear trajectory in the Cartesian space between the point 1 (0.5 m, 0.6 m, 0.7 m), Figure 2a, and point 2 (0.3 m, 0.8 m, 0.9 m), Figure 2b, using a fifth degree polynomial movement low (Figure 3) with the end-effector maximum acceleration reaching 1 m/s^2 while the linear motor 3 develops a maximum acceleration of 5 m/s^2 (Figure 4c).

Starting from desired motion of the end-effector (link 7), Figure 3, the needed motions of the drive motors are determined, Figure 4.

a)

b)

c)
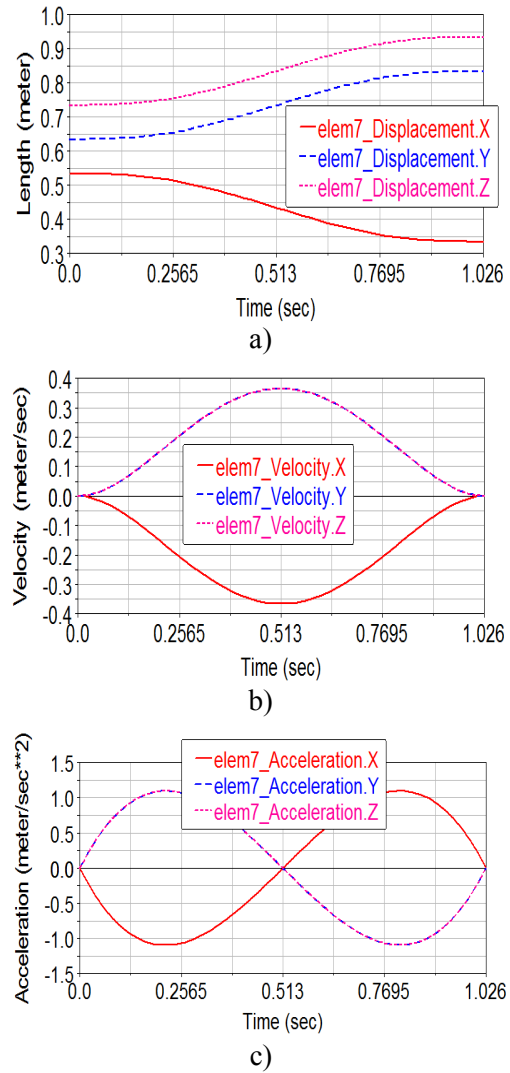
Fig. 3. *The imposed end-effector motion: displacements (a), velocities (b), and accelerations (c)*
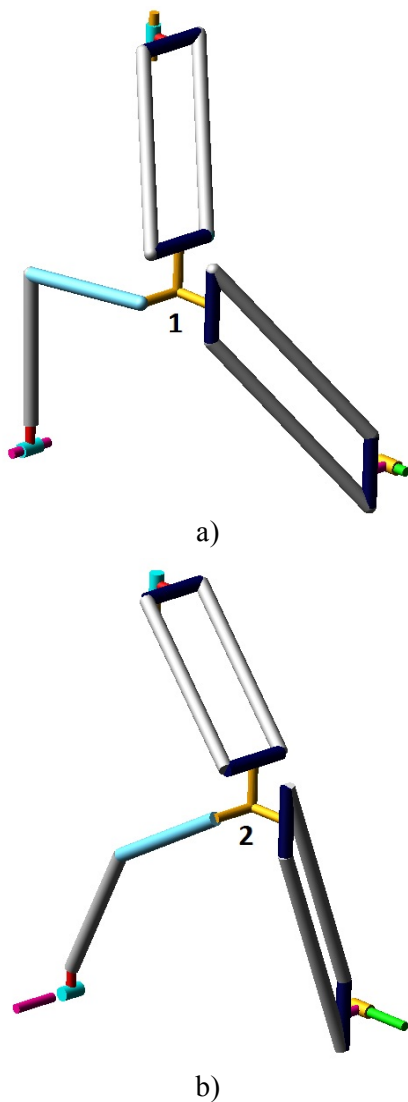

a)

b)

Fig. 2. *ADAMS model of the parallel robot of 1PRRR+2PRPaR type in rigid links hypothesis represented at the beginning (a) and at the end (b) of the trajectory*

4. Dynamical Simulation in the Rigid vs. Flexible Links Hypothesis

Based on the dynamical model developed by applying the Lagrange with multipliers methods in rigid links hypothesis [5], a

numerical simulation has obtained in Maple software considering the input values form Table 1.

a)

b)

c)

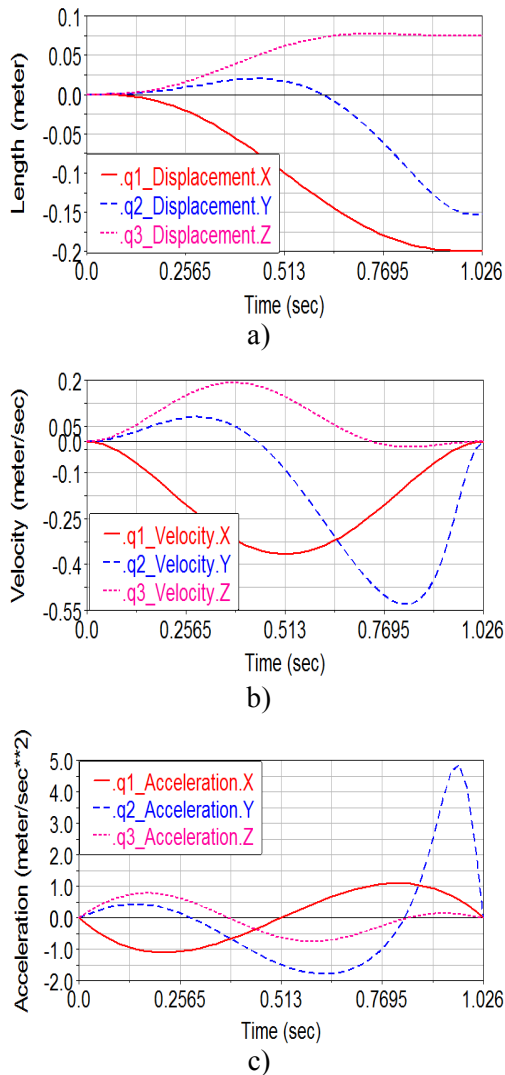Fig. 4. *The motion needed in the linear motor drives : displacements (a), velocities (b), and accelerations (c)*

Also, numerical simulations are done in the Adams software in both rigid and flexible link assumptions. In this study, the natural flexibility of the links 3a and 4a (Figure 1) was only considered.

Starting from the Adams model obtained in rigid links hypothesis (Figure 5a), a new

model with flexible links was derived used ADAMS AutoFlex module. In this way, the influence of flexible links 3a and 4a on the dynamic behaviour of this parallel robot (Figure 5b) was obtained considering only the natural frequency smaller then 2500Hz (Figure 6).

Table 1

Geometric and mass parameters

$l_{3a} = l_{4a}$	0.63 [m]
$l_{3b} = l_{3c}$	0.15 [m]
$l_{4b} = l_{4c}$	0.95[m]
$l_{7a} = l_{7b} = l_{7c}$	0.2 [m]
$m_{3a} = m_{4a}$	9.68 [kg]
$m_{3b} = m_{3c}$	2.32 [kg]
$m_{4b} = m_{5b}$	7.35 [kg]
$m_{4c} = m_{5c}$	7.35 [kg]
$m_{6b} = m_{6c}$	2.32 [kg]

a)   b)
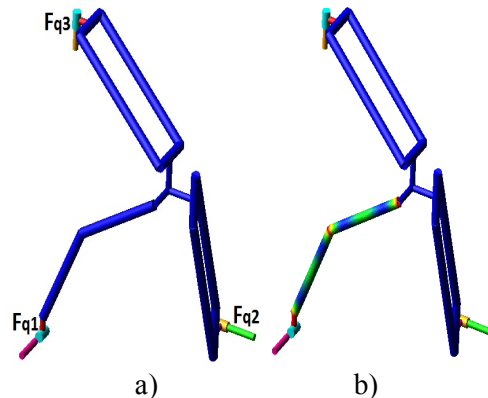
Fig. 5. *The Adams models of robot with: rigid links (a), and flexible links (b)*

Regarding the dynamic behavior of the parallel robot in rigid links hypothesis, the Figure 7 shows that the maximum driving force is achieved in the X linear motor (Fq1) with decoupled motion (more than 700 N).

The parallel robot with flexible links encounters variations of the driving forces with large amplitude and high frequencies in the first part of the trajectory (Figure 7). The maximal value of the driving forces in the flexible robot are about two times

bigger than in the case of the parallel robot with rigid links.

	Nat. Freq.	Enabled	Displacment IC
1	-3.0579658927E-003		
2	-7.3524394299E-004		
3	-5.8411686458E-004		
4	-5.152192861E-004		
5	-1.0098949619E-004		
6	5.4861672295E-004		
7	677.8209817009	*	(none)
8	683.7772146225	*	(none)
9	1832.1215059333	*	(none)
10	1832.5402560479	*	(none)
11	2847.888098881		
12	3465.5283198386		
13	5211.4004721048		
14	6151.9901024597		
15	7671.428160172		
16	1.4176900339E+004		
17	1.4286642396E+004		
18	2.2580234734E+004		

Fig. 6. *Natural frequency of the parallel robot of 1PRRR+2PRPaR type in the flexible links hypothesis*

6. Conclusion

A kinematic and dynamic simulation of maximally regular parallel robots [3], with application to the coupled topology, has been presented in this paper starting from the analytical models detailed in [1] and [5].

The numerical kinematic simulations point out the kinematic behavior of the robot: decoupled motion on the X axis and coupled motions for the other two axis (Y and Z). Also, higher accelerations in the motor drives are needed (up to 5 time bigger in the Y linear motor) to generate a desired end-effector acceleration (e.g. 1 m/s^2).

Dynamic simulations in the rigid links' hypothesis allow to obtain the driving forces developed by the linear motors, where a maximum force of 700 N is developed by the X motor drive.
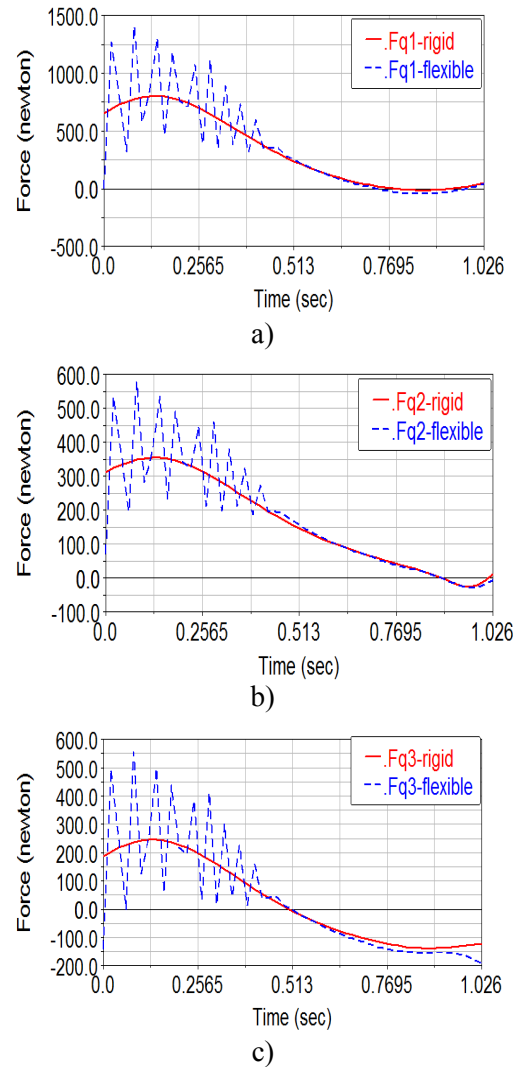

a)

b)

c)

Fig. 7. *The variation of driving force Fq1 (a), Fq2 (b) and Fq3 (c) in rigid (red-continuous line) and flexible (blue-dash line) hypothesis*

When the flexible links assumption is taken into consideration for one arm (arm *a* with the most flexible links, Figure 1) and its natural frequencies up to 2500 Hz, the dynamic results show a major influence of the links' flexibility on the driving force variations.

In conclusion, kinematic and dynamic simulations for a parallel robot using ADAMS software are presented in this

paper, including the study of the influence of the link flexibility.

References

1. Cretescu, N., Neagoe, M., Saulescu, R.: *Kinematic modelling and VR simulation of a 3DOF medical parallel robot with one decoupled motion.* In: Advanced Materials Research **837** (2014), p. 567-572.
2. Gherman, B., Pisla, D., Vaida, C., Plitea, N.: *Development of inverse dynamic model for a surgical hybrid parallel robot with equivalent lumped masses.* In: Robotics and Computer-Integrated Manufacturing **28** (2012) Issue 3, p. 402-415.
3. Gogu, G.: *Structural synthesis of parallel robots. Part 1: Methodology.* Springer Verlag, 2008.
4. Khoukhi, A., Baron, L., Balazinski, M.: *Constrained multi-objective trajectory planning of parallel kinematic machines.* In: Robotics and Computer-Integrated Manufacturing **25** (2009), p. 756-769.
5. Neagoe, M., Cretescu, N., Saulescu, R.: *Dynamic modelling of a 3DOF medical parallel robot with one decoupled motion.* In: Advanced Materials Research **837** (2014), p. 594-599.
6. Stan, S.D., Manic, M., Maties, M., Balan, R.: *Kinematics Analysis, Design, and Control of an Isoglide3 Parallel Robot (IG3PR).* In: IECON08, The 34th Annual Conference of the IEEE Industrial Electronics Society, Nov. 10-13, 2008, Orlando, Florida, p. 2636-2641.
7. Yen, P.-L., Lai, C.-C.: *Dynamic modeling and control of a 3-DOF Cartesian parallel manipulator*, Mechatronics **19** (2009), p. 390-398.
8. Zhao, Y., Gao, F.: *Dynamic formulation and performance evaluation of the redundant parallel manipulator.* In: Robotics and Computer-Integrated Manufacturing **25** (2009), p. 770-781.

Burkhard Corves
Erwin-Christian Lovasz
Mathias Hüsing
Inocentiu Maniu
Corina Gruescu *Editors*

New Advances in Mechanisms, Mechanical Transmissions and Robotics

Proceedings of
The Joint International Conference of the
XII International Conference on Mechanisms
and Mechanical Transmissions (MTM) and the
XXIII International Conference on Robotics
(Robotics '16)

Springer

Burkhard Corves · Erwin-Christian Lovasz · Mathias Hüsing · Inocentiu Maniu · Corina Gruescu
Editors

New Advances in Mechanisms, Mechanical Transmissions and Robotics

Proceedings of The Joint International Conference of the XII International Conference on Mechanisms and Mechanical Transmissions (MTM) and the XXIII International Conference on Robotics (Robotics '16)

This volume presents the proceedings of the Joint International Conference of the XII International Conference on Mechanisms and Mechanical Transmissions (MTM) and the XXIII International Conference on Robotics (Robotics '16), that was held in Aachen, Germany, October 26th–27th, 2016. It contains applications of mechanisms and transmissions in several modern technical fields such as mechatronics, biomechanics, machines, micromachines, robotics and apparatus. In connection with these fields, the work combines the theoretical results with experimental testing. The book presents reviewed papers developed by researchers specialized in mechanisms analysis and synthesis, dynamics of mechanisms and machines, mechanical transmissions, biomechanics, precision mechanics, mechatronics, micromechanisms and microactuators, computational and experimental methods, CAD in mechanism and machine design, mechanical design of robot architecture, parallel robots, mobile robots, micro and nano robots, sensors and actuators in robotics, intelligent control systems, biomedical engineering, teleoperation, haptics, and virtual reality.

Engineering

▶ springer.com

Burkhard Corves · Erwin-Christian Lovasz
Mathias Hüsing · Inocentiu Maniu
Corina Gruescu
Editors

New Advances in Mechanisms, Mechanical Transmissions and Robotics

Proceedings of The Joint International Conference of the XII International Conference on Mechanisms and Mechanical Transmissions (MTM) and the XXIII International Conference on Robotics (Robotics '16)

Editors
Burkhard Corves
RWTH Aachen University
Aachen
Germany

Erwin-Christian Lovasz
University Politehnica of Timisoara
Timişoara
Romania

Mathias Hüsing
RWTH Aachen University
Aachen
Germany

Inocentiu Maniu
University Politehnica of Timisoara
Timişoara
Romania

Corina Gruescu
University Politehnica of Timisoara
Timişoara
Romania

Kinematic and Dynamic Analysis of a 4DOF Parallel Robot with Flexible Links

N. Cretescu, M. Neagoe and R. Saulescu

Abstract The paper deals with the dynamic behaviour of a 4DOF parallel robot with decoupled motions, three orthogonal translations and one rotation, in a comparative approach of flexible versus rigid links, and also the influence of friction in the four active prismatic joints. The ADAMS software and its AUTOFLEX module were used to model the parallel robot and further to identify the end-effector motion errors on a representative trajectory, due to the natural flexibility of the robot links, and the variation of the actuating forces needed in the input joints with both links flexibility and active joints friction. The obtained numerical results show significant resultant errors of the end-effector from the planned trajectory, generated by link elastic deformations, and important errors of actuating forces (up to 300 %) in the assumption of both link flexibility and active joint friction. The results are useful for robot designers to optimally select the actuators and appropriate design the control system to ensure trajectory high accuracy on the robot workspace.

Keywords Parallel robot · ADAMS modelling · AUTOFLEX module · Flexible link · Friction · Analysis

1 Introduction

The parallel robots are closed kinematic chain type mechanisms, composed by a mobile platform (the end-effector) connected to the fixed base by two or more kinematic chains called limbs or legs [4]. Comparing with serial manipulators, parallel robots have the advantages of higher speeds and precision, higher loads and

N. Cretescu (✉) · M. Neagoe (✉) · R. Saulescu
RESREC Research Centre, Transilvania University of Brasov, Brasov, Romania
e-mail: ncretescu@unitbv.ro

M. Neagoe
e-mail: mneagoe@unitbv.ro

R. Saulescu
e-mail: rsaulescu@unitbv.ro

thinness of links. As consequence, the link flexibility under heavy operational conditions can be an important factor influencing significantly the end-effector trajectory accuracy and the driving forces/torques in active joints. Furthermore, friction forces in robot joints influence directly the driving generalised forces and implicitly the design of the actuating system by appropriate choice of actuators.

The link flexibility was approached in many works [1, 2, 5–10], using different modelling methods aiming especially to develop dynamic models and to study the robot mechanism behaviour in the assumption of elastic deformations of robot links. A dynamic finite element analysis of a planar fully parallel robot with flexible links is developed in [9]. By formulating and solving a set of linear ordinary differential equations of motion, the influence of mechanism configurations at high speed motions on the elastic vibrations was highlighted. A numerical kinematical and dynamical modelling in rigid and flexible links hypothesis was presented in [1, 2], using a simplified CAD model developed in ADAMS software and analysed as flexible link system in ADAMS AutoFlex module.

The dynamic behaviour a flexible space robot with joint friction was analysed in [6] by developing the dynamic equations using Jourdain's velocity variation principle and the single direction recursive construction method, concluding that the Coulomb friction model is limited in describing the nonlinear features of friction. Furthermore, an active controller of a flexible space robot considering joint friction was designed, studied and validated using ADAMS software [5]. A review of the main principal methods used in literature for kinematical and dynamical analysis of flexible mechanical systems is presented in [10].

The paper aims at presenting representative results on the influence of the link flexibility and active joint friction on the dynamic behaviour of parallel robots, based on a case study of the 4DOF Isoglide4 manipulator [3] by approaching the robot modelling in ADAMS software and ADAMS Autoflex module to highlight their effect on the end-effector motion accuracy and the driving forces.

2   Problem Formulation

The paper deals with the modelling and simulation of the Isoglide4 parallel robot with decoupled motions [3], Fig. 1, in the assumption of flexible links 3a, b, c, d and 4a, b, c, d and considering friction in the four prismatic active joints q1...q4.

This parallel robot (Fig. 1) is composed by four arms (a, b, c and d), containing each 3 revolute joints with parallel axes, and connected to the end-effector 6 through revolute joints. And additional load 6' is added in the centre of mass (cm) of the mobile platform 6. The end-effector has three decoupled translational motions (along X, Y and Z axis) and one coupled rotational motion (on Y axis) obtained through differential motion of the two vertical linear drivers. This robot is included in a parallel mechanism family proposed in literature [4] as parallel tool machine, raising multiple issues on the link flexibilities and joint frictions.

Fig. 1 Kinematical scheme
of the Isoglide4 parallel robot
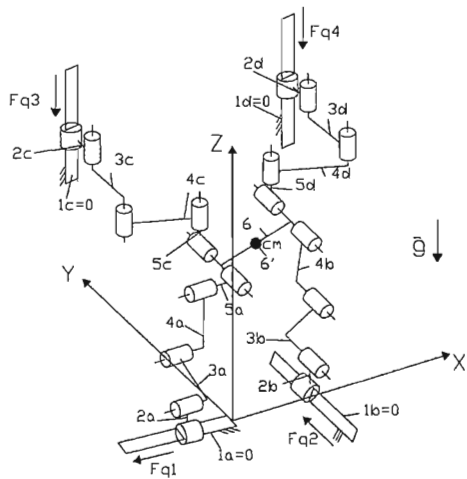
This study is based on the CAD model developed in the ADAMS software considering the following assumptions:

- the robot links are modelled using simple shape steel bodies: cylinders and parallelepipeds, with physical properties systematized in Table 1. The masses of links 5a, c, d are not significant and thus neglected;
- the gravity acts in the negative sense of the Z axis;
- a supplementary mass 6′ of 10 kg is used as robot load;
- using ADAMS AutoFlex module, the links 3 and 4 of each arm are transformed into flexible links; their natural frequencies up to 1000 Hz are considered in simulations;
- the open loop control is applied in the parallel robot simulations;

Table 1 Geometric and mass parameters (according to Fig. 1)

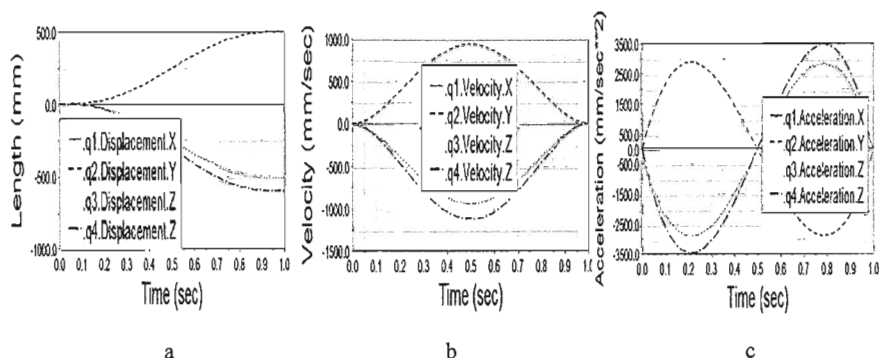| Lengths		Masses	
$l_{2a} = l_{2b} = l_{2c} = l_{2d}$	130 mm	$m_{2a} = m_{2b} = m_{2c} = m_{2d}$	17.10 kg
l_{3a}	677 mm	m_{3a}	26.90 kg
l_{3b}	711 mm	m_{3b}	28.65 kg
l_{3c}	752 mm	m_{3c}	22.81 kg
l_{3d}	638 mm	m_{3d}	23.58 kg
l_{4a}	792 mm	m_{4a}	31.98 kg
l_{4b}	698 mm	m_{4b}	27.99 kg
l_{4c}	630 mm	m_{4c}	28.99 kg
l_{4d}	702 mm	m_{4d}	28.97 kg
l_6	300 mm	m_6	17.00 kg
l_5	120 mm	m_5	0 kg

Fig. 2 Motion generated in the active joints q1, q2, q3 and q4: **a** displacement, **b** velocity, **c** acceleration

- the numerical simulations are carried out considering a representative linear trajectory in the Cartesian space between two points, using a fifth degree polynomial movement low in each active joint (Fig. 2, q1 and q3 have identical motion lows), which allow the end-effector maximum acceleration reaching 5.5 m/s^2, while the linear actuators develop a maximum acceleration of 3.5 m/s^2 and a maximum velocity of ~1 m/s; the strokes of the driving motions along the X (q1), Y (q2) and respectively Z (q3) axis are each of 500 mm and the coupled rotational motion along Y axis is done by the difference between the motions q3 and q4 (the q4 stroke equals 600 mm;
- the coefficient of friction in active joints are 0.016 (static) and 0.01 (dynamic).

Starting from these data, a comparative analysis on the kinematic and dynamic behaviour of the Isoglide4 parallel robot with flexible vs. rigid links, in both assumptions of considering and neglecting the friction in the active joints, is performed in the next chapters. The motion errors on a planned trajectory, due to the link flexibility, are investigated; the influence of friction and link flexibility on the driving forces is also approached in the paper.

3 Effects of Links Flexibility on Robot Behaviour

Based on the CAD simplified rigid link model developed in the ADAMS software (Fig. 3a), the flexible link robot model (Fig. 3b) is obtained using ADAMS AutoFlex module.

The links elasticity influence on the robot kinematic behaviour is highlighted in Fig. 4 by drawing the time variation of the resultant motion (displacement— Fig. 4a, velocity—Fig. 4b and acceleration—Fig. 4c) of the mobile platform mass centre (cm, Fig. 1) in relation to the ideal trajectory achieved by the robot with rigid links. The results show that the elasticity has a significant impact on the end-effector
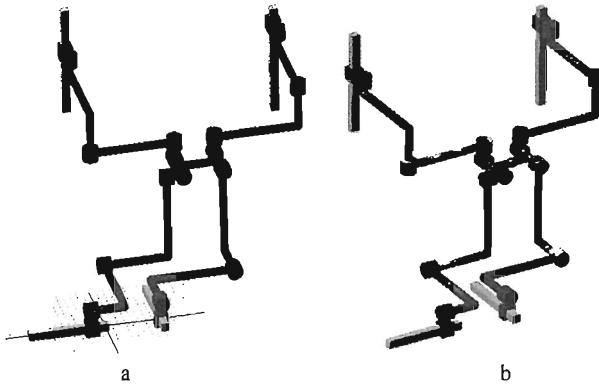
Fig. 3 ADAMS model of parallel robot in the initial position on the selected trajectory: **a** rigid links model and **b** flexible links model

motion, causing an oscillating evolution of the kinematic parameters relative to the planned trajectory and hence significant displacement, velocity and acceleration errors. Thus, for the considered trajectory (Fig. 2) the maximum resultant displacement error reaching worth ~45 mm is recorded at the trajectory ends (Fig. 4a) due to inertial effect. The maximum resultant errors of the velocity on the trajectory reach values up to 15 mm/s (Fig. 4b), and the resultant acceleration records errors up to 7500 mm/s^2 (Fig. 4c), i.e. acceleration maximum relative errors of ~125 %. Larger errors are registered for the angular motion of the mobile platform, e.g. velocity relative errors up to 175 % (Fig. 4d).

Fig. 4 End-effector motion magnitude (the length of the resultant vector) on the planned trajectory, in rigid (*red—continuous line*) and flexible link hypothesis (*blue—dashed line*): **a** the resulting displacements, **b** the resulting linear velocities, **c** the resulting linear accelerations, **d** the angular velocities

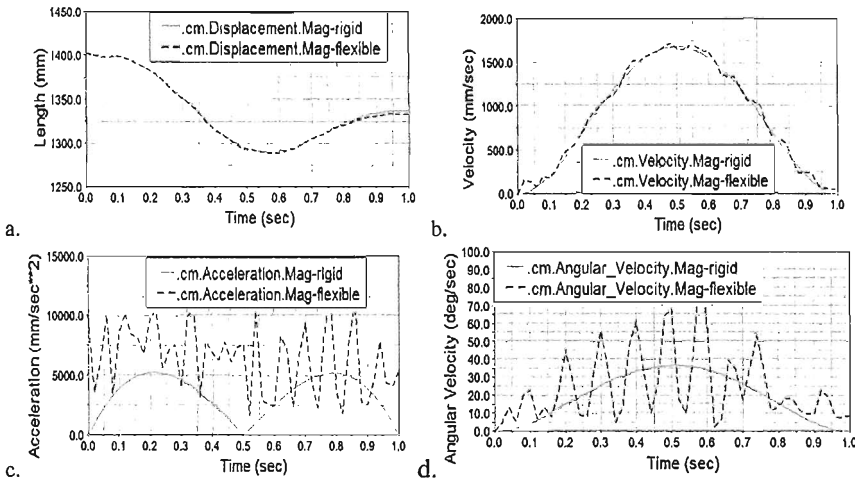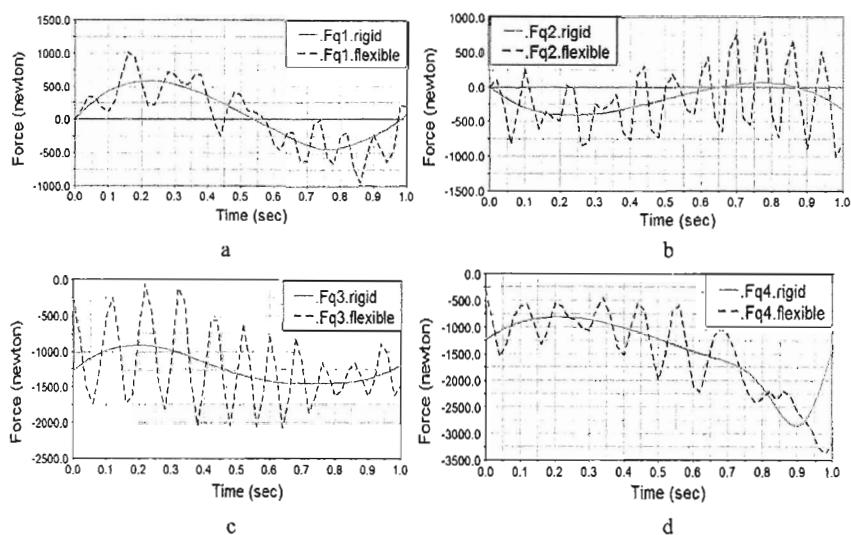**Fig. 5** Driving forces needed in the active joints: **a** q1, **b** q2, **c** q3 and **d** q4, in rigid links hypothesis (*red—continuous line*) and flexible links hypothesis (*blue—dashed line*) (color figure online)

The links elasticity influence on the robot dynamic behaviour is determined by analyzing the evolution of the axial forces in the active joints (q1...q4) and their errors in relation to the ideal case of rigid links. The obtained results (Fig. 5) show a relatively high frequency oscillatory regime of active forces, with negative impact on the robot operation due to the additional rapid varying loads on the linear actuators. It can be remarked that all four actuators are affected by the links elasticity effects to a similar extent, the driving force relative errors registering maximum values of approximately 100 % (Fig. 5).

4 Influence of Friction on Driving Forces

The joint friction influences the robot dynamic behaviour in both assumptions of rigid and flexible links, having a major impact on the driving forces in the active joint, as Fig. 6 shows. The normal forces in the active prismatic joints, transmitted to the base link, generate additional resistant friction forces for the linear actuators and thus changing the magnitude of the driving forces. In the case of rigid links robot, the driving forces with friction are registering significant absolute errors in relation with the ideal joints assumption for the active joints q1 (up to 475 N, Fig. 6a, b) and q2 (up to 700 N, Fig. 6c, d), and friction has less influence on the other two vertical actuators (Fig. 6e–h).

The links flexibility increases in some extent the impact of friction forces on the driving forces, but keep the same frequency profile of active forces variation
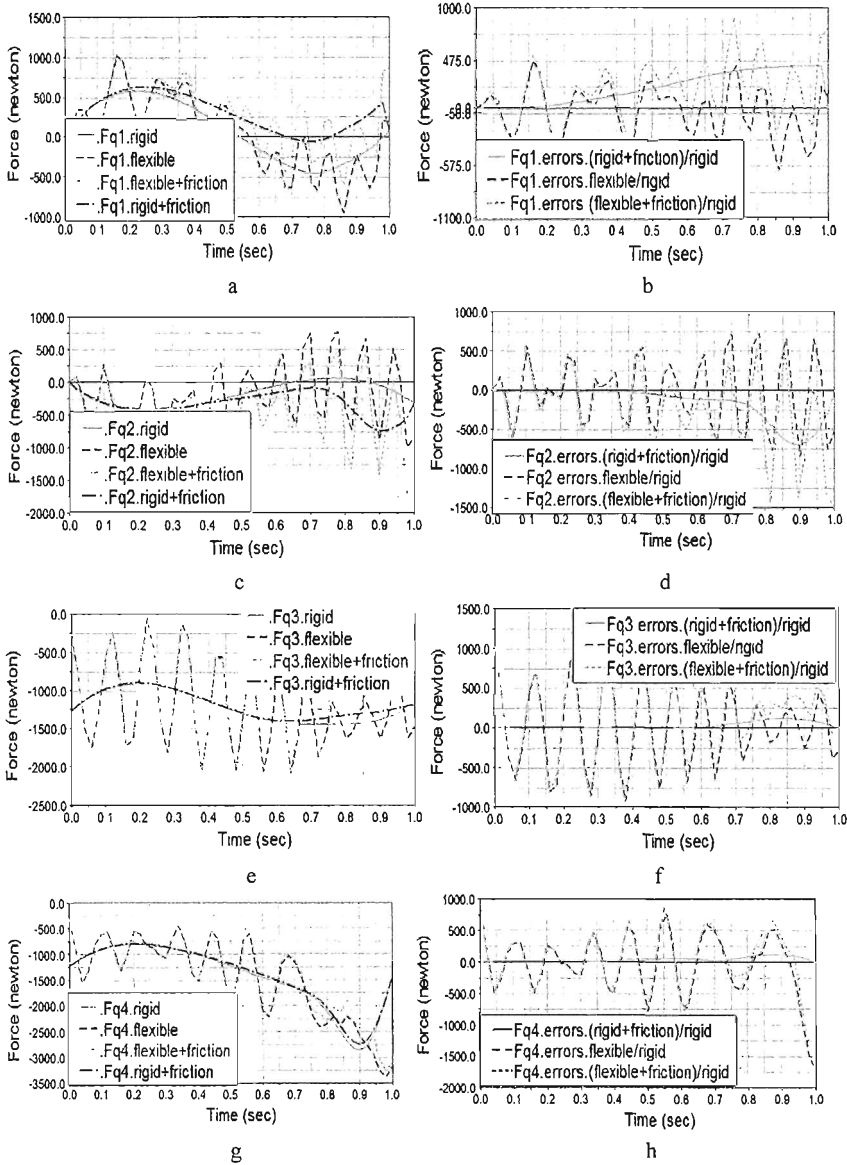
Fig. 6 **a, c, e, g** Driving forces: *red*—rigid link hypothesis, *blue*—flexible link hypothesis, *dark blue*—rigid link hypothesis with friction in active prismatic joints, *pink*—flexible link hypothesis with friction in active prismatic joints; **b, d, f, h** absolute errors of active forces, relative to the rigid links case: *green*—rigid links and joint friction, *blue*—flexible links, *red*—flexible links and joint friction (color figure online)

comparing with the no friction assumption. Comparing with the rigid link robot without friction, it can be highlighted that the driving forces are doubled when only the elasticity is considered and are tripled if the joint friction occurs, mainly for the active joints q1 (Fig. 6a) and q2 (Fig. 6c).

5 Conclusions

This comparative study of the Isoglide4 parallel robot with flexible links and friction in the four active prismatic joints in relation with its ideal variant (rigid link and no friction assumption), allows us to draw the following conclusions:

- the link flexibility has a significant influence on the robot trajectory accuracy, large variations of the end-effector displacements, velocities and especially accelerations can occur from the planned motion trajectory;
- the link flexibility has an important influence on the time variation of driving forces, increasing both the forces magnitude and frequency;
- the joint friction generates relevant additional resistance forces and thus increases the driving forces.

According to the presented results and conclusions, the designers of parallel robots should develop deep knowledge on the kinematic and dynamic behaviour of the robot with flexible links and joint friction in order to identify the best solutions for a high accuracy operation and appropriate selection of the actuators according to the real power and force requirements. Also, a future work will aim at comparing the simulation results with real robot measurements.

References

1. Cretescu, N.R.: Kinematic and Dynamic Simulation of a 3DOF Parallel Robot. Bulletin of the Transilvania University of Brasov, vol. 8 (57) No. 1, Series I—Engineering Sciences, ISSN 2065-2119 (Print), ISSN 2065-2127 (CD-ROM), pp. 73–78 (2015)
2. Cretescu, N., Neagoe, M.: Rigid versus flexible link dynamic analysis of a 3DOF Delta type parallel manipulator. Appl. Mech. Mater. **762**, 101–106 (2015). Trans Tech Publications, Switzerland, ISBN: 978-3-03835-444-4. http://www.scientific.net
3. Gogu, G.: Mobility criterion and overconstraints of parallel manipulator. In: Proceeding of CK005 (2005)
4. Gogu G.: Structural synthesis of parallel robots. Part 1: Methodology. Springer (2008)
5. Liu, X.-F., Li, H.-Q., Chen, Y.-J., Cai, G.-P.: Dynamics and control of space robot considering joint friction. Acta Astronaut. **111**, 1–18 (2015)
6. Liu, X.-F., Li, H., Wang, J., Cai, G.: Dynamics analysis of flexible space robot with joint friction. Aerosp. Sci. Technol. 164–176 (2015)
7. Lovasz, E.-C., Perju, D., Modler, K.-H., Modler, M., Gruescu, C.M., Maniu, I., Comşa, A.: On the structural analysis of the mechanisms with elastic connections. In: The 11th IFToMM International Symposium on Science of Mechanisms and Machines, Springer Series Mechanisms and Machine Science, vol. 18, pp. 59–67 (2014)

8. Modler, N., Modler, K.-H., Hufenbach, W., Lovasz, E.-C., Perju, D., Margineanu, D.: A design of compliant mechanism with integrated actuators. In: 10th International Symposium on Science of Mechanisms and Machines SYROM, Brasov, pp. 655–664 (2010)
9. Piras, G., Cleghorn, W.L., Mills, J.K.: Dynamic finite-element analysis of a planar high-speed, high-precision parallel manipulator with flexible links. Mech. Mach. Theory **40**(7), 849–862 (2005)
10. Shabana, A.: Flexible multibody dynamics review of past and recent development. Multibody Sys. Dyn. **1**, 189–222 (1997)

Dynamic modelling of an Isoglide T3 type parallel robot

Nadia Cretescu[1] and Mircea Neagoe[1]

[1] Renewable Energy Systems and Recycling R&D Center, Transilvania University of Brasov, Romania

ncretescu@unitbv.ro, mneagoe@unitbv.ro

Abstract. The dynamic modelling of parallel robots rise difficult development issues due to the structural, kinematic and dynamic complexity of parallel mechanisms. The paper presents the application of a dynamic approach aiming at reducing the modelling complexity by replacing the parallel robotic structure with simpler open kinematic chains derived from the parallel structure. This method was successfully applied to obtain the closed-form dynamic model of an Isoglide T3 parallel robot and it was validated by numerical simulations using the ADAMS software.

Keywords: Parallel robots, dynamic modelling, closed-form dynamic model, simulation, ADAMS software.

1   Introduction

The parallel robots are closed kinematic chain type mechanisms, composed by a mobile platform connected to the base by two or more kinematic arms (legs or limbs). For each arm a simple open or a complex kinematic chain can be associated [1].

The parallel robots have the advantages of higher speeds and precision, higher loads and stiffness comparing with serial manipulators. The most important drawback is related their reduced workspace.

Different approaches can be applied to obtain the dynamic model of parallel robots, e.g. Euler-Lagrange method, Lagrange equations with multipliers, Newton-Euler method, were applied in literature aiming at identifying their dynamic behaviour [2-7]. A dynamic modelling method for hybrid robotic structures is presented in [8]. The direct and inverse dynamic models of the robotic arms and the mobile platform were obtained by using the Newton Euler equations, where Jacobian matrices are also involved.

The influence of the load-rigidity correlation on the dynamic response of a medical Triglide parallel robot was identified using ADAMS simulations in the hypothesis of rigid and elastic connecting rods [9]. The same approach was applied for a 4 DOF parallel robot of type T3R1with decoupled motions [10]. The Lagrange with multipliers method was used in [11] to obtain the analytical dynamic models of two parallel robots with two and three degrees of coupling, respectively, followed by a virtual simulation in SimMechanics environment.

The Lagrange equations of second kind is used in this paper to derive the closed-form dynamic model of an Isoglide T3 parallel robot, considering the rigid link hypothesis, based on an approach presented by Ibrahim [12]. The structural and kinematic analysis is presented in Section 3, followed by the analytical dynamic modelling of the three open arms and the end-effector platform and the projection of the dynamic equations in the space of active joints (Section 4), developed using the Maple software. The close-form dynamic model is numerically simulated and validated in the ADAMS environment software (Section 5). The conclusions of the study are drawn in the section 6.

2   Problem formulation

The dynamic modelling of parallel type robotic structures, used in this paper, is based on an algorithm proposed by Ibrahim [12] and composed of the following steps:
1) breaking the kinematic joints between the mobile platform (end-effector) and the component robotic arms;
2) inverse dynamic modelling of each open robotic arm with serial kinematic chain configuration, considering the joint variables as independent generalized coordinates;
3) inverse dynamic modelling of the end-effector platform based on the operational variables associated to the parallel robot, considering known the end-effector motion;
4) projection of the dynamic equations obtained for the open robotic arms and the mobile platform into the space of the independent joint variables (in the active joints) of the parallel robot through Jacobian matrices.
The dynamic modelling of the robot arms, considered after removing their connections with the end-effector platform, can be done using known approaches applied to serial robots, such as the Newton-Euler method or Lagrange equations of the second kind.
The inverse dynamic model of the end-effector platform can be described through the Newton-Euler equations, which allow to obtain the forces and moments applied on a rigid body with known motion.
The inverse dynamic modelling algorithm of each robotic arm, isolated from the parallel robot, has the following steps:
- establishing the kinetic energy of the component kinematic links;
- establishing the potential energy of the component kinematic links;
- expressing the Lagrangian of the robotic arm;
- deriving the inverse dynamic equations for each arm.
The generalized forces (forces and torques) resulting in the inverse dynamic models of the end-effector platform and the robotic arms, considered independently, are reduced in the space of active joints and thus the actuating generalized forces are obtained by applying the superposition principle.

3 Geometric and Kinematic Modelling

The Isoglide T3 robot has a three degrees of freedom (DOF) parallel structure of 3<u>T</u>RRR type (3 **T**ranslation, **R**otation, **R**otation, **R**otation) with three translational inputs and three translational outputs (Fig.1). It is composed by a mobile end-effector platform (4) connected to the base by three arms $a, b\ c$, each one composed by three links ($1_i, 2_i, 3_i$, where $i = a, b, c$) and four kinematic joints: one active prismatic joint disposed along the axis of the global coordinate system $O_0X_0Y_0Z_0$ (denoted by q_i, $i = a$, b, c) and 3 passive revolute joints characterized by the relative angular displacements $\varphi_{1i}, \varphi_{2i}, \varphi_{3i}$, where $i = a, b, c$. The four joints have parallel axes to each other.

The three output motions of the end-effector along the axes X_0, Y_0 and Z_0 are decoupled. Therefore, each output motion is commanded from a single motor: the output motion along the X_0 axis is controlled by the active joint q_a, the one along the Y_0 axis by the active joint q_b, and the one along Z_0 axis by the active joint q_c. In addition, the input motions are transmitted unchanged to the outputs [13]. Therefore, this parallel robot type is also called "maximally regular" [14, 15] and refers to the particular case of Jacobian matrix that equals the identity matrix.
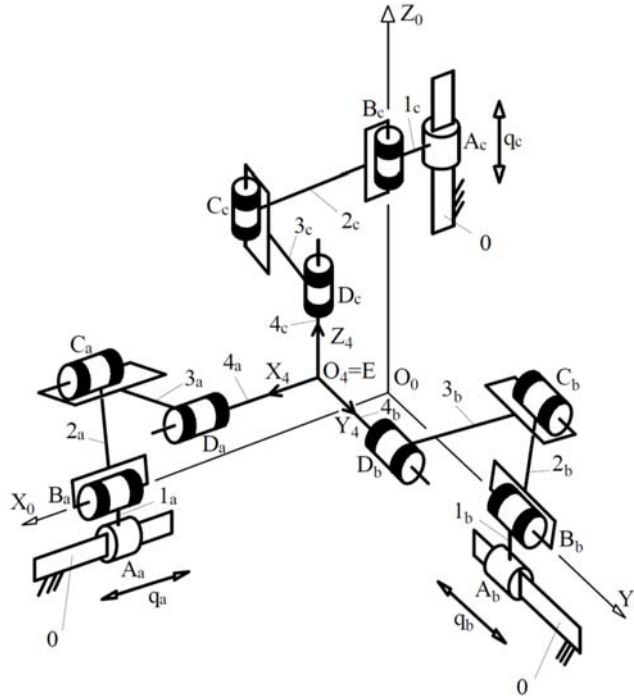

Fig. 1. Kinematic diagram of an Isoglide T3 parallel robot

The traveling coordinate system method [16] was used to obtain the direct and inverse geometric and kinematic models of the Isoglide T3 parallel robot. The results of the direct geometric model is the absolute translational displacement function, i.e. the displacements of the end-effector characteristic point $E(x_E, y_E, z_E) \equiv O_4$ in relation with the relative displacements in the active joints (q_a, q_b, q_c):

$$\begin{cases} x_E = q_a - l_{4a} \\ y_E = q_b - l_{4b} \\ z_E = q_c - l_{4c} \end{cases} \tag{1}$$

where l_{4a}, l_{4b}, l_{4c} represent the lengths of the mobile platform 4 in the direction of the axes of the local coordinate system $O_4X_4Y_4Z_4$ as depicted in Fig. 1.

The inverse geometric model allows to establish the dependence of the relative displacements in the active joints (q_a, q_b, q_c), in relation with the end-effector Cartesian coordinates (x_E, y_E, z_E):

$$\begin{cases} q_a = x_E + l_{4a} \\ q_b = y_E + l_{4b} \\ q_c = z_E + l_{4c} \end{cases} \tag{2}$$

The direct kinematic model expresses the dependences of the end-effector speeds $(\dot{x}_E, \dot{y}_E, \dot{z}_E)$ and acceleration $(\ddot{x}_E, \ddot{y}_E, \ddot{z}_E)$ on the relative linear speeds $(\dot{q}_a, \dot{q}_b, \dot{q}_c)$ and accelerations $(\ddot{q}_a, \ddot{q}_b, \ddot{q}_c)$ in the active joints, through the robot Jacobian matrix J_e:

$$\begin{bmatrix} \dot{x}_E \\ \dot{y}_E \\ \dot{z}_E \end{bmatrix} = J_e \cdot \begin{bmatrix} \dot{q}_a \\ \dot{q}_b \\ \dot{q}_c \end{bmatrix} \quad \text{and} \quad \begin{bmatrix} \ddot{x}_E \\ \ddot{y}_E \\ \ddot{z}_E \end{bmatrix} = \dot{J}_e \cdot \begin{bmatrix} \dot{q}_a \\ \dot{q}_b \\ \dot{q}_c \end{bmatrix} + J_e \cdot \begin{bmatrix} \ddot{q}_a \\ \ddot{q}_b \\ \ddot{q}_c \end{bmatrix} \tag{3}$$

where J_e and $\dot{J}_e$ are define by relations:

$$J_e = \begin{bmatrix} \dfrac{\partial x_E}{\partial q_a} & \dfrac{\partial x_E}{\partial q_b} & \dfrac{\partial x_E}{\partial q_c} \\ \dfrac{\partial y_E}{\partial q_a} & \dfrac{\partial y_E}{\partial q_b} & \dfrac{\partial y_E}{\partial q_c} \\ \dfrac{\partial z_E}{\partial q_a} & \dfrac{\partial z_E}{\partial q_b} & \dfrac{\partial z_E}{\partial q_c} \end{bmatrix} = \begin{bmatrix} 1 & 0 & 0 \\ 0 & 1 & 0 \\ 0 & 0 & 1 \end{bmatrix} \quad \text{and} \quad \dot{J}_e = \begin{bmatrix} 0 & 0 & 0 \\ 0 & 0 & 0 \\ 0 & 0 & 0 \end{bmatrix}. \tag{4}$$

As a result, the kinematical model is expressed by:

$$\begin{bmatrix} \dot{x}_E \\ \dot{y}_E \\ \dot{z}_E \end{bmatrix} = \begin{bmatrix} \dot{q}_a \\ \dot{q}_b \\ \dot{q}_c \end{bmatrix} \quad \text{and} \quad \begin{bmatrix} \ddot{x}_E \\ \ddot{y}_E \\ \ddot{z}_E \end{bmatrix} = \begin{bmatrix} \ddot{q}_a \\ \ddot{q}_b \\ \ddot{q}_c \end{bmatrix}. \tag{5}$$

4   Dynamic modelling

The inverse dynamic modelling begins for the Isoglide T3 parallel robot with the pre-
liminary stage of disconnecting the three arms from the mobile platform, i.e. disassem-
bling the passive revolute joints D_a, D_b and D_c as represented in Fig. 2. Thus, three
separate kinematic open chains of T-R-R type (the arms 1_j-2_j-3_j, $j = a, b, c$) and the end-
effector 4 are obtained.

The three robotic arms a, b and c have a serial structure, formed by the active pris-
matic joints A_j and two passive revolute joints B_j and C_j, $j = a, b, c$, Fig. 2. The three
kinematic joints A_j, B_j and C_j have axes parallel to the axis O_0x_0 for the robotic arm a,
with axis O_0y_0 for the robotic arm b and to the axis O_0z_0 for the robotic arm c, respec-
tively. The independent joint variables (the linear relative displacement in the active
joints A_j) are denoted by q_j, and the dependent ones by φ_{1j} for the joints B_j and by φ_{2j}
for the joints C_j, $j = a, b, c$.

The links of the robotic arms are rigid bodies and characterized by the length l_k (dis-
tance between the axes of the two adjacent joints), the gravity centre G_k, the mass m_k
and the matrix of the moments of inertia J_k established in a local coordinate system with
origin point in the gravity centre G_k, $k = 1_a, 2_a, 3_a, 1_b, 2_b, 3_b, 1_c, 2_c, 3_c$. As a simplifying
hypothesis, the gravity centres G_k are located at middle of the length l_k and the centrif-
ugal moments of inertia are zero (i.e. the axes of the local coordinate system coincide
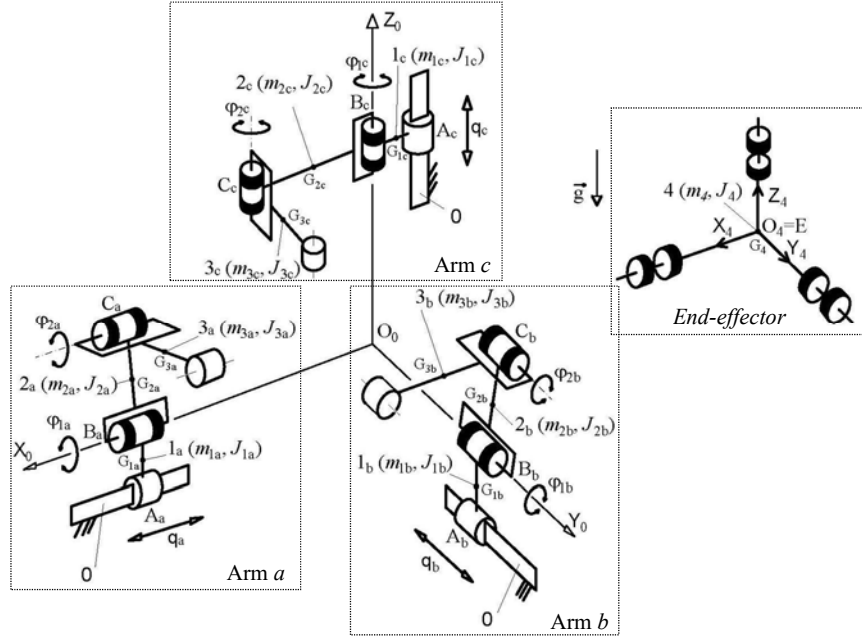with the axes of inertia of the link).

Fig. 2. Dynamic scheme of the Isoglide T3 robot considering the robotic arms detached
from the end-effector platform.

The end-effector platform 4 performs only translational motions, it has the mass m_4 and the gravity centre G_4 in the origin O_4 of the local coordinate system $O_4X_4Y_4Z_4$, as well as the matrix of moments of inertia J_4. The length of the element 4 in the X_4 direction is denoted by l_{4a}, in the Y_4 direction by l_{4b} and in the Z_4 direction by l_{4c}.

The inverse dynamic model of the Isoglide T3 parallel robot is derived based on the following algorithm:

1. Stage I: inverse dynamic modelling of the 3 robotic arms a, b and c, considered as independent serial kinematic chains. The Lagrange equations of second kind are used in this study.
2. Stage II: inverse dynamic modelling of the end-effector platform 4, considered as a rigid body with independent translational motions along the three axes of the global coordinate system $O_0X_0Y_0Z_0$.
3. Stage III: projection of the dynamic equations of the robotic arms and of the end-effector platform in the force space of the active joints A_j, $j = a, b, c$, Fig. 2.

4.1 Inverse dynamic models of the robotic arms

The inverse dynamic modelling based on the Lagrange equations of second kind, in the case of a robotic arm $j = a, b, c$, involves determining the total kinetic energy K_j and the total potential energy P_j, necessary to establish the system Lagrangian L_j:

$$L_j = K_j - P_j = \sum_{i=1}^{3} K_{ij} - \sum_{i=1}^{3} P_{ij} , \tag{6}$$

where K_{ij} represent the kinematical energy of the ith link from the arm j:

$$K_{ij} = \frac{1}{2} m_{ij} v_{Gij}^2 + \frac{1}{2} \omega_{ij}^T J_{Gij} \omega_{ij} , \quad J_{Gij} = \begin{bmatrix} J_{ijxx} & 0 & 0 \\ 0 & J_{ijyy} & 0 \\ 0 & 0 & J_{ijzz} \end{bmatrix}, \tag{7}$$

where m_{ij} is the mass of the link ij, v_{Gij} – the speed of the gravity centre G_{ij}, ω_{ij} – the angular speed vector of the link ij, J_{Gij} – the inertial matrix of the link ij, define in a local coordinate system $O_{ij}x_{ij}y_{ij}z_{ij}$ with the origin O_{ij} in the gravity centre G_{ij} and with the axes parallel to the principal axis of inertia, J_{ijxx}, J_{ijyy}, J_{ijzz} – principal moments of inertia in relation with the axis x_{ij}, y_{ij} and z_{ij}.

The potential energy P_{ij} of the link ij is determined by using:

$$P_{ij} = -m_{ij}\vec{g} \cdot \vec{r}_{Gij} = m_{ij} g \cdot z_{Gij} , \tag{8}$$

where $\vec{r}_{Gij} = x_{Gij}\vec{i}_0 + y_{Gij}\vec{j}_0 + z_{Gij}\vec{k}_0$ is the position vector of the gravity centre G_{ij} in global coordinate system, $\vec{i}_0, \vec{j}_0, \vec{k}_0$ – the unit vectors of the global coordinate system axes, $\vec{g} = -g\vec{k}_0$ is the gravitational acceleration, Fig. 2.

Using the geometric and kinematic models, the Langrangian L_j of the robotic arm j is described by:

$$L_j = \frac{1}{2} A_{0j} \ddot{q}_j^2 + \frac{1}{2} A_{1j} \dot{\varphi}_{1j}^2 + \frac{1}{2} A_{2j} \dot{\varphi}_{2j}^2 + A_{3j} \dot{\varphi}_{1j} \dot{\varphi}_{2j} + A_{4j} g \,, \ j = a, b, c \tag{9}$$

where

$$\begin{cases} A_{0j} = m_{1j} + m_{2j} + m_{3j} \\ A_{1j} = J_{2j} + J_{3j} + m_{2j}c_{2j}^2 + m_{3j}\left(l_{2j}^2 + c_{3j}^2\right) + 2m_{3j}l_{2j}c_{3j} \cos\varphi_{2j} \\ A_{2j} = J_{3j} + m_{3j}c_{3j}^2 \\ A_{3j} = J_{3j} + m_{3j}c_{3j}^2 + m_{3j}l_{2j}c_{3j} \cos\varphi_{2j} \\ A_{4a} = m_{1a}c_{1a} - m_{2a}c_{2a} \sin\varphi_{1a} - m_{3a}l_{2a} \sin\varphi_{1a} - m_{3a}c_{3a} \sin\left(\varphi_{1a} + \varphi_{2a}\right) \\ A_{4b} = m_{1b}c_{1b} - m_{2b}c_{2b} \cos\varphi_{1b} - m_{3b}l_{2b} \cos\varphi_{1a} - m_{3b}c_{3b} \cos\left(\varphi_{1b} + \varphi_{2b}\right) \\ A_{4c} = -\left(m_{1c} + m_{2c} + m_{3c}\right)q_c \end{cases} \tag{10}$$

with notation $J_{2a} = J_{2axx}$, $J_{3a} = J_{3axx}$, $J_{2b} = J_{2byy}$, $J_{3b} = J_{3byy}$, $J_{2c} = J_{2czz}$, $J_{3c} = J_{3czz}$, and $c_{1j} = B_j G_{1j}$, $c_{2j} = B_j G_{2j}$ and $c_{3j} = C_j G_{3j}$ (Fig. 2).

After performing the calculus according to Lagrange equations, the inverse dynamic model of a robotic arm j is expressed by:

$$\begin{bmatrix} F_j \\ \tau_{1j} \\ \tau_{2j} \end{bmatrix} = M_j \cdot \begin{bmatrix} \ddot{q}_j \\ \ddot{\varphi}_{1j} \\ \ddot{\varphi}_{2j} \end{bmatrix} + V_j \begin{bmatrix} \dot{q}_j \\ \dot{\varphi}_{1j} \\ \dot{\varphi}_{2j} \end{bmatrix} + G_j \,, j = a, b, c \tag{11}$$

where: Fj-, τ_{ij}-, M_j represents the matrix of inertial coefficients, V_j - the matrix of centrifugal and Coriolis coefficients, and G_j - the vector of gravitational terms:

$$M_j = \begin{bmatrix} A_{0j} & 0 & 0 \\ 0 & A_{1j} & A_{3j} \\ 0 & A_{3j} & A_{2j} \end{bmatrix} \tag{12}$$

$$V_j = \begin{bmatrix} 0 & 0 & 0 \\ 0 & -2m_{3j}l_{2j}c_{3j} \sin\varphi_{2j}\dot{\varphi}_{2j} & -m_{3j}l_{2j}c_{3j} \sin\varphi_{2j}\dot{\varphi}_{2j} \\ 0 & m_{3j}l_{2j}c_{3j} \sin\varphi_{2j}\dot{\varphi}_{1j} & 0 \end{bmatrix} \tag{13}$$

$$G_a = \begin{bmatrix} 0 \\ m_{2a}c_{2a} \cos\varphi_{1a} + m_{3a}(l_{2a} \cos\varphi_{1a} + c_{3a} \cos(\varphi_{1a} + \varphi_{2a})) \\ m_{3a}c_{3a} \cos(\varphi_{1a} + \varphi_{2a}) \end{bmatrix} \tag{14a}$$

$$G_b = \begin{bmatrix} 0 \\ -m_{2b}c_{2b}\sin\varphi_{1b} - m_{3b}(l_{2b}\sin\varphi_{1b} + c_{3b}\sin(\varphi_{1b}+\varphi_{2b})) \\ -m_{3b}c_{3b}\sin(\varphi_{1b}+\varphi_{2b}) \end{bmatrix} \quad (14b)$$

$$G_c = \begin{bmatrix} m_{1c}+m_{2c}+m_{3c} \\ 0 \\ 0 \end{bmatrix} \quad (14a)$$

4.2 Inverse dynamic model of the end-effector platform

As the mobile platform can only perform translational motions, and considering the Eq. (5), the inverse dynamic model is expressed by:

$$F_4 = \begin{bmatrix} F_{4x} \\ F_{4y} \\ F_{4z} \end{bmatrix} = \begin{bmatrix} m_4\ddot{q}_a \\ m_4\ddot{q}_b \\ m_4(\ddot{q}_c - g) \end{bmatrix}. \quad (15)$$

4.3 Projection of the dynamic equations in the force space of the active joints

The dynamic model of a robotic arm j can be projected in the force space of the active joints by applying the principle of virtual power:

$$\begin{bmatrix} F_j \\ \tau_{1j} \\ \tau_{2j} \end{bmatrix}^T \cdot \begin{bmatrix} \dot{q}_j \\ \dot{\varphi}_{1j} \\ \dot{\varphi}_{2j} \end{bmatrix} = \begin{bmatrix} F_{a.j} \\ F_{b.j} \\ F_{c.j} \end{bmatrix}^T \cdot \begin{bmatrix} \dot{q}_a \\ \dot{q}_b \\ \dot{q}_c \end{bmatrix}, j = a, b, c \quad (16)$$

where $F_{a.j}$, $F_{b.j}$ and $F_{c.j}$ represent the components of the forces in the active joints generated by the dynamic effects of the robotic arm j.
It is known that:

$$\begin{bmatrix} \dot{q}_j \\ \dot{\varphi}_{1j} \\ \dot{\varphi}_{2j} \end{bmatrix} = J_{qj} \cdot \begin{bmatrix} \dot{q}_a \\ \dot{q}_b \\ \dot{q}_c \end{bmatrix} \rightarrow \begin{bmatrix} F_{a.j} \\ F_{b.j} \\ F_{c.j} \end{bmatrix} = J_{qj}^T \begin{bmatrix} F_j \\ \tau_{1j} \\ \tau_{2j} \end{bmatrix} \quad (17)$$

where

$$
J_{qj} = \begin{bmatrix} \dfrac{\partial q_j}{\partial q_a} & \dfrac{\partial q_j}{\partial q_b} & \dfrac{\partial q_j}{\partial q_c} \\[2.5ex] \dfrac{\partial \varphi_{1j}}{\partial q_a} & \dfrac{\partial \varphi_{1j}}{\partial q_b} & \dfrac{\partial \varphi_{1j}}{\partial q_c} \\[2.5ex] \dfrac{\partial \varphi_{2j}}{\partial q_a} & \dfrac{\partial \varphi_{2j}}{\partial q_b} & \dfrac{\partial \varphi_{2j}}{\partial q_c} \end{bmatrix}.
\tag{18}
$$

The absolute positions of the central points of the passive joint D_j, $j = a, b, c$ can be expressed depending on both the operational variables (x_E, y_E, z_E) and on the joint variables $(q_j, \varphi_{1j}, \varphi_{2j})$. The relationships thus obtained make possible to obtain the partial derivatives in the matrix (18):

$$
J_{qa} = \begin{bmatrix} 1 & 0 & 0 \\[2ex] 0 & \dfrac{\cos(\varphi_{1a} + \varphi_{2a})}{l_{2a} \sin \varphi_{2a}} & \dfrac{\sin(\varphi_{1a} + \varphi_{2a})}{l_{2a} \sin \varphi_{2a}} \\[3ex] 0 & \dfrac{-l_{2a} \cos \varphi_{1a} - l_{3a} \cos(\varphi_{1a} + \varphi_{2a})}{l_{2a} l_{3a} \sin \varphi_{2a}} & \dfrac{-l_{2a} \sin \varphi_{1a} - l_{3a} \sin(\varphi_{1a} + \varphi_{2a})}{l_{2a} l_{3a} \sin \varphi_{2a}} \end{bmatrix}
\tag{19a}
$$

$$
J_{qb} = \begin{bmatrix} 1 & 0 & 0 \\[2ex] 0 & \dfrac{\sin(\varphi_{1b} + \varphi_{2b})}{l_{2b} \sin \varphi_{2b}} & \dfrac{\cos(\varphi_{1b} + \varphi_{2b})}{l_{2b} \sin \varphi_{2b}} \\[3ex] 0 & \dfrac{-l_{2b} \sin \varphi_{1b} - l_{3b} \sin(\varphi_{1b} + \varphi_{2b})}{l_{2b} l_{3b} \sin \varphi_{2b}} & \dfrac{-l_{2b} \cos \varphi_{1b} - l_{3b} \cos(\varphi_{1b} + \varphi_{2b})}{l_{2b} l_{3b} \sin \varphi_{2b}} \end{bmatrix}
\tag{19b}
$$

$$
J_{qc} = \begin{bmatrix} 1 & 0 & 0 \\[2ex] 0 & \dfrac{\cos(\varphi_{1c} + \varphi_{2c})}{l_{2c} \sin \varphi_{2c}} & \dfrac{\sin(\varphi_{1c} + \varphi_{2c})}{l_{2c} \sin \varphi_{2c}} \\[3ex] 0 & \dfrac{-l_{2c} \cos \varphi_{1c} - l_{3c} \cos(\varphi_{1c} + \varphi_{2c})}{l_{2c} l_{3c} \sin \varphi_{2c}} & \dfrac{-l_{2c} \sin \varphi_{1c} - l_{3c} \sin(\varphi_{1c} + \varphi_{2c})}{l_{2c} l_{3c} \sin \varphi_{2c}} \end{bmatrix}
\tag{19c}
$$

Similarly, the dynamic equations of the end-effector platform are projected into the force space of the active joints using:

$$
\begin{bmatrix} F_{a.4} \\ F_{b.4} \\ F_{c.4} \end{bmatrix} = J_e^T \begin{bmatrix} F_{4x} \\ F_{4y} \\ F_{4z} \end{bmatrix}
\tag{20}
$$

where J_e is the identity matrix according to Eq. (4).

By applying the superposition principle for the projected dynamic equations, the to-tal driving forces in the active joints A_j, $j = a$, b, c are:

$$
\begin{bmatrix} F_{A_a} \\ F_{A_b} \\ F_{A_c} \end{bmatrix} = \begin{bmatrix} F_{a.a} \\ F_{b.a} \\ F_{c.a} \end{bmatrix} + \begin{bmatrix} F_{a.b} \\ F_{b.b} \\ F_{c.b} \end{bmatrix} + \begin{bmatrix} F_{a.c} \\ F_{b.c} \\ F_{c.c} \end{bmatrix} + \begin{bmatrix} F_{a.4} \\ F_{b.4} \\ F_{c.4} \end{bmatrix}.
$$

(21)

5   Simulation results

The closed-form dynamic model described by Eq. (21), obtained by using the Maple software, was simulated on a test trajectory implemented both on Maple and ADAMS software, that allows the modelling and simulation of mechanisms as multibody systems (MBS) [17]. The CAD model of the Isoglide T3 parallel robot (Fig. 3) includes bodies of simple cylindrical shape; this ADAMS model can be used for validation of the closed-form model and to deliver the necessary input data in numerical simulations related to the inertial link properties, Table 1.

Table1. Geometric and inertial properties of the robot links

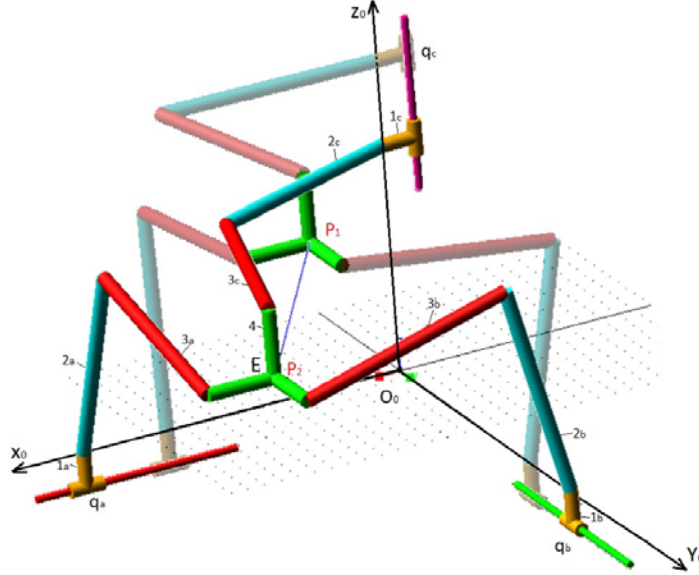| Link/ body	Length [m]	Mass [kg]	Principal moments of inertia [kg·m2]		
			Jxx	Jyy	Jzz
$1j$	0.1	0.98	$9.14 \cdot 10^{-4}$	$9.14 \cdot 10^{-4}$	$1.96 \cdot 10^{-4}$
$2j$	0.63	6.17	0.204	$1.235 \cdot 10\text{-}3$	0.204
$3j$	0.63	6.17	0.204	$1.235 \cdot 10\text{-}3$	0.204
4	0.20	5.66	$5.302 \cdot 10^{-2}$	$5.302 \cdot 10^{-2}$	$5.302 \cdot 10^{-2}$
$j = a, b, c$					

Fig. 3. ADAMS model of the Isoglide T3 parallel robot and its positions at the trajectory ends

The numerical simulations were performed on a trajectory defined in the joint space, characterized by:
- motion duration t = 10 s;
- strokes in active joints $\Delta q_a = \Delta q_b = 0.25$ m and $\Delta q_c = - 0.25$;
- linear trajectory between the points $P_1(0.7, 0.8, 0.9)$ and $P_2(0.95, 1.05, 0.65)$;
- time interpolation functions: fifth degree polynomials, as represented in Fig. 4 for the active prismatic joint A_a.

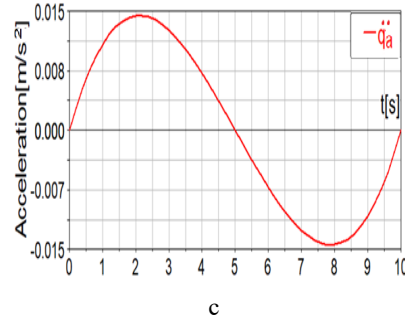The simulations on the selected test trajectory (Fig. 3) allowed obtaining the driving forces as depicted in Fig. 5…7.

c
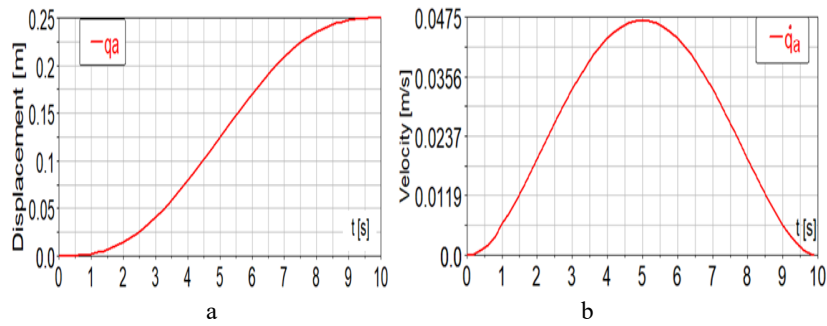
Fig. 4. Simulated motion for the active joint A_a: linear displacement q_a (a); linear speed $\dot{q}_a$ (b); linear acceleration $\ddot{q}_a$ (c).
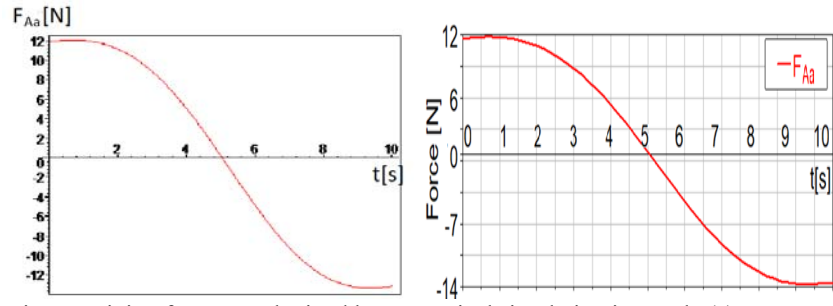

Fig. 5. Driving force F_{Aa} obtained by: numerical simulation in Maple (a); ADAMS simulation (b).
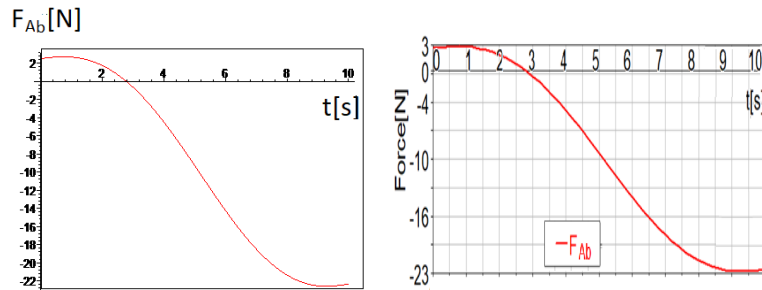

Fig. 6. Driving force F_{Ab} obtained by: numerical simulation in Maple (a); ADAMS simulation (b).
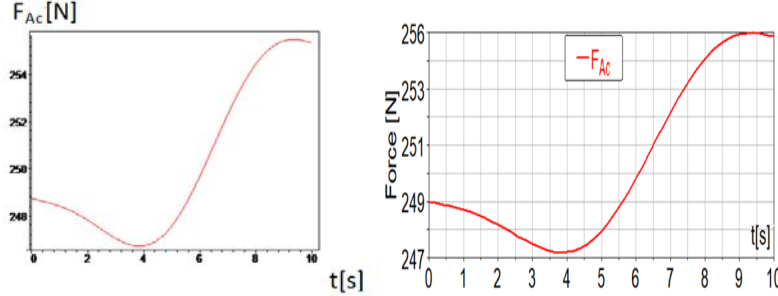
Fig. 7. Driving force F_{Ac} obtained by: numerical simulation in Maple (a); ADAMS simulation (b).

The analysis of the results obtained by numerical simulation of the closed-form model (Maple) and of the CAD model (ADAMS), it can be noticed that the driving forces have identical time variations for the same active joint in both cases (Figs. 5... 7). Thus, it can be concluded that the closed-form inverse dynamic model is validated by ADAMS simulation. It can also be observed that:

- the driving forces F_{Aa} and F_{Ab} follow the shape as the displacements imposed in the active joints (Fig. 5 and 6); the maximum values of the driving forces are ~12 N for the F_{Aa} force and ~22 N for the F_{Ab} force, respectively;
- the force F_{Ac} has higher values in relation to the other two driving forces (ranges between ~ 249 N up to ~ 255 N), due to the gravitational forces directed in the negative direction of the $O_0 z_0$ axis.

6   Conclusion

The paper presents the inverse dynamic modelling of an Isoglide T3 parallel robot, using the approach of preliminary decomposing the parallel structure into open kinematic chains by disassembling the revolute joints between the robotic arms and the end-effector platform.

The application of the investigated inverse dynamic modelling for the Isoglide T3 parallel robot allowed to highlight the following aspects:

- By dismantling the revolute joints with the mobile platform, the parallel structure was decomposed into three serial robotic arms of TRR type and the end-effector link with translational motion;
- The inverse dynamic models of the three robotic arms, considered as independent mechanisms, were derived using the Lagrange equations of the second kind. The dynamic model of the mobile platform resulted based on the Newton's second law of motion;
- The driving forces were obtained by projecting the dynamic equations of the robotic arms and end-effector platform on the force space of the active joints, based on Jacobian matrices determined in the kinematic analysis stage;

- − The closed-form of the inverse dynamic model was developed using the Maple software, that also allowed numerical simulation;
- − The inverse dynamic model was validated by developing the CAD model of Iso-glide T3 parallel robot and by simulating its dynamic behaviour using the ADAMS software.

The main advantages of the applied dynamic modelling method refer to the simplicity of its application: the complex modelling of a parallel structure is reduced to simpler modelling of serial structures (the robotic arms) and the end-effector platform, followed by the projection of their dynamic equations in the force space of the active joint through Jacobian matrices.

References

1. Gogu G., Structural synthesis of parallel robots. Part 1: Methodology, Springer Verlag, (2008).
2. Lee, K.M. , Shah, D.K. , Dynamic analysis of a three-degrees-of-freedom in-parallel actuated manipulator, IEEE Journal of Robotics and Automation, 4, pp. 361-368, (1988).
3. Bhattacharya, S., Nenchev, D.N., Uchiyama, M., A recursive formula for the inverse of the inertia matrix of a parallel manipulator, Mechanism and Machine Theory, 33 (7), pp. 957-964, (1998).
4. Liu, M-J., Li, C-X., Li, C-N., Dynamics analysis of the Gough–Stewart platform manipulator, IEEE Transaction on Robotics and Automation, 16 (1), pp. 94-98, (2000).
5. Dasgupta, B, Mruthyunjaya, T.S., A Newton–Euler formulation for the inverse dynamics of the Stewart platform manipulator, Mechanism and Machine Theory, 33 (8), pp. 1135-1152, (1998).
6. Dasgupta, B., Choudhury, P. , A general strategy based on the Newton–Euler approach for the dynamic formulation of parallel manipulators, Mechanism and Machine Theory, 34 (6), pp. 801-824, (1999).
7. Khalil, W., Guegan, S., Inverse and direct dynamic modeling of Gough–Stewart robots, IEEE Transactions on Robotics and Automation, 20 (4), pp. 754-762, (2004).
8. Ibrahim, O., Khalil, W., Inverse and direct dynamic models of hybrid robots, Mechanism and Machine Theory, pp 627-640, Vol 45, (2010).
9. Rat, N.R, Neagoe, M., Diaconescu, D., Stan, S.D. Dynamic simulations regarding the influence of the load-rigidity correlation on the working accuracy of a medical Triglide parallel robot, ISSN 1392 – 1207, MECHANIKA 17(2), pp 178-181, (2011).
10. Rat, N., Rizk, R., Gogu, G., Neagoe, M., Comportement des robots parallèles à mouvements découplés et corps déformables, Congrès Français de Mécanique, (2005).
11. Raţ, N.R., Neagoe, M., Stan, S.D. ,Comparative Dynamic Analysis of Two Parallel Robots, The 2010 International Conference on Robotics (ROBOTICS'10), Vols. 166-167 ,pp 345-356, (2010).
12. Ibrahim, O., Contribution a la modelisation dynamique des robots parallels et des robots hybrids, PHD thesis, L'Ecole Centrale de Nantes et l'Universite de Nantes, (2006).
13. Gogu, G., Structural synthesis of fully-isotropic translational parallel robots via theory of linear transformations, European Journal of Mechanics A/Solids 23, pp. 1021–1039, (2004).
14. Gogu, G., *Structural synthesis of parallel robots*, Part 1: Methodology, Springer Verlag, (2008).

15. Gogu, G., *Structural synthesis of parallel robots*, Part 3: Topologies with planar motion of the moving platform, Springer Verlag, (2010).
16. Gogu, G., Optimization on the modeling of industrial robots (in Romanian), PHD thesis, Transilvania University of Brasov, (1995).
17. Costa, A., Jones, R.P., Automitive Vehicle Chassis Simulation for Motion Control Studies using Multibody Systems (MBS) Modelling Techniques, SAE Paper No. 921443, (1992).

Dynamic Analysis of a Delta Parallel Robot with Flexible Links and Joint Clearances

Nadia Cretescu [1], Mircea Neagoe [1,*] and Radu Saulescu [2]

1 Renewable Energy Systems and Recycling R&D Centre, Faculty of Product Design and Environment, Transilvania University of Brasov, 500036 Brasov, Romania; ncretescu@unitbv.ro
2 Design of Mechanical Elements and Systems R&D Centre, Faculty of Product Design and Environment, Transilvania University of Brasov, 500036 Brasov, Romania; rsaulescu@unitbv.ro
* Correspondence: mneagoe@unitbv.ro; Tel.: +40-268-413-000

Abstract: Delta robot is a lightweight parallel manipulator capable of accurately moving heavy loads at high speed and acceleration along a spatial trajectory. This intensive dynamic process may have a significant impact on the end-effector trajectory precision and motor behavior. The paper highlights the influence on the dynamic behavior of a Delta robot by considering individual and combined effects of clearances and friction in the spherical joints, as well as the flexibility of the rod elements. The CAD modeling of the Delta robot and its motion simulation on a representative spatial trajectory where the maximum allowed values of speed and acceleration are reached were performed using the Catia and Adams software packages. The obtained results show that the methods used were successfully applied and the effects are mutually interconnected, but not cumulative.

Keywords: parallel robot; Delta manipulator; dynamic; flexible link; joint clearance; joint friction; modelling; simulation

1. Introduction

The Delta parallel robot (DPR) is a three-degree-of-freedom (3-DOF) translational manipulator that consists of a fixed base linked to a mobile platform by three arms. The first model of the Delta parallel robot was invented in 1987 by Reymond Clavel [1] as a suitable structure for high-speed and high-acceleration tasks, specially used for pick and place operations, but also for packaging, sorting, precision positioning, and other applications.

In the industry, parallel robots have light structures and usually operate at high speeds and accelerations with heavy payload; as a result, negative kinematic and dynamic effects may intervene in the operation due to joint clearances and frictions or link flexibility. Preliminary knowledge of the behavior of these robots represents a critical asset for their optimal design.

Various studies related to the analytical modeling (both kinematic and dynamic approaches) of parallel robots but also their CAD modelling and simulation can be found in the literature. To the best of our knowledge, no relevant works have been identified that address the idea of analyzing the cumulative effect of the flexibility of elastic elements in combination with the clearances and friction from the spherical joints. These three parameters can have a major role in the dynamic behavior of parallel robots. The analysis of the effects of these factors is exemplified in the paper on the case study of a Delta parallel robot (DPR).

A new DPR is proposed and developed in [2], along with its dynamic optimization. A direct and inverse pose modeling method for a DPR is addressed in [3] based on ADAMS, and a DPR kinematic model is presented in [4], completed by a closed-form inverse dynamic model using the Newton laws, a formulation called "in two spaces". An analytical approach for the dimensional synthesis of a Delta parallel robot is presented in [5]. The analytical solution presented, with dimensional optimization for the link length, aims to find the

DPR workspace. A dynamic dimensional synthesis using the pressure/transmission angle constraints of a DPR is described in [6]. Two types of pressure angle are defined, and thus direct and indirect singularities can be identified.

The kinematic calibration and sensitivity analysis for a DPR is described in [7], a method which can be used successfully for other parallel robots.

An experimental verification of a newly developed DPR, based on the dynamic model derived by using the Hamilton's principle, is presented in [8]. An inverse dynamic model is developed using the Euler–Lagrange approach, a model validated with real torques data obtained from of a model of the Delta parallel robot developed by SIPRO [9].

Other approaches to dynamic DPR modeling are presented in [10], for example, the Lagrange equations, Newton–Euler formulation and the Principle of Virtual Work. An analysis of an analytical dynamic model of the Delta robot was presented in [11] and another analytical model was validated by experimental data [12]. Different methods for dynamic modeling of parallel robots are presented in [13–17], with numerical simulation and experimental validation.

In addition, the kinematic modeling of parallel robots, especially the Delta robot, has been extensively addressed in the literature [18–22] including forward and inverse modeling and kinematic optimization.

The numerical simulation of parallel robots is an attractive topic, mainly using MATLAB software (https://en.wikipedia.org/wiki/MATLAB) [23,24] or MATLAB simulation validated by experimental research [25,26].

In dynamic studies, various assumptions can be considered, such as rigid vs. flexible links (analytical or numerical), ideal condition vs. friction and clearance in joints. The effect of link flexibility is analyzed for different parallel robots by using ADAMS software (https://hexagon.com/products/product-groups/computer-aided-engineering-software/adams) compared with rigid link case [27–29]. An alternative approach to obtaining the analytical model of a DPR with flexible links is presented in [30].

An optimal trajectory planning for a DPR is carried out in [31] aiming to suppress robot vibration by developing an elasto-dynamic model assuming flexible links, and a polynomial function in the operating space was considered. The dynamical model of a parallel robot considering link flexibility was developed in [32] based on co-rotational and rigid finite elements.

Several scholars have analyzed the phenomenon of friction in spherical joints. The stability analysis of a ball joint based on Coulomb and Stribeck-type model was addressed in [33]. Nonlinear periodic solutions were obtained depending on the ball joint friction parameters. The error modeling for a DPR has been analyzed in [34] by considering joint clearances.

Thus, there are works that separately deal with the influence of these factors on the kinematic and dynamic behavior of the DPR, some through analytical modeling and most through numerical simulation using specialized software, but without identifying relevant results regarding the cumulative effect of these three factors (link flexibility, friction and joint clearance).

The main problems of DPR highlighted in the literature are systematized in the Introduction:

(a) kinematic and dynamic modeling and simulation of DPR;
(b) optimizations of the dynamic model;
(c) new methods for solving the dynamic model;
(d) analytical modeling with experimental verification;
(e) the influence of the flexibility of DPR elements using different software;
(f) the analysis of the friction in joints of DPR;
(g) errors produced by joint clearances of DPR.

This paper addresses the following gap identified in the literature: to the best of the authors' knowledge, there is a lack of significant scientific works dealing with the cumulative effects of link flexibility, joint friction and joint clearance on the dynamic

behavior of parallel robots. Therefore, the proposed research is conducted on a Delta parallel robot using a CAD model obtained in the CATIA software (https://en.wikipedia.org/wiki/CATIA) and deriving specific simulations in the ADAMS software.

The rest of the paper is organized as follows: Section 2 presents the problem formulation; Section 3 proposes seven simulation scenarios and discusses the obtained results; and Section 4 draws final conclusions.

2. Problem Formulation

The effect of element flexibilities, frictions and clearances can be studied numerically by developing a CAD model of the analyzed robot in the first stage, for example, using the CATIA software, followed in the second stage by the ADAMS analysis. Since ADAMS does not easily allow the creation of elements with complex shapes, it was decided to develop the CAD model in CATIA and then export the 3D bodies (in an IGES format) to ADAMS. Thus, a CAD model can be obtained in ADAMS that reflects the properties of the existing physical robot as accurately as possible.

In this analysis, we consider the case study of a Delta Siax D3-1600 parallel robot (Figure 1a, [35]). Its simplified CAD model (without motors) at a 1:1 scale was represented in CATIA (Figure 1b) and then transferred to ADAMS (Figure 1c). The Delta Siax D3-1600 is a three degree-of-freedom (3-DOF) robot (the end-effector performs three independent translations). It is composed of a fixed platform (0) and a mobile platform (4), interconnected by three arms, A, B and C, each of them with a driving element (1) connected to the base by a motor drive (R). Each arm has a parallelogram-type kinematic chain with two flexible elements (2 and 3) and four passive spherical couples each (S_{2k1}, S_{2k2} and S_{3k1}, S_{3k2}, where $k = A, B, C$—Figure 1d). The three arms are equiangularly distributed (Figure 1e) in relation to the global coordinate system ($X_0Y_0Z_0$) of the robot, with the origin located at point O (Figure 1d). The Delta robot has attached to the end-effector (4) a payload in the form of a cylinder (5) with a mass of 5 kg. The characteristic point P is the origin of the mobile coordinate system of the end-effector and it travels a spatial trajectory established so as to reach the maximum velocity and acceleration according to the values specified in Table 1.

Table 1. Delta SIAX D3-1600 parallel robot: main characteristics.

Parameter	Value
Total mass	80 kg
Maximum payload	5 kg
Maximum end-effector speed	8 m/s
Maximum end-effector acceleration	120 m/s^2

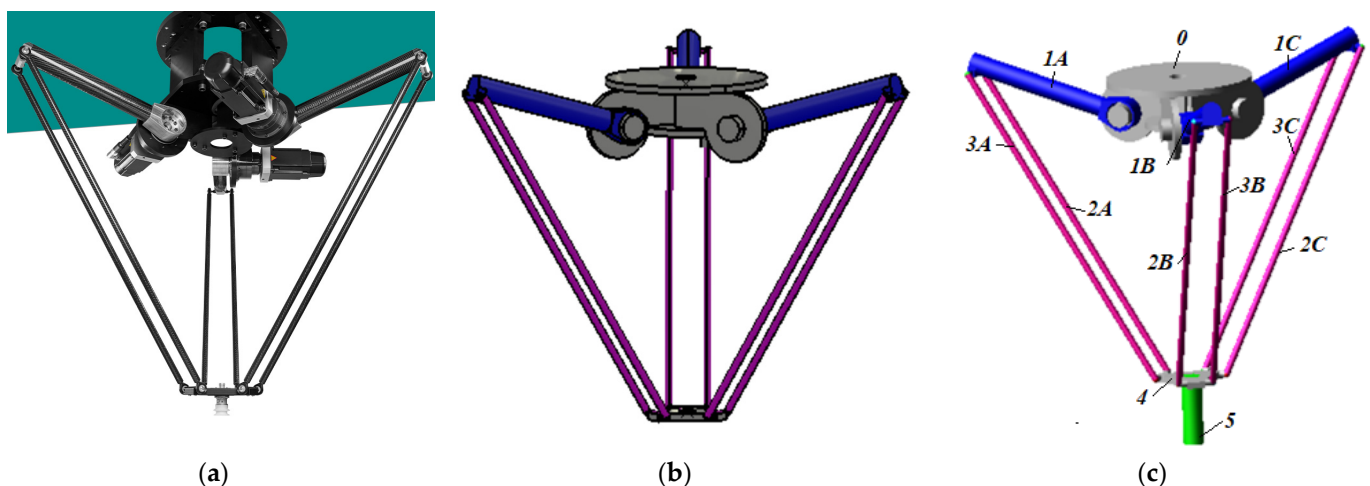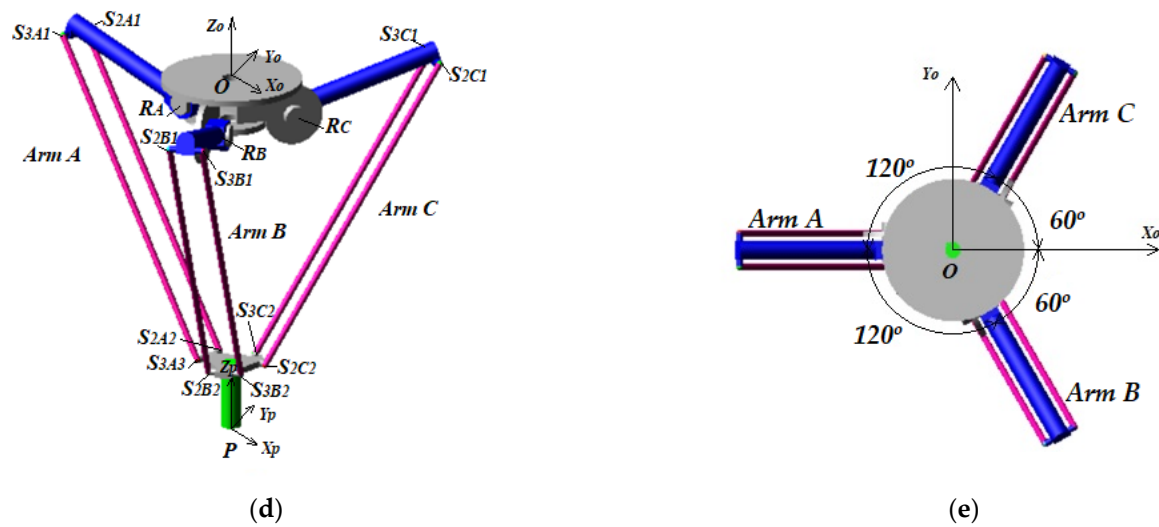| (a)	(b)	(c)

Figure 1. *Cont.*

(d)

(e)

Figure 1. Delta parallel robot: (**a**) Delta Siax D3-1600 type robot; (**b**) CATIA model without payload; (**c**) ADAMS model with payload; (**d**) ADAMS model parametrisation; (**e**) arm arrangement.

The geometrical, mass and material properties of the robot's component bodies are key factors in determining its dynamic behavior. In the proposed analysis, the following assumptions have been made:

- Elements 0, 1, 4 and 5 are rigid solid bodies;
- Rod Elements 2 and 3 have higher elastic characteristics than the other elements due their dimensions, see Table 2;
- All bodies are made of steel.

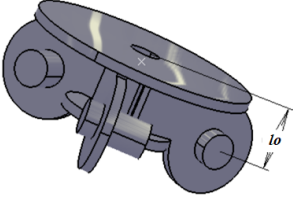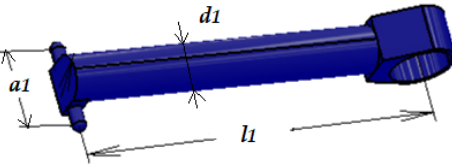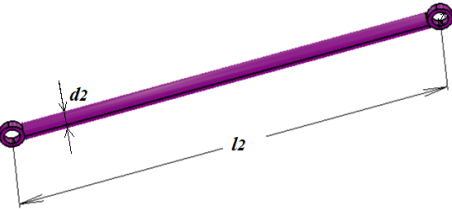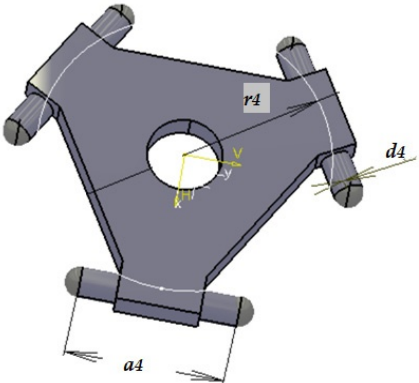**Table 2.** Geometrical and mass details of the Delta robot bodies.
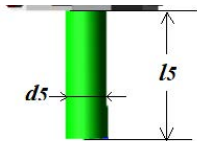
Body	CAD Model	Parameters
Fixed platform (0)		l_0 = 125 mm
Crank (1)		l_1 = 500 mm m_1 = 1.58 kg d_1 = 62 mm a_1 = 106 mm
Rod element (2 and 3)		$l_2 = l_3$ = 1106 mm $m_2 = m_3$ = 0.34 kg $d_2 = d_3$ = 20 mm

Body	CAD Model	Parameters
Mobile platform (4)		$m_4 = 0.46$ kg $d_4 = 20$ mm $a_4 = 106$ mm $r_4 = 97$ mm
Payload (5)		$l_5 = 212$ mm $m_5 = 5$ kg $d_5 = 50$ mm

The reference model of the Delta robot is based on the assumptions of an ideal mechanism, where all bodies are rigid solids, all kinematic joints are ideal (no clearance, no friction), and the characteristic point P follows a trajectory that reaches maximum allowed values of speed and acceleration. Thus, the fifth degree polynomial function was chosen to generate the movement trajectory in the joint space as well as a short trajectory travel time of 0.2 s, the time resulting from the simultaneous provision of the conditions for the robot to touch the P_0P_1 trajectory (Figure 2), the maximum speed of the end-effector $v_{Pmax} = 8$ m/s and the maximum acceleration $a_{Pmax} = 120$ m/s^2 (see Table 1).
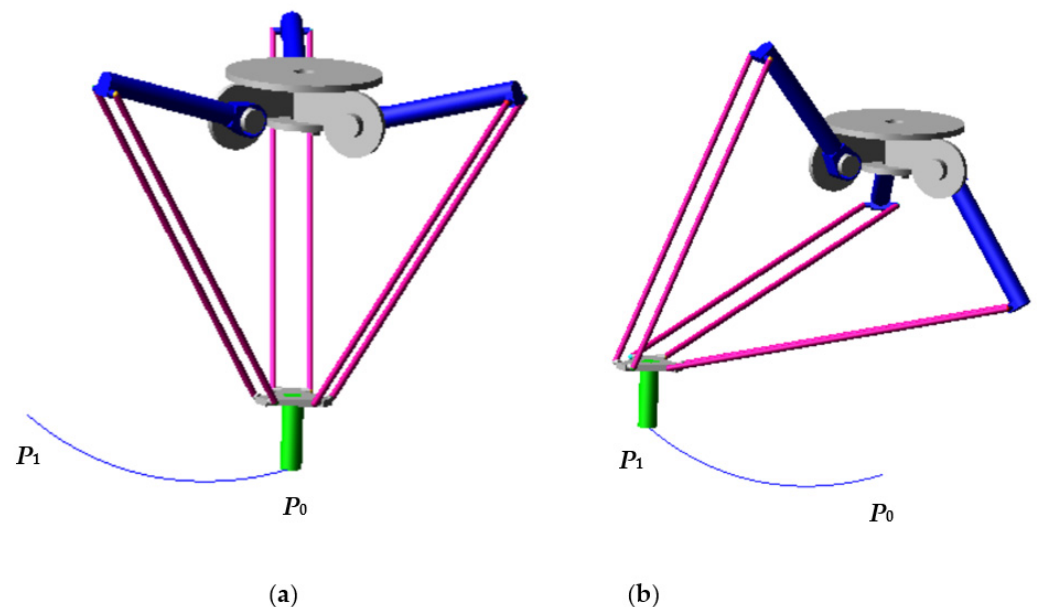
Figure 2. Cartesian trajectory of the Delta robot: (**a**) initial position; (**b**) final position.

The starting position of the Cartesian trajectory (P_0) corresponds to the initial position of the robot where all three motor torques R_A, R_B and R_C are in the zero position and Elements 1 are arranged in a horizontal plane (parallel to X_0Y_0, see Figure 1d). The trajectory in the Cartesian space P_0P_1 is a spatial curve obtained by applying an angular

displacement of 70° in the positive direction of the joint axis R_A, 41° in the positive direction of the coupling axis R_B and of 36° in the negative direction of the joint axis R_C (Figure 3a). Along this trajectory, the maximum angular velocity of 656°/s in joint A, 384°/s in joint B and 292°/s in joint C is reached (Figure 3b), as well as the maximum angular accelerations of 10,103°/s² (engine A), 5124°/s² (engine B) and 4500°/s² (engine C), as shown in Figure 3c.
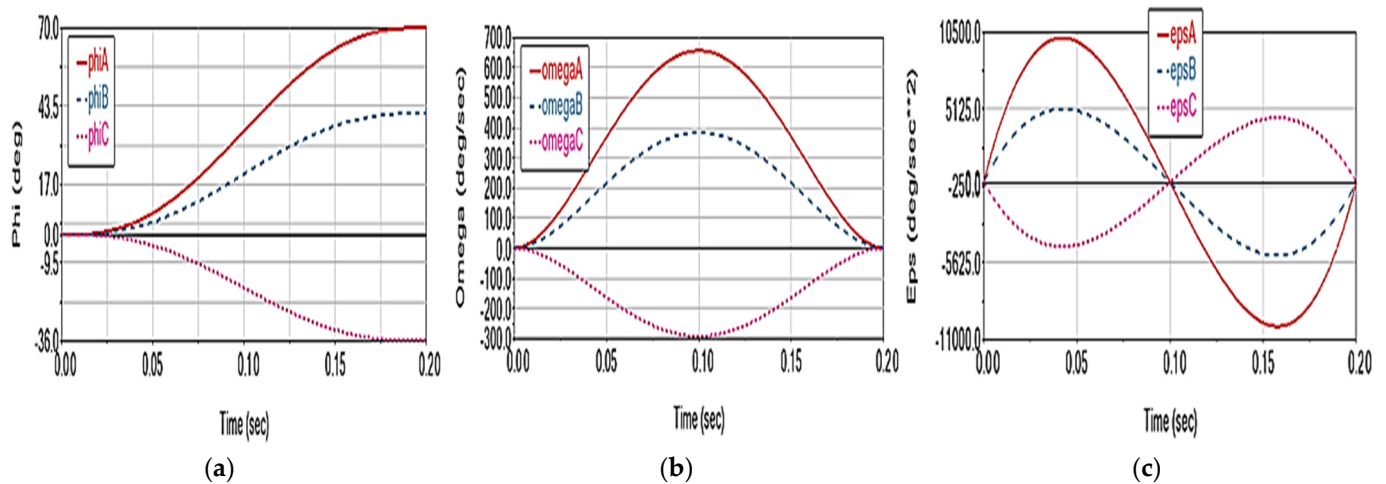

Figure 3. Motion trajectories in the active joint space (R_A, R_B and R_C): (**a**) angular displacement; (**b**) angular velocity and (**c**) angular acceleration.

When polynomial movement trajectories of the fifth degree are applied to the active joints, a Cartesian trajectory P_0P_1 is obtained. This trajectory is characterized by the displacement of the characteristic point P along all three axes of the global coordinate system $X_0Y_0Z_0$ (Figure 4), and it reaches a final position of $r_P = 1.245$ m (Figure 5a). The trajectory also reaches a maximum speed of $v_P = 8$ m/s at 0.1 s (Figure 5b) and a maximum acceleration of $a_P = 120$ m/s² at approximately 0.052 s and 0.158 s (Figure 5c).

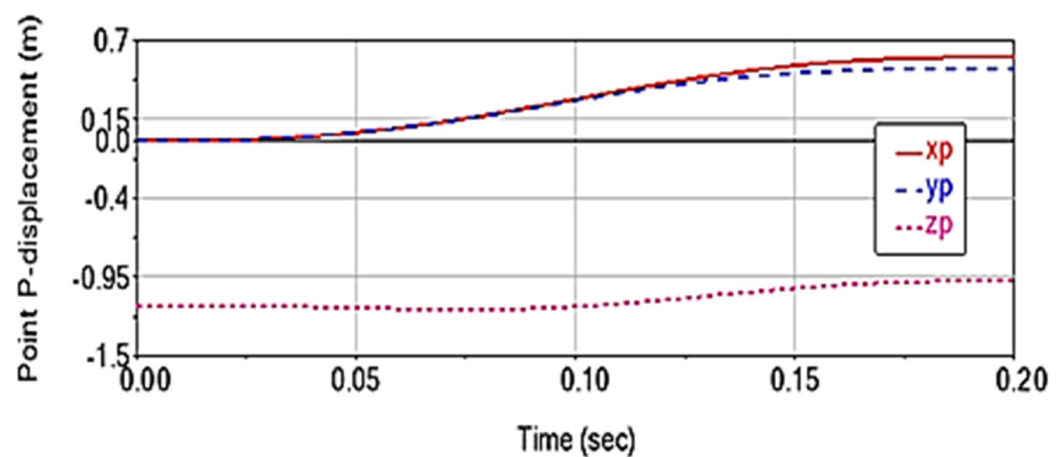**Figure 4.** End-effector displacement components for the Delta robot reference model.

The torque in the active joints (Figure 6) on the stated trajectory has the allure of angular acceleration (see Figure 3c); higher values of the moment *TA* are observed due to the higher angular accelerations (and consequently higher values of angular speeds and displacements) compared to the other two active torques.
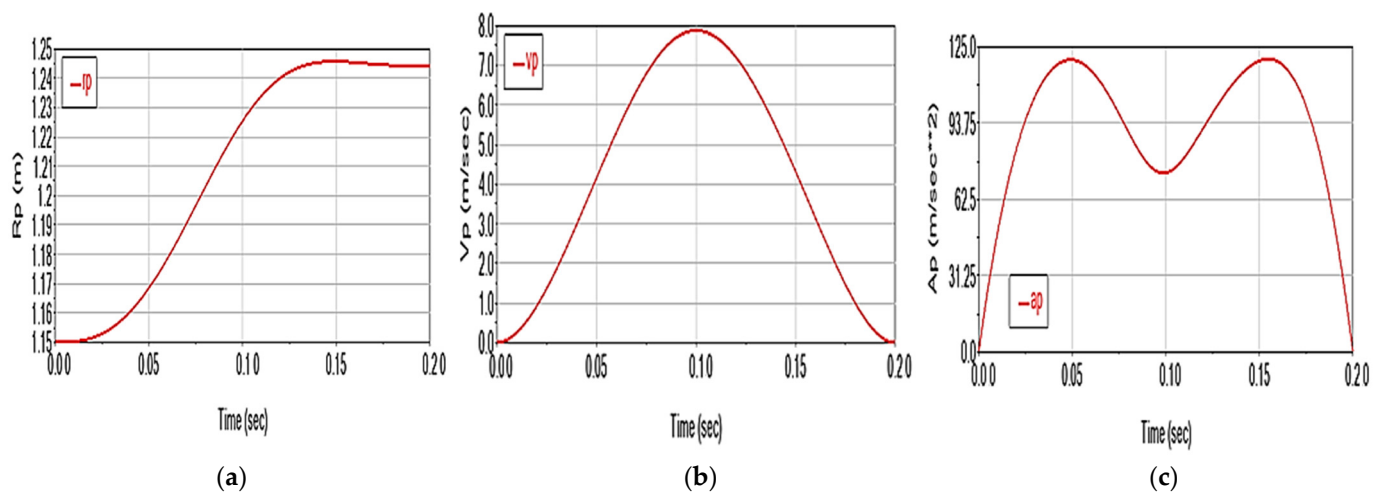
Figure 5. End-effector motion for the Delta robot reference model (magnitude of): (**a**) displacement; (**b**) velocity and (**c**) acceleration.
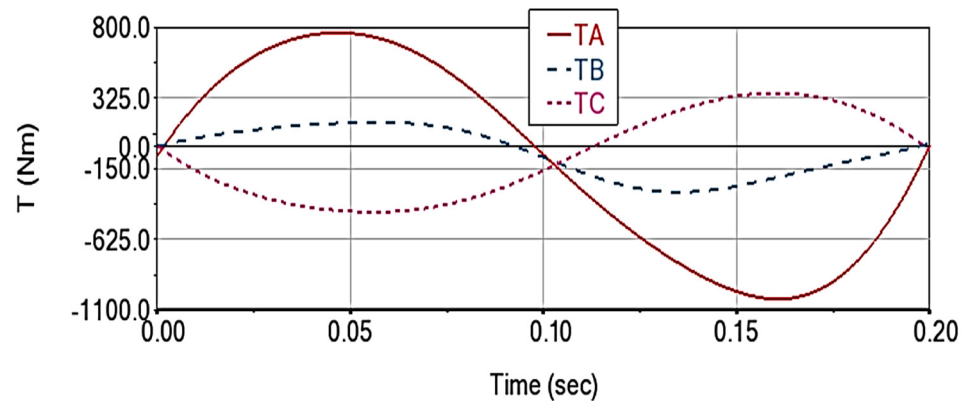

Figure 6. Driving torques (*TA*, *TB* and *TC*) for the Delta robot reference model.

Under these considerations, the aim of this study is to analyze the kinematic and dynamic effects of these three factors, both individually and in combination:

- Friction on spherical joints;
- Clearances on spherical joints;
- Elasticity of the flexible rod elements (2 and 3).

Thus, the comparative analysis of the Delta robotic structure is presented in seven dynamic simulation scenarios, taking as reference the previously defined ideal model. The study makes the following assumptions:

- Scenario 1: considers only the frictions from the passive spherical joints (S_2k_1, S_2k_2 and S_3k_1, S_3k_2, $k = A, B, C$) assuming steel/steel friction with lubricant.
- Scenario 2: considers only the elasticity of Elements 2 and 3 and only allows natural frequencies lower than 250 Hz.
- Scenario 3: considers only the play in the passive spherical joints with the value of 0.1 mm.
- Scenario 4: combines Scenario 1 and Scenario 2.
- Scenario 5: combines Scenario 1 and Scenario 3.
- Scenario 6: combines Scenario 2 and Scenario 3.
- Scenario 7: combines Scenario 1, Scenario 2 and Scenario 3.

3. Results and Discussions

The influence of each of the three factors considered (Scenarios 1–3) as well as their combination (Scenarios 4–7) was analyzed by comparison with the reference model (ideal case) in order to identify

(a) kinematic (displacements, speeds and accelerations of the characteristic point) and dynamic (driving torques) deviations generated by these factors. These deviations are denoted generically with $e\_X\_p = X\_p - X$, where $X = r_P, v_P, a_P, TA, TB, TC, p$ is the considered parameter (μ—friction, *e*—elasticity, *c*—clearance), and X_p is the value of the X variable in the assumption of considering the *p* factor, X obtained in the ideal case;

(b) the coupling effect of the factors, i.e., the extent to which they are independent variables and whether their effects can be considered additive phenomena.

3.1. Scenario 1

In this scenario, we start from the ideal case of the robot structure, to which the friction in the spherical joints S_{2k1}, S_{2k2} and $S_{3k1}, S_{3k2}, k = A, B, C$ is added, taking into account steel/steel friction with lard oil lubricant with the 0.11 static friction coefficient and the 0.084 dynamic coefficient [36].

As is known, friction in kinematic joints does not influence the motion transmission function but has an effect on the dynamic behavior of the robot. The friction from the spherical joints has a moderate effect on the diving torques (about 0.007%, Figure 7), resulting in deviations of up to 0.508 N·m for *TA* (Figure 7a), 0.207 N·m for *TB* (Figure 7b) and 0.241 N·m for *TC* (Figure 7c).
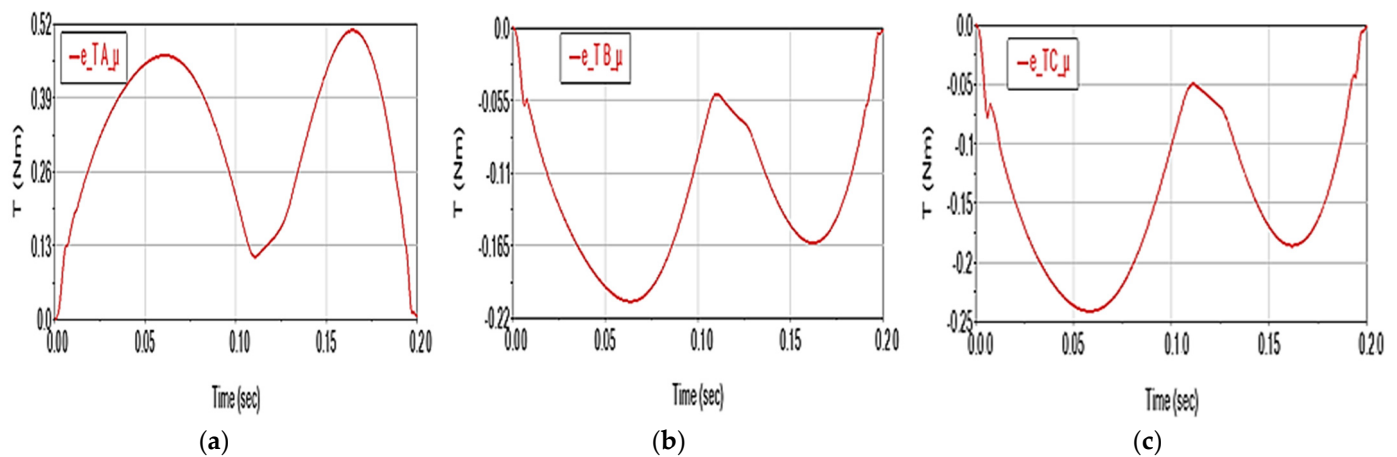

(a)   **(b)**   **(c)**

Figure 7. The driving torque deviations in the hypothesis of considering the friction from the spherical joints (Scenario 1): (**a**) arm A; (**b**) arm B; (**c**) arm C.

A variation of these deviations is noted for all three driving torques, with a profile similar to the acceleration a_p (see Figure 5c) and in correlation with the moment variation (Figure 6):

- the deviation values $e\_Tk\_μ, k = A, B, C$ are directly proportional to the absolute values of the moments *Tk*;
- friction leads to an increase in the driving torques value during the acceleration phase (0.0–0.1 s interval) and helps the motors to brake during the deceleration phase (0.1–0.2 s).

3.2. Scenario 2

In the hypothesis of considering the flexibility of the flexible elements of the Delta parallel robot (Elements 2 and 3 on each arm, see Figure 8) and limiting the analysis to the first 10 vibration modes (with natural frequencies lower than 250 Hz, as the effect of

higher frequencies is negligible—the principal characteristics are presented in Figure 9), the results represented in Figure 10 (motion deviations) and Figure 11 (torque deviations) are obtained.
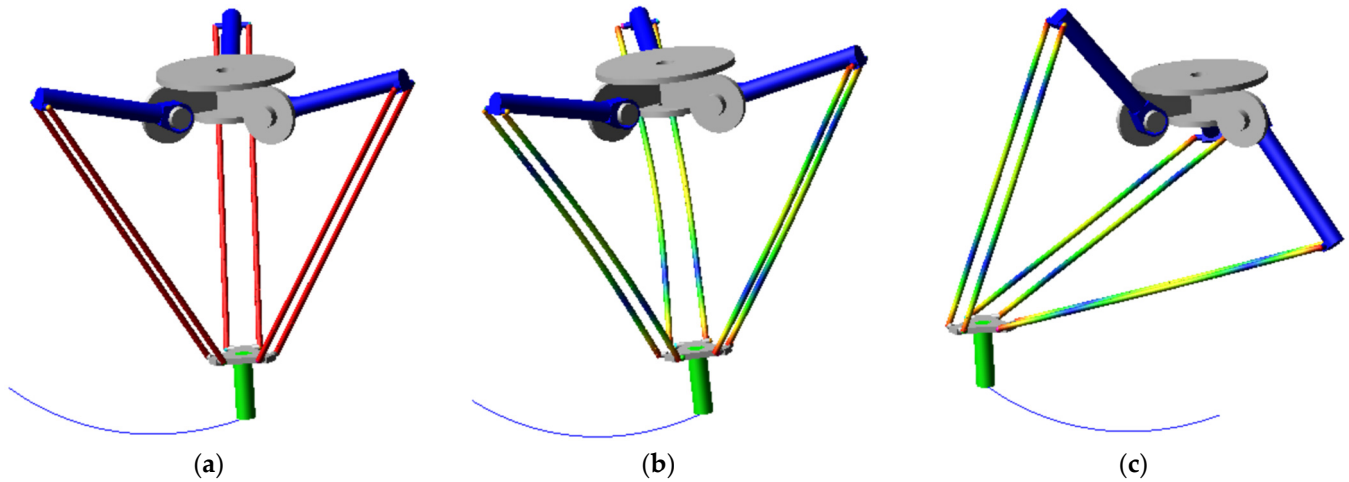

(a)   (b)   (c)

Figure 8. The CAD model of the Delta robot: (**a**) in ideal case, and with flexible links at (**b**) trajectory start point P_0; (**c**) trajectory end point P_1.

Mode	Natural Freq. (Hz)	Generalized Stiffness
1	1.1518958978e−03	5.2382497388e−05
2	7.9683124725e−04	2.5066427918e−05
3	6.7322190739e−04	1.7892713855e−05
4	4.2411675126e−04	7.1011811048e−06
5	1.0216174116e−03	4.1203708769e−05
6	1.2931285196e−03	6.6015074361e−05
7	7.8683948112e+01	2.4441734563e+05
8	7.8720880107e+01	2.4464684450e+05
9	2.1644260022e+02	1.8494611889e+06
10	2.1655696823e+02	1.8514162115e+06
11	4.2357073107e+02	7.0829083423e+06
12	4.2377863224e+02	7.0898630547e+06
13	8.0134291407e+02	2.5351084259e+07
14	8.0253908819e+02	2.5426824477e+07
15	1.2399320219e+03	6.0695359596e+07
16	1.2422770737e+03	6.0925159870e+07
17	2.2897598814e+03	2.0698535591e+08
18	2.6876483924e+03	2.8517052887e+08
19	6.4453936151e+03	1.6400558051e+09
20	7.1969750670e+03	2.0448418881e+09
21	1.8387634416e+04	1.3347854309e+10
22	2.0763778650e+04	1.7020507986e+10
23	2.9980545194e+04	3.5248185976e+10
24	3.4802008438e+04	4.7815461595e+10

```
Mass          : 2.677430125 kg
CM Location   : 0.148144261, 0.3609460597, −0.4755363783 meter, meter, meter
Inertia Tensor : (relative to the Local Body Reference Frame)
        IXX   : 1.205559104 kg-meter**2
        IYY   : 0.877780897 kg-meter**2
        IZZ   : 0.483000689 kg-meter**2
        IXY   : 0.175740214 kg-meter**2
        IZX   : −0.1281618898 kg-meter**2
        IYZ   : −0.3546979703 kg-meter**2
```
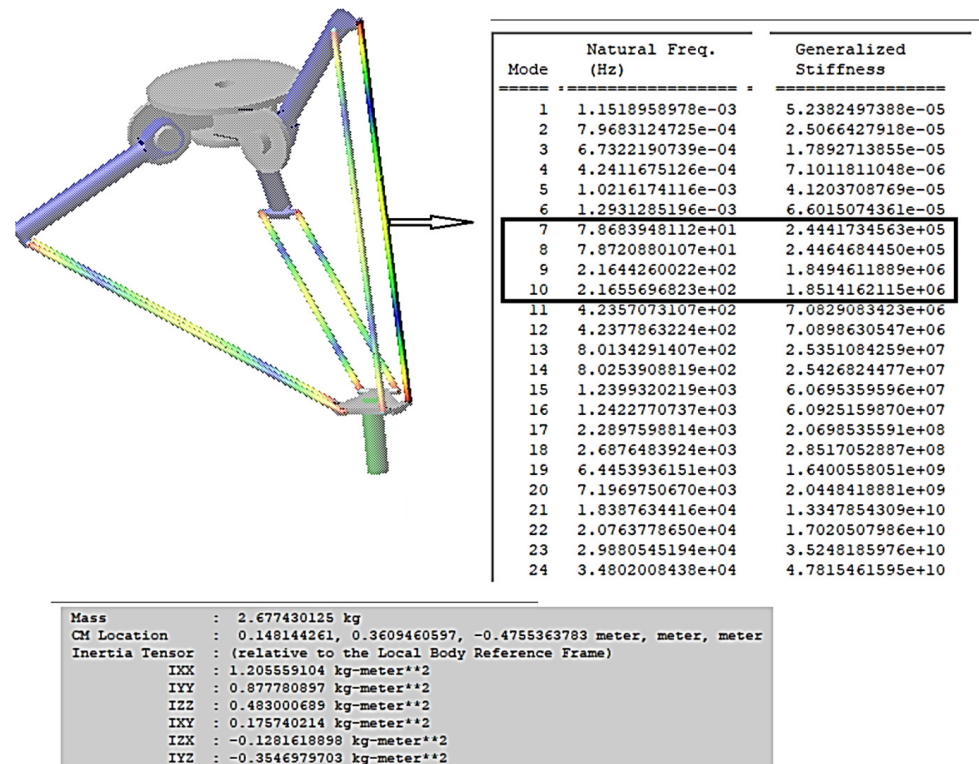
Figure 9. The principal modes of vibration (Hz), generalized stiffness (N/m) and mass properties (including CM and inertia tensor) of rods.

Taking into account the natural properties of the rod elements (Table 2), the ADAMS dynamic simulation leads to low deviations from the theoretical trajectory of the effector ($e\_rp < 4.2 \cdot 10^{-6}$ m, Figure 10a), the speed deviation of up to $3.1 \cdot 10^{-4}$ m/s for (Figure 10b) and deviations of up to 5 m/s^2 for acceleration (i.e., max. 4.2%, Figure 10c). The largest deviations e_vp and e_ap occur at around 0.042 s and 0.158 s, respectively, the moments of time at which the acceleration a_p is at its maximum (see Figure 5c).
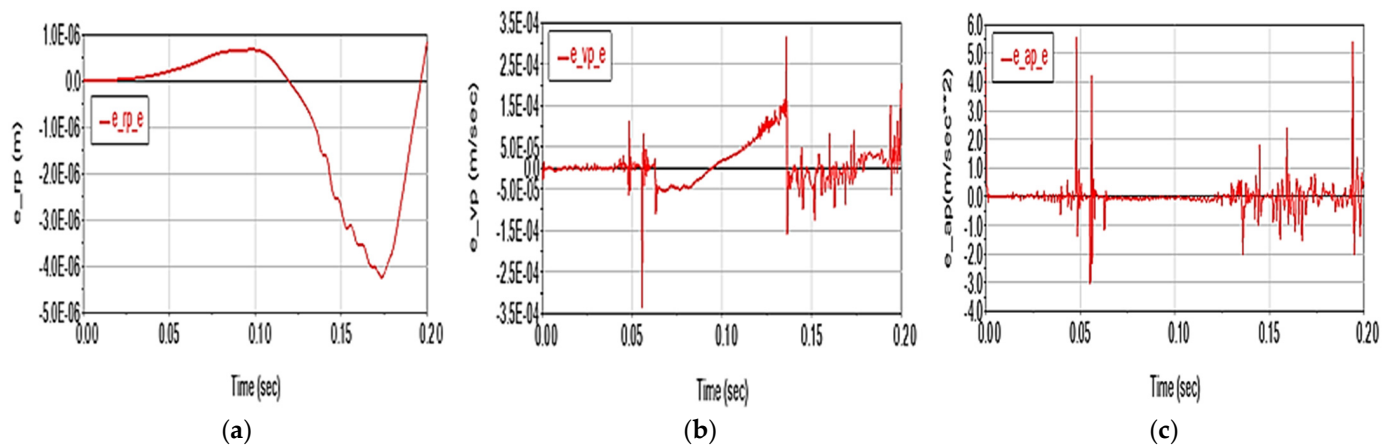
Figure 10. Kinematic deviations in Scenario 2 for (**a**) displacement; (**b**) velocity and (**c**) acceleration.
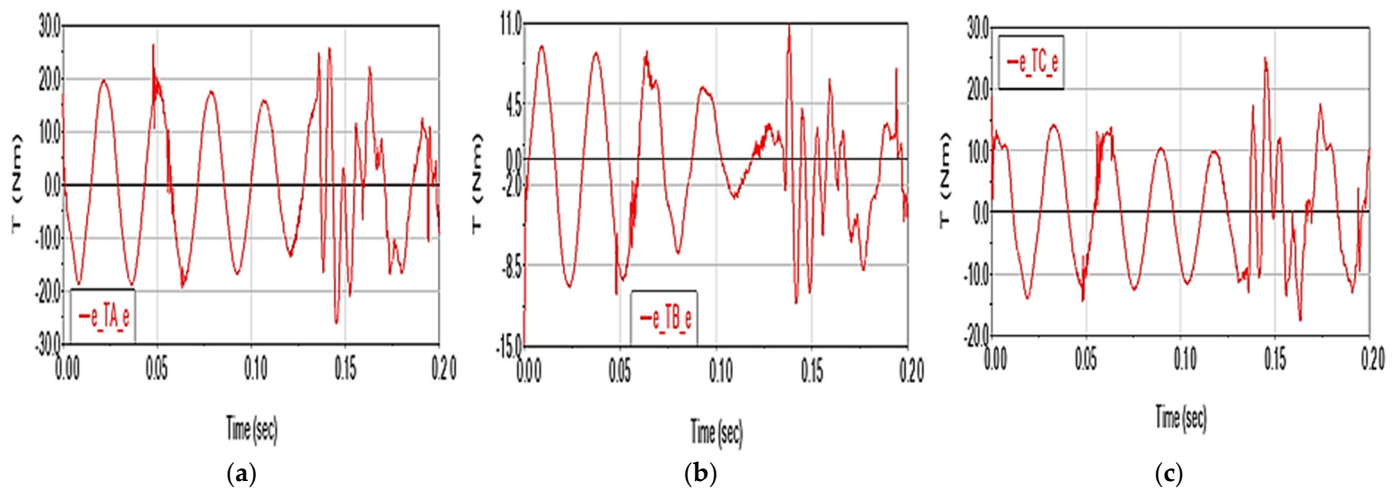

Figure 11. Driving torque deviations in Scenario 2 for (**a**) arm A; (**b**) arm B and (**c**) arm C.

The driving torque deviations have an oscillatory evolution (seven oscillations with a period of approx. 0.025 s) characterized by maximum values of ~26.4 N·m for *TA* (Figure 11a), ~10.8 N·m for *TB* (Figure 11b) and ~25.3 N·m for *TC* (Figure 11c). The maximum deviations are recorded in the case of the engine in joint A (~0.035%). An instability phenomenon occurs at the time of ~0.15 s, corresponding to the maximum acceleration zone of the characteristic point.

3.3. Scenario 3

In this subsection, we analyze the influence of the clearances in the spherical, using a single value of 0.1 mm for all 12 joints S_{2k1}, S_{2k2} and S_{3k1}, S_{3k2}, $k = A$, B, C. Under these conditions, the deviation of the characteristic point in the initial position is 0.2 mm.

The deviation from the characteristic point trajectory is up to $1.18 \cdot 10^{-4}$ m (Figure 12a), with a velocity deviation of up to 0.0035 m/s (Figure 12b) and an acceleration of up to 0.068 m/s^2 (Figure 12c). Compared to Scenario 2, the displacement deviation on the trajectory is significantly higher (~20 times higher), but the deviation of the acceleration on the trajectory is much lower (~70 times lower).
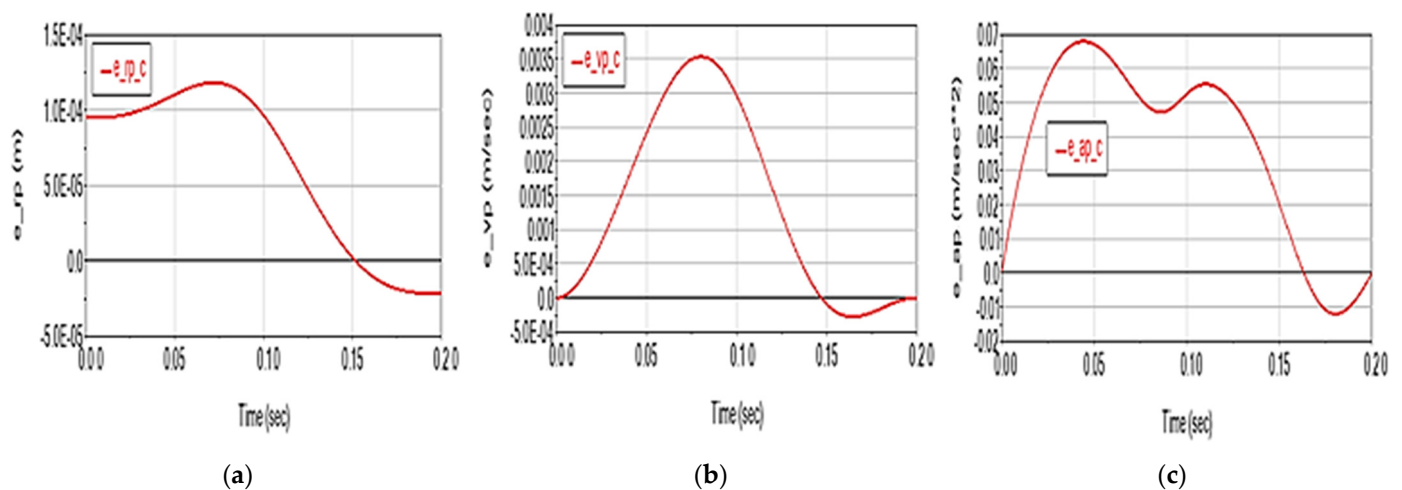
Figure 12. Kinematical deviation in Scenario 3 for (**a**) displacement; (**b**) velocity and (**c**) acceleration.

The influence of the spherical joint clearances on the driving torques is moderate, about 10–20 times lower than in Scenario 2, but 2–3 times higher than in Scenario 1. A deviation of up to 1.7 N·m can be highlighted for *TA* (Figure 13a), up to 0.49 N·m for *TB* (Figure 13b) and up to 0.47 N·m for *TC* (Figure 13c). The extreme values of the deviations are also recorded around the values of 0.042 s and 0.158 s, which are co-responsible for the extreme values of the driving motors (Figure 6).
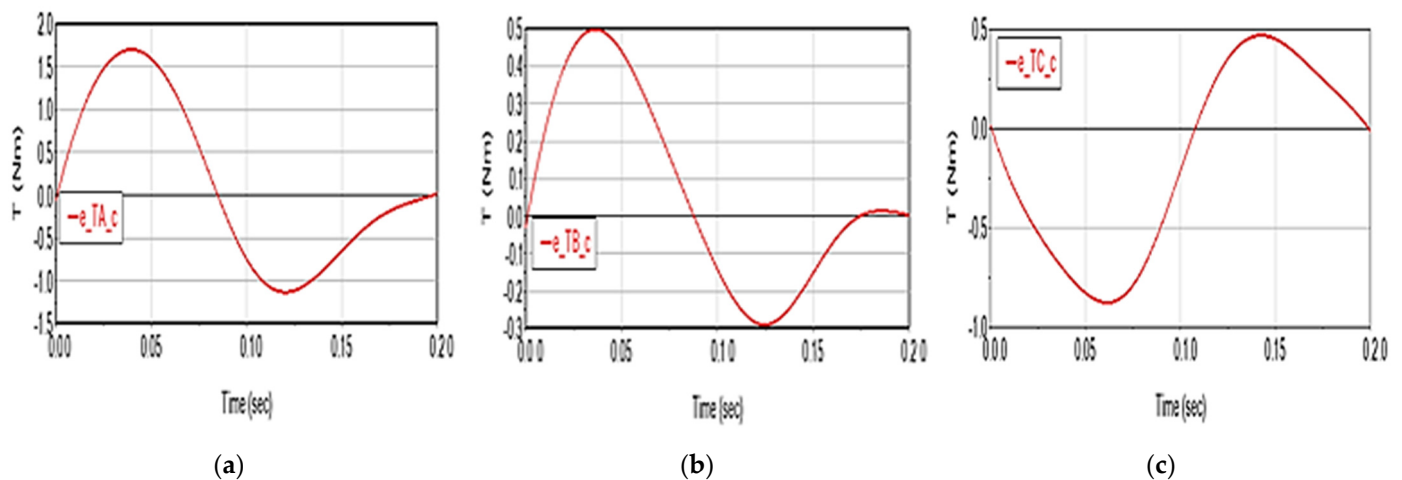

Figure 13. Driving torque deviations in Scenario 3 for (**a**) arm A; (**b**) arm B and (**c**) arm C.

3.4. Scenario 4

In this subsection, we analyze the cumulative influence of friction in the spherical joints and elasticity of the rod elements. We compare and analyze the cumulative resulting deviations with the sum of the deviations identified in Scenarios 1 and 2 to identify the coupling effect between these two factors.

Figure 14 shows the kinematic behavior of the Delta robot with the elastic elements and the joint friction, highlighting both the deviations of the effector motion from the ideal case (red, solid line) and the differences from the case of summing the separate effects of the two factors (blue, dashed line). For the characteristic point displacement (Figure 14a), it can be observed that the cumulative effect of the factors leads to a deviation (in absolute value) of up to a maximum of $4.23 \cdot 10^{-6}$ m (compared to a maximum of $\sim 4 \cdot 10^{-6}$ m for the case of summing the effects), up to $4.2 \cdot 10^{-4}$ m/s for velocity (Figure 14b) compared to the maximum of $3.5 \cdot 10^{-4}$ m/s for the additive case, and up to ~ 6 m/s^2 for acceleration (Figure 14c) compared to the maximum ~ 6 m/s^2 for the case of summing the effects. These

results highlight that the kinematic effects of the two factors (friction in the spherical joints and the elasticity of the elements) are not additive.
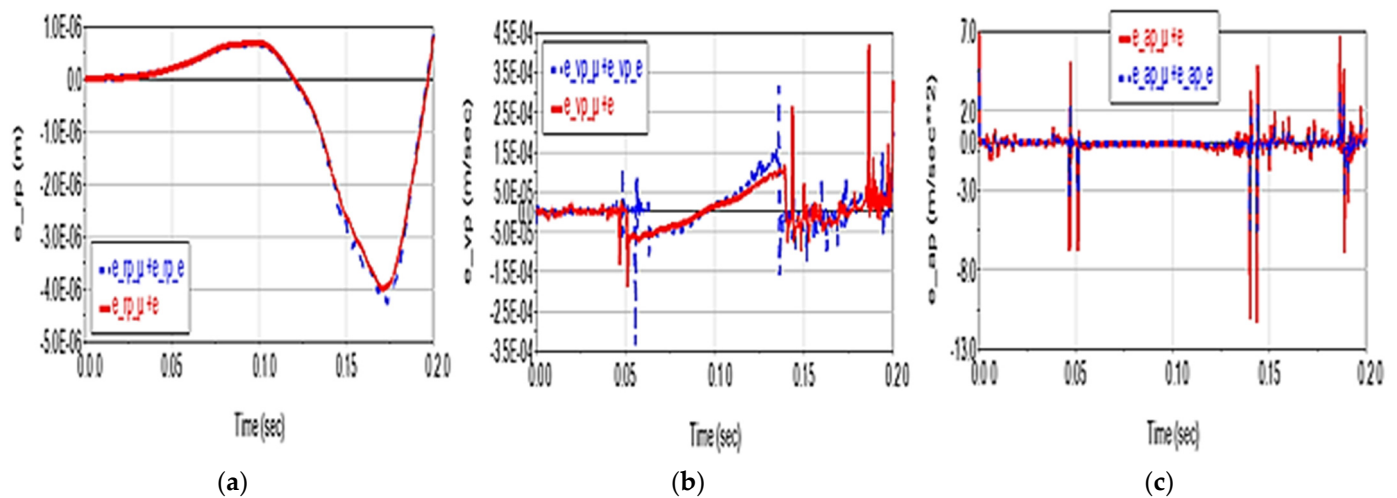

Figure 14. Motion deviations in Scenario 4 (red solid line) and the additive effect of friction and elasticity factors (blue dashed line) for (**a**) displacement; (**b**) velocity and (**c**) acceleration.

Similar to the motion case, the cumulative effect of the two factors results in a decrease in the maximum values of the driving torque deviations compared to the additive case (Figure 15). Therefore, it can be concluded that these factors have no significant coupling effect. Friction (with less significance) does not affect the shape of the deviation curve, but rather contributes to better curve shapes for the torque deviation values.
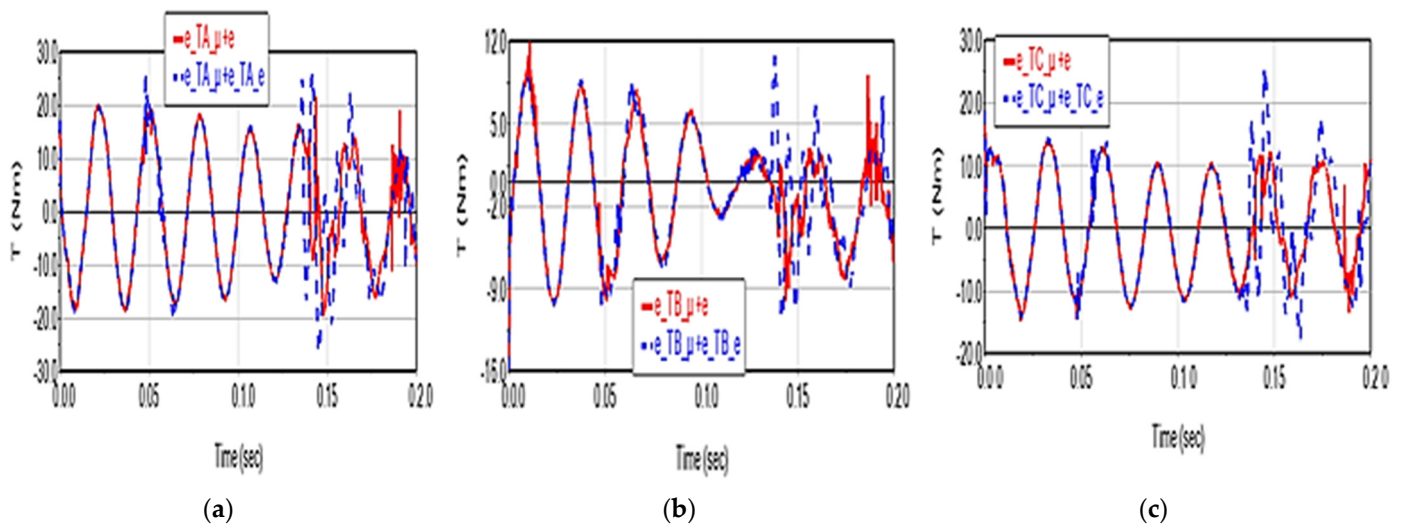

Figure 15. Driving torque deviations in Scenario 4 (red solid line) and the additive effect of friction and elasticity factors (blue dashed line) for (**a**) arm A; (**b**) arm B and (**c**) arm C.

3.5. Scenario 5

The kinematic deviations from the theoretical movement trajectory are shown in Figure 16. In the case of displacement, it can be seen that the cumulative effect of these two factors leads to a deviation similar to that observed in the simulative case. As a result, the effects of the two factors on the kinematic behavior of the Delta parallel robot are not cumulative and their coupling results in the same deviations.
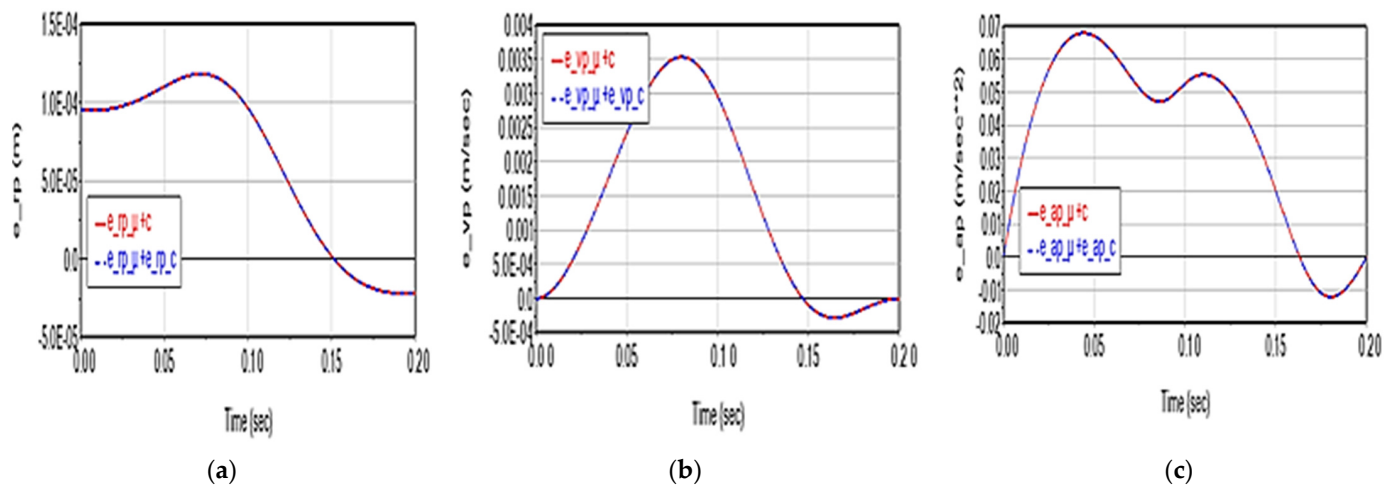
Figure 16. Motion deviations in Scenario 5 (red solid line) and the additive effect of friction and clearance factors (blue dashed line) for (**a**) displacement; (**b**) velocity and (**c**) acceleration.

The cumulative effect of the two factors manifests similarly in the case of motor moments: it leads to the increase in deviations up to 2.12 N·m (additive case) for *TA* torque (Figure 17a), up to 0.36 N·m (*TB* torque, Figure 17b), 1.11 N·m (*TC* torque, Figure 17c). The moment deviations still have the same value also in the case of summing the effects, when their values are the same compared to the case of summing the effects, without affecting the shape of the curves.
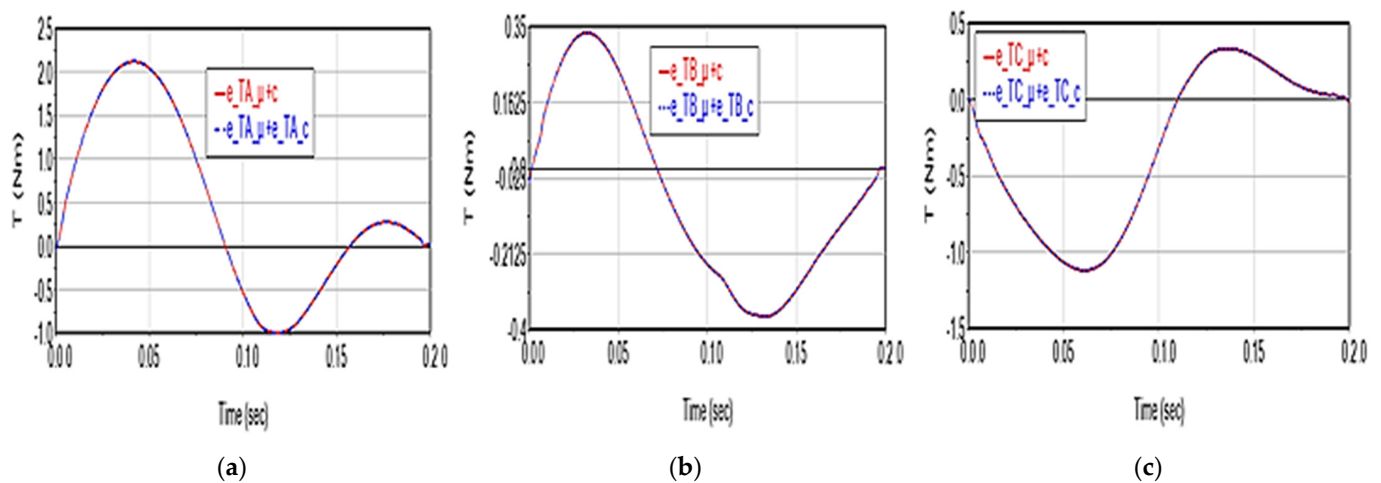

Figure 17. Driving torque deviations in Scenario 5 (red solid line) and the additive effect of friction and clearance factors (blue dashed line) for (**a**) arm A; (**b**) arm B and (**c**) arm C.

3.6. Scenario 6

The combination between the flexibility of the rod elements and the clearances in the spherical joints (0.1 mm) has almost no effect in the displacement and velocity of the characteristic point. However, the "picks" in the acceleration are considered reduced and the cumulative effect is taken into consideration (Figure 18).
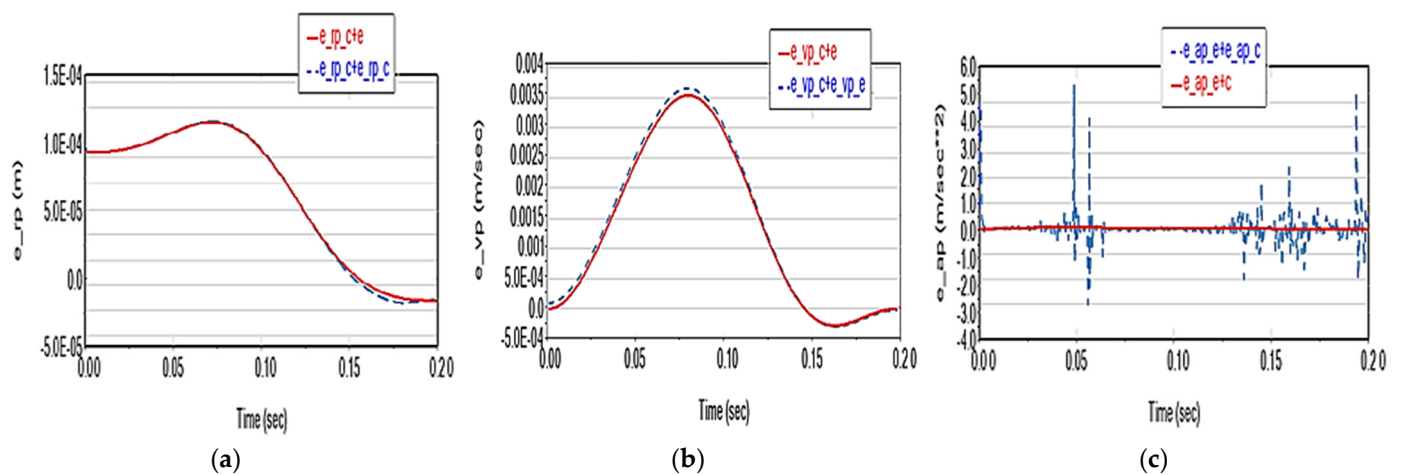
Figure 18. Motion deviations in Scenario 6 (red solid line) and the additive effect of clearance and elasticity factors (blue dashed line) for (**a**) displacement; (**b**) velocity and (**c**) acceleration.

In this scenario, the moment deviations have a relatively constant harmonic pitch and amplitude variation, the maximum values reaching ~50 N·m vs. ~20 N·m (in the additive case) for *TA* (Figure 19a), to ~30 N·m vs. ~10 N·m for *TB* (Figure 19b), 20 N·m vs. 22 N·m for *TC* (Figure 19c).
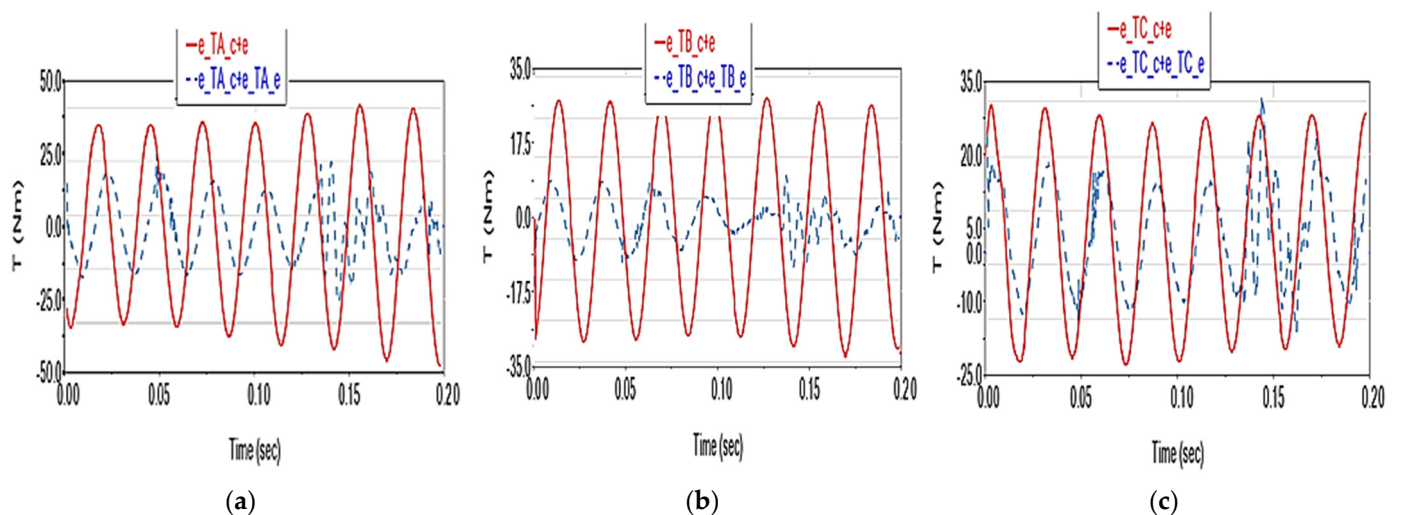

Figure 19. Driving torque deviations in Scenario 6 (red solid line) and the additive effect of clearance and elasticity factors (blue dashed line) for (**a**) arm A; (**b**) arm B and (**c**) arm C.

3.7. Scenario 7

In this scenario, the cumulative effects of the three factors (friction, flexibility and clearance) on the kinematic and dynamic behavior of the Delta robot are not considered. ADAMS simulations that consider the simultaneous action of those three factors resulted in values of kinematic deviations that are approximately the same values for displacement and speed (Figure 20). However, for acceleration, smaller values are emphasized due to the better numerical integration in ADAMS compared to summing the deviations generated individually by each factor (Figure 20c).
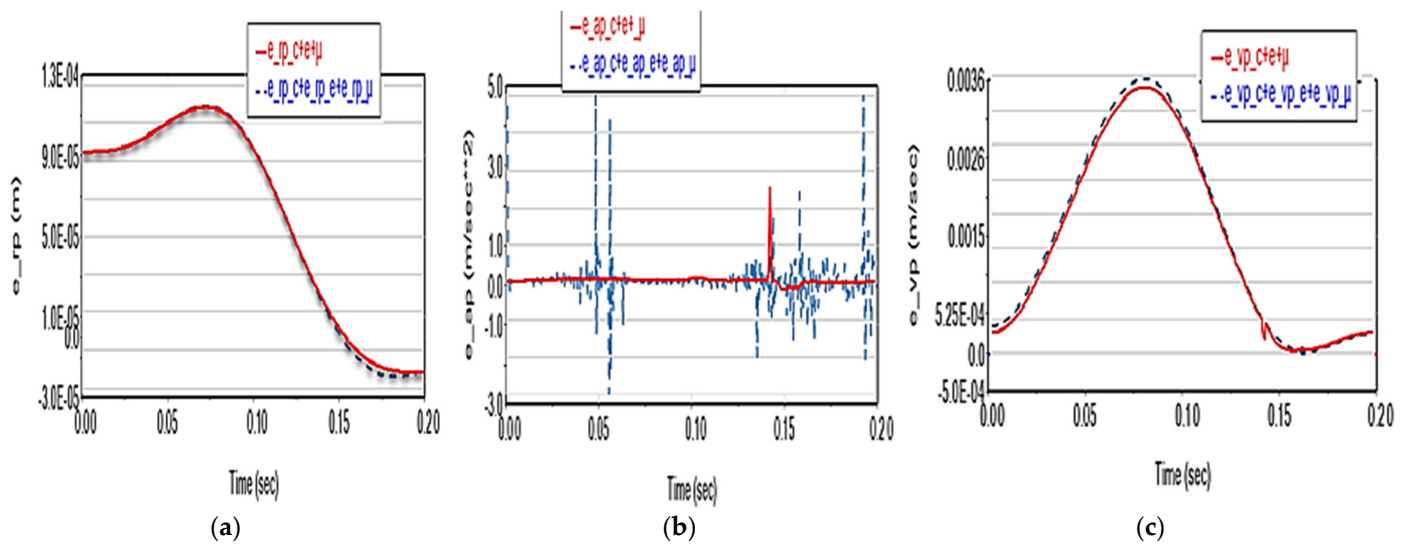
Figure 20. Motion deviations in Scenario 7 (red solid line) and the additive effect of friction, elasticity and clearance factors (blue dashed line) for (**a**) displacement; (**b**) velocity and (**c**) acceleration of the characteristic point.

The maximum deviation of the driving torques shows the same type of harmonic variation as in the scenarios where the elasticity factor is considered. It reaches ~120 N·m vs. ~20 N·m (in the additive case) for *TA* (Figure 21a), ~80 N·m vs. ~10 N·m for *TB* (Figure 21b) and ~70 N·m vs. ~10 N·m for *TC* (Figure 21c).
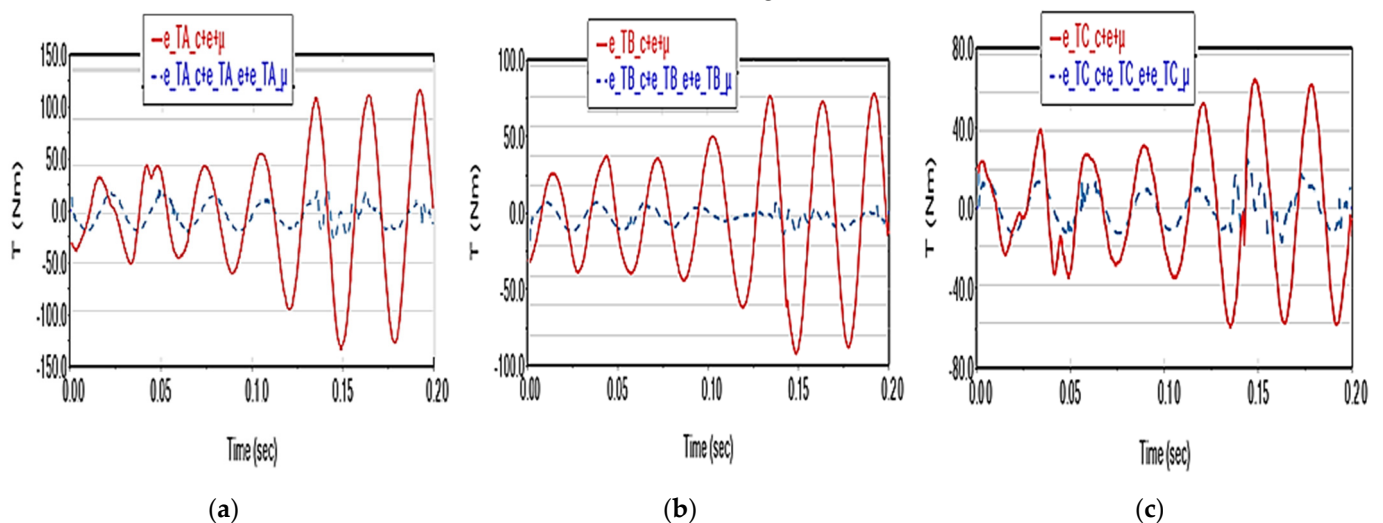

Figure 21. Driving torque deviations in Scenario 7 (red solid line) and the additive effect of clearance, friction and elasticity factors (blue dashed line) for (**a**) arm A; (**b**) arm B and (**c**) arm C.

4. Conclusions

A new approach is employed in this paper by analyzing the impact of three factors on the kinematic and dynamic behavior of the Delta parallel robot: the elasticity of the robot's supple elements (rod elements), friction and clearance in the spherical joints. For this purpose, the analysis was carried out for the case study of a Delta SIAX 3-1600-type robot based on the 3D models developed in CATIA and simulated in the ADAMS software.

The following summarizes the effects of these factors' actions on the movement trajectory:

- Friction has an insignificant influence on the movement parameters of the characteristic point (displacement, speed, acceleration);

- The elasticity of the elements causes practically negligible deviations in the displacement on the trajectory (of the order of 10^{-6} m), small deviations on velocity (of the order of 10^{-4} m/s), but significant in the acceleration (of up to 5 m/s^2);
- Joint clearances (considered at the value of 0.1 mm) have a substantial effect on the characteristic point displacement (deviations of the order of 10^{-4} m), moderate on velocity (of the order of 10^{-3} m/s) and relatively negligible on acceleration (of order 10^{-2} m/s^2);
- The coupling of any two of these factors results in the cumulative effects on kinematics and dynamics, except in Scenario 6, where the deviations reach values three times higher than those in the case of the individual effects summation;
- The coupling of the three factors leads, from a kinematic point of view, to a slight reduction in deviations, except for acceleration, where a significant reduction in deviations, and especially in picks, can be observed, leading to a better numerical integration solution;
- Regarding dynamics, the effects of the three factors are the following:
- Friction in the joints causes a practically insignificant variation in the driving torques (of the order of 10^{-1} N·m) compared to their nominal values of the order of 103 N·m (<750 N·m);
- The elasticity of the elements has a substantial impact on driving torques (deviations of up to 25 N·m, i.e., 3.3%, with a harmonic evolution);
- Joint clearances have a moderate effect on driving torques (<2 N·m);
- When two factors are combined (except in Scenario 6), the deviations can reach vaues up to two times higher compared to the case of the summation of individual effects and values up to three times higher when all three factors are combined.

For all factor coupling scenarios (S4–S7), the study observed that individual effects are not always cumulative. The coupling of factors can increase deviation values when the clearances and elasticities in the joints are considered simultaneously. Consequently, it is not recommended to simulate these factors separately and sum their effects. Since the phenomena are not linear, a combined approach of the factors is necessary to obtain relevant results. The authors propose to validate the conclusions of this theoretical study resulting from numerical simulations in the ADAMS software through experimental means in the future.

Author Contributions: Conceptualization, M.N. and N.C.; methodology, N.C., M.N. and R.S.; software, N.C. and R.S.; validation, M.N., N.C. and R.S.; formal analysis, M.N. and N.C.; investigation, N.C. and R.S.; resources, N.C., M.N. and R.S.; data curation, M.N. and R.S.; writing—original draft preparation, N.C.; writing—review and editing, M.N. and R.S; visualization, N.C and R.S.; supervision, M.N. All authors have read and agreed to the published version of the manuscript.

Institutional Review Board Statement: Not applicable.

Informed Consent Statement: Not applicable.

Data Availability Statement: Not applicable.

Conflicts of Interest: The authors declare no conflict of interest.

References

1. Clavel, R. Dispositif Pour le Déplacement et le Positionnement d'un Elément dans L'espace. Google Patents WO1987003528A1, 18 June 1987.
2. Angel, L.; Bermudez, J.; Munoz, O. Dynamic optimization and building of a parallel delta-type robot. In Proceedings of the International Conference on Robotics and Biomimetics, Shenzhen, China, 12–14 December 2013; pp. 444–449. [CrossRef]
3. Zhang, J.; Shi, L.; Gao, R.; Lian, C. A Method for obtaining direct and inverse pose solutions to Delta parallel robot based on ADAMS. In Proceedings of the International Conference on Mechatronics and Automation, Changchun, China, 9–12 August 2009; pp. 1332–1336. [CrossRef]

4. Guglielmetti, P.; Longchamp, R. A closed form inverse dynamics model of the delta parallel robot. *IFAC Proc. Vol.* **1994**, *27*, 51–56. [CrossRef]

5. Dastjerdi, A.H.; Sheikhi, M.M.; Masouleh, M.T. A complete analytical solution for the dimensional synthesis of 3-DOF delta parallel robot for a prescribed workspace. *Mech. Mach. Theory* **2020**, *153*, 103991. [CrossRef]

6. Zhang, L.; Mei, J.; Zhao, X.; Huang, T. Dimensional synthesis of the Delta robot using transmission angle. *Robotica* **2011**, *30*, 343–349. [CrossRef]

7. Huiping, S.; Qingmei, M.; Ju, L.; Jiaming, D.; Guanglei, W. Kinematic sensitivity, parameter identification and calibration of a non-fully symmetric parallel Delta robot. *Mech. Mach. Theory* **2021**, *161*, 104311.

8. Miller, K. Experimental Verification of Modeling of Delta Robot Dynamics by Direct Application of Hamilton's Principle. In Proceedings of the IEEE International Conference on Robotics and Automation (ICRA), Nagoya, Japan, 21–27 May 1995; pp. 532–537.

9. Falezza, F.; Vesentini, F.; Di Flumeri, A.; Leopardi, L.; Fiori, G.; Mistrorigo, G.; Muradore, R. A novel inverse dynamic model for 3-DoF delta robots. *Mechatronics* **2022**, *83*, 102752. [CrossRef]

10. Brinker, J.; Corves, B.; Wahle, M. A comparative study of inverse dynamics based on clavel's delta robot. In Proceedings of the 14th World Congress in Mechanism and Machine Science, Taipei, China, 25–30 October 2015; pp. 25–30.

11. Codourey, A. Dynamic modelling and mass matrix evaluation of the delta parallel robot for axes decoupling control. In Proceedings of the IEEE/RSJ International Conference on Intelligent Robot and Systems, Osaka, Japan, 4–8 November 1996; Volume 3, pp. 1211–1218.

12. Asadi, F.; Heydai, A. Analitical dynamic modeling of Delta robot with experimental verification. *Proc. Inst. Mech. Eng. Part K J. Multi-Body Dyn.* **2020**, *234*, 623–663.

13. Rat, N.R.; Neagoe, M.; Gogu, G.; Stan, S.D. Dynamic analysis of an Isoglide3-T3 parallel robot. In Proceedings of the Annals of DAAAM 2009 & Proceedings of the 20th International DAAAM Symposium "Intelligent Manufacturing & Automation: Theory, Practice & Education", Vienna, Austria, 25–28 November 2009; p. 15.

14. Cretescu, N.; Neagoe, M. Dynamic Modelling of an Isoglide T3 Type Parallel Robot. In *New Advances in Mechanisms, Mechanical Transmissions and Robotics MTM&Robotics*; Springer International Publishing: Cham, Switzerland, 2020; pp. 235–248. [CrossRef]

15. Raţ, N.R.; Neagoe, M.; Stan, S.D. Comparative Dynamic Analysis of Two Parallel Robots. In *Solid State Phenomena*; Trans Tech Publications Ltd.: Stafa-Zurich, Switzerland, 2010; pp. 345–356.

16. Rat, N.; Neagoe, M.; Gogu, G. Theoretical and Experimental Research on the Dynamics of a 4DOF Isoglide 4-T3R1 Parallel Robot. In Proceedings of the SYROM 2009: 10th IFToMM International Symposium on Science of Mechanisms and Machines, Brasov, Romania, 12–15 October 2009; pp. 387–396. [CrossRef]

17. Rat, N.R.; Neagoe, M.; Diaconescu, D.; Stan, S.D. Dynamic analysis of a Triglide parallel robot. In Proceedings of the 4th International Conference on Human System Interaction (HSI), Yokohama, Japan, 19–21 May 2011; pp. 245–249.

18. Robert, L.; Williams, I.I. The Delta Parallel Robot: Kinematics Solutions, Mechanical Engineering. Ph.D. Thesis, Ohio University, Athens, Ohio, 2016.

19. Hamdoun, O.; Bakkali, L.E.; Baghli, F.Z. Analysis and Optimum Kinematic Design of a Parallel Robot. In Proceedings of the 10th International Conference Interdisciplinarity in Engineering, Tirgu Mures, Romania, 6–7 October 2016.

20. Hugo, H.; Joan, L. The Forward and Inverse Kinematics of a Delta Robot, Chapter. In Proceedings of the Advances in Computer Graphics: 37th Computer Graphics International Conference, CGI 2020, Geneva, Switzerland, 20–23 October 2020. [CrossRef]

21. Gosselin, C.; Angeles, J. The Optimum Kinematic Design of a Planar Three-Degree-of-Freedom Parallel Manipulator. *J. Mech. Transm. Autom.* **1988**, *110*, 35–41. [CrossRef]

22. Cheng, L.; Guohua, C.; Yongyin, Q. Safety Analysis via Forward Kinematics of Delta Parallel Robot using Machine Learning. *Saf. Sci.* **2019**, *117*, 243–249.

23. Swaraj, Z.; Sharad, K.P. Matlab Toolbox for Kinematic Analysis and Simulation of Dexterous Robotic Grippers. In Proceedings of the 12th Global Congress on Manufacturing and Management, GCMM 2014, Procedia Engineering, Vellore, India, 8–10 December 2014; Volume 97, pp. 1886–1895.

24. Carmelo, M.; Stephen, G.P.; Pascual, I.N.; Ian, C. Robotic path Planning for Non-Destructive Testing—A Custom MATLAB Toolbox, Approach. *Robot. Comput.-Integr. Manuf.* **2016**, *37*, 1–12.

25. Ma, L.; Dexue, B.; Zhipeng, X. Mechanism Simulation and Experiment of 3-DOF Parallel Robot Based on MATLAB. In Proceedings of the 2015 International Power, Electronics and Materials Engineering Conference, Dalian, China, 16–17 May 2015.

26. Shehata, M.; Elshami, M.; Bai, Q.; Zhao, X. Parameter Estimation for Multibody System Dynamic Model of Delta Robot from Experimental Data. *IFAC-PapersOnLine* **2021**, *54*, 72–77. [CrossRef]

27. Cretescu, N.; Neagoe, M.; Saulescu, R. Kinematic and Dynamic Analysis of a 4DOF Parallel Robot with Flexible Links. In Proceedings of the Joint International Conference of the XII International Conference on Mechanisms and Mechanical Transmissions (MTM) and the XXIII International Conference on Robotics (Robotics '16), Aachen, Germany, 26–27 October 2016; pp. 473–481.

28. Cretescu, N.R.; Neagoe, M. Rigid versus Flexible Link Dynamic Analysis of a 3DOF Delta Type Parallel Manipulator. *Appl. Mech. Mater.* **2015**, *762*, 101–106. [CrossRef]

29. Rat, N.R.; Neagoe, M. Rigid vs. flexible links dynamic analysis of a 3DOF parallel robot. In Proceedings of the 3rd IEEE International Conference on ASME 2009, DEST '09, San Diego, CA, USA, 30 August–2 September 2009; pp. 534–539.

30.   Kuo, Y.-L. Mathematical modeling and analysis of the Delta robot with flexible links. *Comput. Math. Appl.* **2016**, *71*, 1973–1989. [CrossRef]

31.   Wu, M.; Mei, J.; Zhao, Y.; Niu, W. Vibration reduction of delta robot based on trajectory planning. *Mech. Mach. Theory* **2020**, *153*, 104004. [CrossRef]

32.   Kermanian, A.; Kamali, E.A.; Taghvaeipour, A. Dynamic analysis of flexible parallel robots via enhanced co-rotational and rigid finite element formulations. *Mech. Mach. Theory* **2019**, *139*, 144–173. [CrossRef]

33.   Weiss, C.; Morlock, M.M.; Hoffmann, N.P. Friction induced dynamics of ball joints: Instability and post bifurcation behavior. *Eur. J. Mech.-A/Solids* **2014**, *45*, 161–173. [CrossRef]

34.   Li, Y.; Shang, D.; Fan, X.; Liu, Y. Motion Reliability Analysis of the Delta Parallel Robot considering Mechanism Errors. *Math. Probl. Eng.* **2019**, *2019*, 3501921. [CrossRef]

35.   SIPRO. Available online: https://www.sipro.vr.it/en/delta-robot/delta-robot-SIAX-D3-1600.html (accessed on 4 November 2022).

36.   Engineeringlibrary. Available online: https://engineeringlibrary.org/reference/coefficient-of-friction (accessed on 4 November 2022).